國立臺灣大學工學院土木工程學系

碩士論文

Department of Civil Engineering
College of Engineering
National Taiwan University

Master's Thesis

半乾旱與乾旱地區永續雨水收集適址之最佳化方法

An Optimized Method for Sustainable Rainwater Harvesting Sites in Semi-Arid and Arid regions

胡卡林

Abdikarim Hassan Hussein

指導教授：何昊哲 博士

Advisor: Hao-Che Ho, Ph.D.

中華民國 114 年 7 月

July 2025

doi:10.6342/NTU202503692

國立臺灣大學碩士學位論文

NATIONAL TAIWAN UNIVERSITY
MASTER'S THESIS ACCEPTANCE CERTIFICATE

半乾旱與乾旱地區永續雨水收集適址之最佳化方法

An Optimized Method for Sustainable Rainwater Harvesting Sites in Semi-Arid and Arid regions

本論文係 胡卡林 (R12521324 在國立臺灣大學土木工程學系水利工程組完成之碩士學位論文，於民國114年07月23日承下列考試委員審查通過及口試及格，特此證明。

The undersigned, appointed by the Department of Civil Engineering, Hydraulic Engineering on 23 July,2025 have examined a Master's Thesis entitled above presented by Abdikarim Hassan Hussein (R12521324) candidate and hereby certify that it is worthy of acceptance.

口試委員 Oral examination committee:

何昊哲 (指導教授 Advisor)

李鴻源

葉克家

系主管Director: 葛宇甯

Acknowledgement

I am deeply thankful to Almighty Allah for his infinite mercy, guidance, and strengths throughout my academic journey. This achievement would not have been possible without his ongoing support.

I express my profound gratitude to my advisor, Professor Hao-Che Ho, for his exceptional mentorship, insightful feedback, and support. His expertise and thoughtful guidance have been crucial in shaping this research and seeing it through to completion.

I wish to express my sincere gratitude to the faculty and administrative staff of the Department of Civil Engineering at the National Taiwan University for their unwavering support and professionalism.

I owe a great deal of gratitude to my lab-mates and colleagues, and I am profoundly appreciative of my dear friends Ahmed, Abdishakour, and Simeon, whose unwavering support during my injury enabled me to continue my studies. Their generosity, motivation, and practical help were immensely important to me.

I extend my heartfelt gratitude to my cherished parents and family for their unwavering love, sacrifices, and steadfast faith. Their unwavering support is a continual source of strength and motivation. I am grateful to my siblings for their prayers, encouragement, and steadfast presence throughout this journey.

Finally, I am deeply grateful to everyone who played a role, whether directly or indirectly, in bringing this academic project to fruition. Your support, in all its forms, is greatly appreciated.

doi:10.6342/NTU202503692

Abstract

Rainwater harvesting (RWH) is a sustainable solution for mitigating water scarcity, particularly in regions experiencing irregular and declining precipitation. This research focuses on the Southern Province of Zambia, a region that is becoming increasingly susceptible to climate fluctuations and the resulting challenges to sustained water security. Despite previous studies have explored RWH, there remains a significant shortfall in developing integrated frameworks that are spatially optimized to address the unique requirements of semi-arid regions. Here, the study developed a hybrid model integrating Geographic Information Systems (GIS) with Multi-Criteria Decision Analysis (MCDA) to delineate suitable zones for RWH implementation. In the evaluation, twelve criteria were taken into account, addressing physical, environmental, and socio-economic factors, with the Standardized Precipitation Index (SPI) serving as a climatic indicator. The Fuzzy Analytic Hierarchy Process (Fuzzy-AHP) was applied to assess the relative weights of the criteria, identifying rainfall, curve number, and slope as the most influential factors. Suitability maps were generated and classified into five categories including not and low suitable regions, most, highly, and moderately suitable. Results from Fuzzy-AHP and the Technique for Order of Preference by Similarity to Ideal Solution (TOPSIS) indicated that 62% and 37.5% of the study area, respectively, are favorable for RWH. The northern and southwestern regions exhibited the highest suitability due to their advantageous physical and socio-economic conditions. Sensitivity analysis, conducted by varying the fuzziness degree (FD), confirmed the robustness of the model. Validation through TOPSIS revealed a 63% spatial agreement and 67% accuracy, supporting reliability of the model. This research presents a reproducible, affordable, and climate-adaptive approach for sustainable RWH site selection and informed water resource planning in drought-prone regions.

doi:10.6342/NTU202503692

Keywords: Rainwater Harvesting (RWH), Geographic Information Systems (GIS), Fuzzy-AHP, TOPSIS, Multi-Criteria Decision Analysis (MCDA), Semi-Arid and Arid Regions (SARs), Selection of Potential Sites.

doi:10.6342/NTU202503692

Table of Contents

doi:10.6342/NTU202503692

doi:10.6342/NTU202503692

List of figures

doi:10.6342/NTU202503692

doi:10.6342/NTU202503692

List of Tables

doi:10.6342/NTU202503692

Chapter 1: Introduction

1.1 Background

Water is essential for maintaining life, promoting development, and supporting the balance of ecosystem. The term is typically characterized by having sufficient water in both quantity and quality to sustain economic activities, human well-being, and the health of ecosystems (Alfonsov et al., 2008). Ensuring a dependable water supply is crucial for supporting household, farming, and industrial activities, especially as the global demand for water has increased dramatically in recent years due to growing pressures from both domestic and agricultural sectors (Buraihi & Shariff, 2015; Wu et al., 2018; Yegizaw et al., 2022). Additionally, Challenges related to water resources have become increasingly critical on a global scale, as numerous regions continue to experience severe water scarcity and prolonged droughts. These conditions deplete irrigation water supplies, leading to widespread crop failures, food shortages, and substantial socioeconomic and environmental losses (Odhiambo et al. 2021; Sopper 1992).

Africa, with a particular emphasis on Southern Africa, exhibits significant vulnerability to drought, a condition exacerbated by climate change. The region's vulnerability largely stems from its dependence on sectors that are sensitive to climate, such as agriculture reliant on rainfall and services based on ecosystems. (Libanda et al., 2019). In Zambia, the recurrence of droughts is largely attributed to variations in rainfall patterns, which are affected by the Inter-Tropical Convergence Zone (ITCZ) and El Niño–Southern Oscillation (ENSO) phenomena (Musonda et al., 2020). These climatic conditions have led to increasingly frequent and severe drought events, resulting in widespread socioeconomic disruption across the country.

doi:10.6342/NTU202503692

In the most recent 2023–2024 drought, approximately 6.6 million individuals across the three provinces were directly impacted. The 2023–2024 agricultural season was identified as the driest in over four decades, characterized by delayed rainfall onset and extended dry spells, resulting in significant disruptions to agriculture, water availability, livestock health, and ecosystem integrity (Water, 2024). Consequently, Zambia is increasingly facing growing challenges in meeting water needs for both household and farming purposes. This highlights the significant need to enhance sustainable water management approaches, particularly by developing and applying rainwater harvesting (RWH) methods.

In response to these growing challenges, RWH is extensively recognized as an efficient strategy for alleviating water scarcity and bolstering water security. This involves the harvesting, conveyance, and storage of precipitation runoff, which can be utilized in domestic, agricultural, and groundwater recharge contexts (Cruz, 2013; Mouhoumed et al. 2024). As stated by Wu et al. (2018) , RWH serves as an essential additional water source, particularly in areas where water is scarce.

RWH systems have been extensively adopted worldwide for various applications including domestic water supply, groundwater recharge, and agricultural purposes. The efficient application of RWH schemes is dependent upon diligent site identification and robust design methodology. To achieve this, relevant studies have utilized multi-criteria decision-making (MCDM) methods to identify the ideal sites for RWH structures, including terracing, ponds, sand dams, check dams, infiltration trenches, percolation tanks, and contour bunds.

Although rainwater harvesting (RWH) is increasingly acknowledged as a viable method to address water shortages, there is a scarcity of research that systematically

doi:10.6342/NTU202503692

pinpoints the best RWH locations in Zambia's Southern Province using a integration of Geographic Information Systems (GIS) and Multi-Criteria Decision-Making (MCDM) techniques. While previous research has largely focused on physical, environmental, and socio-economic aspects, there are still two significant gaps that have not been addressed. First, the Standardized Precipitation Index (SPI), a recognized measure of drought, has been largely excluded from current suitability evaluations, which restricts the consideration of climate variability and the risk of prolonged drought. Second, there is a noticeable absence of systematic evaluations comparing MCDM techniques to determine the spatial consistency and reliability of their outputs in informing planning decisions. This research fills these gaps by integrating SPI into the suitability analysis to improve climate adaptability and by performing a comparative assessment of Fuzzy-AHP and TOPSIS to evaluate the reliability of the models. Additionally, the framework offers a detailed, reproducible GIS–MCDM model specifically designed for the Southern Province, with potential use in other semi-arid areas. The outcomes of this research are designed to steer the strategic deployment of RWH systems and enhance efforts to achieve water security in the context of increasing climate unpredictability.

1.2 Objectives

This study primarily aims to pinpoint sustainable locations for harvesting rainwater by employing a GIS-based framework for MCDM. This framework integrates physical, socioeconomic, and environmental factors to improve the precision, efficiency, and long-term sustainability of sites identification.

doi:10.6342/NTU202503692

1.2.1 Specific objectives

A. To determine and analyze the physical, environmental, and socioeconomic parameters that affect RWH site suitability using GIS and remote sensing data.
B. To analyze the sensitivity of the assigned weights by evaluating the influence of varying degrees of fuzziness on the weighting of selection criteria within the Fuzzy Analytical Hierarchy Process (Fuzzy-AHP) framework
C. Generate and interpret suitability maps derived from the Fuzzy-AHP and the technique for order of preference by similarity to ideal solution (TOPSIS) for the determination of ideal RWH places.
D. To compare outputs from Fuzzy-AHP and TOPSIS models to assess their spatial consistency, agreement, and reliability in supporting RWH planning decisions.

1.3 Thesis Organization

This thesis is structured into six chapters. A comprehensive review of the existing literature on RWH techniques and methodologies used for site selection is presented in chapter two. Chapter three offers a comprehensive summary of the study region, including an explanation of the data sources and the processing methods used. Fourth chapter describes the methodological framework used for the analysis. The findings of the spatial analysis and suitability assessment are presented and critically discussed in Chapter Five. section, chapter six, concludes the paper by summarizing key insights and proposing recommendations for practical applications.

doi:10.6342/NTU202503692

Chapter 2: Literature Review

2.1 Overview of Global and Regional Context of Water Scarcity

Water scarcity is becoming an increasingly pressing global concern, specifically in semi-arid and arid regions (SARs), where the aggregated consequences of climate change and escalating water demand place substantial pressure on traditional water sources (Matomela et al., 2020). As highlighted by Mahmoud and Alazba (2015) and Tiwari et al. (2018), the decreasing availability of freshwater underscores the urgent necessity for innovative and viable approaches to water management. In many developing nations, the crisis is exacerbated by rapid population growth, expansion of agriculture, and rapid urbanization. These factors collectively heighten water demand while diminishing the dependability of the current supply systems under shifting climate conditions.

In recent decades, the growth of the global population has resulted in significant increases in water consumption. According to the FAO (2015), the worldwide need for water is increasing at a pace that is more than twice as fast as population growth. This escalating demand is further exacerbated by the need for irrigated agriculture and industrial development (Yannopoulos et al. 2019). These converging pressures have raised global concerns regarding water scarcity and food security, particularly in regions where rainfall is highly variable and unreliable. Wu et al. (2018) noted that by 2025, approximately 1.8 billion individuals will inhabit areas facing severe water shortages, while nearly two-thirds of the global population will be living in regions under water scarcity.

Countries in the Horn of Africa, such as Somalia, Eritrea, Ethiopia, and Djibouti, face severe water shortages and climate fluctuations that significantly threaten the livelihoods of millions and the region's ecosystems (Mouhoumed et al., 2023). The

doi:10.6342/NTU202503692

situation in Somalia is particularly desperate, with approximately 6.1 million individuals affected by recurrent droughts, resulting in widespread internal displacement (Broek and Hodder, 2022). Studies by Ullah et al. (2022, 2023) and Mwelwa et al. (2024)have indicated that since the 1980s, Southern Africa has been witnessing a steady increase in temperatures coupled with a decline in rainfall. Recurring drought conditions in the region are primarily due to interannual climate fluctuations linked to the El Niño-Southern Oscillation (ENSO), which is a major role in these patterns.

Similar to numerous other developing nations in Africa, Zambia encounters considerable hurdles due to the intertwined issues of socioeconomic development, climate change, and disaster risk.(Ghosh et al., 2024a; Ngoma et al., 2021). These interconnected factors increase the country's risk of experiencing severe weather phenomena such as floods and droughts. For instance, Musonda et al. (2020) highlighted noteworthy spatial differences in the occurrence of droughts throughout Zambia, noting that the southwestern region experienced more intense droughts than the northeastern region. As noted by Kaluba et al. (2017), the region of southern Zambia faces a heightened risk of experiencing both moderate and severe droughts, with these events expected to occur every 3-4 years and 5-10 years, respectively. Their observations indicate that drought occurrences were more frequent and severe in the southern region, whereas northern Zambia experienced relatively stable conditions. These findings collectively highlight the necessity of implementing region-specific drought mitigation strategies, including the development of a water-harvesting infrastructure, to mitigate the adverse impacts of recurrent droughts.

doi:10.6342/NTU202503692

2.2 Global and Regional RWH Practices

In regions with semi-arid and arid climates that rely on agriculture dependent on rainwater, rainfall usually occurs in a few intense bursts, often resulting in significant runoff losses. Within this framework, RWH has emerged as a promising strategy to bolster agricultural resilience. It can provide supplemental irrigation during extended dry spells, thereby aiding the stabilization and enhancement of crop yields (Sacolo & Mkhandi, 2021). Additionally, rainwater collection efficiently captures runoff, which in turn enhances agricultural productivity through methods that are both economically sound and environmentally responsible (Ziadat et al., 2006). Besides its advantages for agriculture, this approach helps lessen the negative impacts of drought and climate change, while also enhancing the dependability and accessibility of water resources.

RWH is increasingly being acknowledged as an environmentally sustainable method to enhance water availability, particularly in regions facing water scarcity. This approach is instrumental in alleviating water shortages, reducing reliance on overexploited groundwater resources, and boosting agricultural productivity, particularly in areas affected by climate variability (Mahmoud and Alazba, 2015; Tiwari et al., 2018; Ziadat et al., 2006). Rainwater harvesting systems are generally categorized into three primary types: in situ techniques that conserve soil moisture, techniques for channeling surface runoff to irrigate crops within a field, and systems designed to gather and store runoff from rooftops or land surfaces into designated containers for both household and farming uses (Falkenmark & Rockström, 2004). Similarly, RWH refers to the process of collecting and storing surface runoff to meet the water demands for household, agricultural, and environmental purposes (Mouhoumed et al., 2024). Beyond augmenting the water supply during arid periods, RWH also aids in flood control and groundwater recharge. Furthermore, the capture and storage of rainwater runoff can mitigate the

doi:10.6342/NTU202503692

limitations associated with the exclusive reliance on rain-fed agriculture in regions lacking irrigation infrastructure (de Winnaar et al., 2007).

RWH techniques have been tailored to accommodate diverse geographical and climatic conditions worldwide. In India, traditional methods such as ponds and tanks have been incorporated into managed aquifer recharge initiatives (Yadav et al. 2022). Similarly, the ridge-furrow RWH technique has been utilized in China as a method for farming water collection. This involves constructing ridges, often covered with a plastic film to boost runoff and minimize infiltration and evaporation, alongside furrows where crops are grown. This setup facilitates effective rainwater collection and enhances soil moisture, thereby alleviating the consequences of drought (Sun et al., 2023; Zhou et al., 2012). Additionally, various RWH methods are practiced in Sri Lanka, ranging from traditional household techniques without dedicated infrastructure to conventional systems that utilize roof catchments and storage tanks. These include informal setups with small barrels and large-scale institutional systems that are supported by community and government initiatives. Notably, these approaches significantly contribute to enhancing household water security, particularly in remote regions (Vijitha et al. 2022).

Australia presented a strong example of large-scale RWH adoption. Nearly 34% of urban households have implemented rainwater harvesting systems, collectively capturing approximately 177 billion liters of water annually and approximately 9% of residential water consumption (Khan et al., 2021). In response to recurring droughts, multiple Australian states have introduced policies and financial incentives to promote the widespread use of RWH, particularly in regions with limited municipal supply (Chubaka et al., 2018). While global examples highlight the success and adaptability of RWH systems, African countries, including Zambia, face unique climatic and infrastructural challenges that necessitate localized approaches to RWH site identification.

doi:10.6342/NTU202503692

In Africa, RWH systems are gradually being considered as practical solutions to persistent water shortages, particularly in sub-Saharan nations where erratic rainfall and limited infrastructure pose severe challenges. Despite the application of various practices to preserve soil and water, the adoption of runoff storage-based RWH techniques remains limited (Rockström, 2000). In response, countries such as Kenya, Ethiopia, and Uganda have promoted small-scale RWH systems, such as roof catchments and surface tanks, to buffer against seasonal variability and drought (Mati et al., 2005). Conversely, large-scale implementation is often constrained by socioeconomic, technical, and policy barriers, underscoring the need for robust spatial tools to support site suitability assessment and long-term planning. In Zambia, although technologies such as rooftop collection systems, small dams, weirs, and boreholes exist in some areas, their adoption remains geographically limited (Handia et al., 2003). This highlights the need for broader integration and strategic scaling of RWH systems to strengthen the national water resource management.

2.3 Key Factors Influencing RWH Site Selection

2.3.1 Factors Considered in Previous Studies

Determining the ideal sites for RWH is crucial for ensuring the effectiveness and sustainability of these interventions. Prior to implementation, a thorough assessment of the physical, environmental, and socioeconomic parameters of the target area is essential to support long-term efficiency and successful incorporation of RWH systems into local water management strategies. Identifying potential locations not only enhances water availability and land productivity but also is essential in mitigating water scarcity and tackling environmental issues, especially in SARs.

doi:10.6342/NTU202503692

Identifying appropriate decision criteria and parameters remains a central challenge in MCDA for RWH, particularly given the increasing scope and complexity of these criteria in recent years (Mouhoumed et al. 2024b). The concept of employing specific physical parameters, such as LULC, soil type, slope, and drainage density, to determine potential sites for RWH was initially introduced in 1995 through the Integrated Mission for Sustainable Development (IMSD) initiative (Chowdhury & Paul, 2021; Mahamoud, 2024). In the literature, the selection of RWH sites has been broadened to incorporate physical, socioeconomic, and environmental factors. As noted by Kahinda et al. (2008), referring to the 2003 standards of the Food and Agriculture Organization (FAO), the determination of suitable RWH locations requires consideration of multiple factors, including topography, climate, hydrology, agronomic requirements, soil properties, and socioeconomic considerations.

Expanding upon this foundation, Rane et al. (2023) assessed suitable dam locations in the Ulhas River Basin in Western Maharashtra, India. The site selection process was based on a diverse set of criteria such as rainfall, curve number, drainage density, geological and geomorphological features, LULC, elevation, soil type, and proximity to critical infrastructure, including roads, rivers, and fault lines. Similarly, Mouhoumed et al. (2024b) conducted a study in the southern basin of Djibouti to map potential RWH sites for managed aquifer recharge (MAR). Their methodological framework incorporated a comprehensive range of indicators including LULC, drainage density, slope, soil texture, watershed area, NDVI, curve number, rainfall, geological characteristics, electrical conductivity, proximity to roads, settlements, and agricultural zones.

doi:10.6342/NTU202503692

2.3.2 Standard Precipitation Index (SPI)

SPI was developed to assess precipitation deficiencies across multiple temporal scales, facilitating the evaluation of drought impacts on diverse water resources (Chisanga et al., 2025). It has since become one of the most commonly utilized tools for assessing drought severity. Among the available drought indices, the SPI is considered the most extensively applied for detecting and characterizing climate-related drought conditions (Chisanga et al., 2025; WMO, 2012). It is crucial to recognize that the widespread use of SPI can be attributed to several significant advantages. First, it is computationally efficient and based on a straightforward methodological framework (Chisanga et al., 2025; Nam et al., 2015). Second, it effectively identified the onset, intensity, duration, and development of drought events. Third, its exclusive dependence on precipitation data makes it particularly useful in areas with scarce hydrometeorological data (Teuling et al., 2013; Chisanga et al., 2025). Koudahe et al. (2017) highlighted that one of the key advantages of the SPI method is its straightforwardness and flexibility for use over various time frames, as it depends only on precipitation data gathered during a designated period.

Several studies have highlighted the notable decline in rainfall across Africa (Koudahe et al. 2017). Consistent with these observations, Iradukunda et al. (2023) and Musonda et al. (2020) highlighted that Zambia is increasingly susceptible to drought because of the diminishing precipitation levels. Expanding on this, Chisanga et al. (2025) employed SPI to examine drought patterns in Zambia over the period 1981–2024. Through their examination, they uncovered a variety of drought conditions ranging from moderate to extreme over different periods. They also observed clear trends in the occurrence, intensity, and duration of these drought episodes.

doi:10.6342/NTU202503692

Despite growing concerns about climate variability, many studies on rainwater harvesting (RWH) site selection have yet to adequately incorporate climate index factors, thereby limiting their capacity to address the long-term impacts of climate change (B. A. Ahmad et al., 2024). The Standardized Precipitation Index (SPI), a well-established tool for monitoring drought conditions(WMO, 2012), remains underutilized within GIS-based multi-criteria decision analysis (MCDA) frameworks for identifying suitable RWH locations. This study Seeks RWH site selection techniques by incorporating SPI as a dynamic climatic factor, allowing for a more precise depiction of temporal precipitation changes and enhancing the overall reliability of spatial suitability evaluations. By including the SPI, the model's capacity to detect and prioritize areas susceptible to drought is improved, thus facilitating climate-adaptive and cost-efficient RWH planning. By integrating SPI with physical and socioeconomic elements, this method offers a more comprehensive and contextually appropriate assessment of site suitability, especially in areas frequently experiencing rainfall shortages.

2.4 GIS-Based MCDA for Identifying RWH Sites

Given the growing demand for affordable and time-efficient approaches to identifying potential locations for RWH interventions, Ammar et al. (2016)organized the methods typically utilized over the past 30 years to determine ideal places for RWH in regions characterized by arid to semi-arid climates into four principal categories. The first category emphasizes the integration of GIS with Remote Sensing (RS) technologies. Forzieri et al. (2008) used these techniques to identify ideal locations for both subsurface and surface RWH systems in Kidal and Mali. The second group integrated hydrological modeling using GIS and RS. In this context, de Winnaar et al. (2007) utilized this method to identify optimal sites for collecting runoff in South Africa, whereas Gupta et al. (1997) estimated potential RWH zones in Rajasthan, India, using a similar combination.

doi:10.6342/NTU202503692

The third group involved MCDA combined with hydrological modeling (HM), RS, and GIS. For example, Elewa et al. (2012) utilized this comprehensive approach to determine suitable runoff harvesting locations on Egypt's Sinai Peninsula. Similarly, Weerasinghe et al. (2011) evaluated the allocation of water-collecting storage in the São Francisco and Nile catchments in Brazil. The fourth category combined MCA with GIS and RS alone. Prominent instances include the research conducted by Al-Adamat et al. (2010), which utilized this approach to determine optimal places for RWH ponds in Jordan.

GIS-based MCDA has become an effective and widely adopted approach for collecting, managing, analyzing, and visualizing both spatial and non-spatial data to support informed and evidence-based decision making (Coskun & Musaoglu, 2004; Padmavathy et al., 1993). As stated by Al-Adamat et al. (2010), GIS, remote sensing, and HM techniques have been widely utilized to determine and evaluate potential sites for water-capturing projects within the framework of water resource planning. Among the different MCDA approaches, AHP is particularly notable for its robust ability to derive the relative importance of multiple assessment criteria. Approaches involving GIS, RS, and HM have been broadly adopted to determine ideal locations for water-harvesting schemes. In analyses utilizing GIS, decision-making processes frequently employ approaches such as Weighted Linear Combination (WLC) and Boolean operators to determine and rank viable sites based on various criteria (Al-Adamat et al., 2010).

In southeastern Botswana, a comparative study by Mosase et al. (2017) evaluated the effectiveness of both the conventional AHP and its fuzzy logic-enhanced version in identifying suitable sites for rainwater harvesting (RWH). Their findings demonstrated that the Fuzzy-AHP approach yielded superior results, offering greater precision in delineating suitable areas than the conventional AHP method. Similarly, Mouhoumed et

doi:10.6342/NTU202503692

al. (2024b) explored the feasibility of rainwater harvesting (RWH) in Djibouti's southeastern basin using a comprehensive decision-making framework. This framework integrates fuzzy AHP with the VIKOR method to evaluate and prioritize optimal RWH sites. Hassan et al. (2025) employed a GIS-based MCDM method to identify potential RWH zones in the Kerbala Desert region of Iraq.

Furthermore, Mouhoumed et al. (2023) assessed suitable sites for managed aquifer recharge (MAR) in Djibouti by utilizing a comprehensive method that integrated Fuzzy-AHP with TOPSIS. Tavakoli et al. (2025) introduced a comprehensive flood risk mapping strategy for South Khorasan, Iran, which integrates the Analytic Hierarchy Process–Weighted Linear Combination (AHP–WLC) with the Fuzzy Ordered Weighted Averaging (FOWA) method. This approach was utilized to map out areas at risk of flooding and to propose long-term solutions for reducing these risks. Similarly, Baalousha et al. (2023) conducted a comparative evaluation of AHP and Fuzzy-AHP methodologies to assess flood exposure risks in the arid regions of Qatar, employing these two frameworks to highlight their performance.

Despite the widespread application of integrated MCDA techniques, including AHP, Fuzzy-AHP, and MIF, in conjunction with TOPSIS or VIKOR for RWH site identification (Mouhoumed et al., 2023, 2024b; Rane et al., 2023), There is a considerable gap in research that quantitatively examines how effectively these methods' outputs align in terms of spatial distribution. Although change detection techniques have been extensively used to identify changes in time-series analyses of LULC (Kafi et al., 2014; Mahendra et al., 2024; Tahraoui & Kheddam, 2024; Usman et al., 2015), their application in the comparison of suitability maps generated through integrated MCDA approaches for RWH remains unexplored. Specifically, pixel-level comparison tools such as change detection

doi:10.6342/NTU202503692

have not been employed to evaluate categorical differences among MCDA-derived suitability outputs.

Confusion matrix analysis is a well-established method for assessing classification accuracy (Banko, 1998; Foody, 2001), it has not yet been used to examine the consistency between RWH suitability maps produced by different MCDA techniques. Additionally, although Spearman's rho coefficient is frequently used to evaluate the robustness and direction of consistent relationships between attributes (Ali & Al-Hameed, 2022), its application to pixel-based suitability scores extracted from the raster outputs of methods such as Fuzzy-AHP and TOPSIS is limited. For instance, Sazakli et al. (2007)utilized Spearman's rho to investigate the relationship between microbiological and chemical factors in rainwater collected in Greece. However, this method has not yet been used to evaluate spatial agreement in RWH suitability models. This study addresses these methodological gaps by employing the Compute Change Raster tool, confusion matrix analysis, and Spearman's rank correlation to systematically evaluate the spatial consistency between suitability maps generated using Fuzzy-AHP and TOPSIS. This approach provides a thorough framework for assessing the consistency and reliability of MCDM results in the selection of RWH sites.

doi:10.6342/NTU202503692

Chapter 3: Study Area and Data

3.1 Study Area

Zambia is a landlocked country situated in Southern Africa bordered by eight other nations: Zimbabwe, Tanzania, Mozambique, Namibia, the Democratic Republic of Congo, Angola, Botswana, and Malawi. Situated between latitudes of 8 °S and 18 °S and longitudes of 22 °E and 34 °E, the country experiences a wide range of climatic conditions. The amount of rainfall each year shows considerable variation, with the northern regions receiving an average of around 1,400 mm, while the southern areas get about 700 mm; Temperatures typically fluctuate from 15°C in the winter months to 30°C during the summer (Ghosh et al., 2024b)

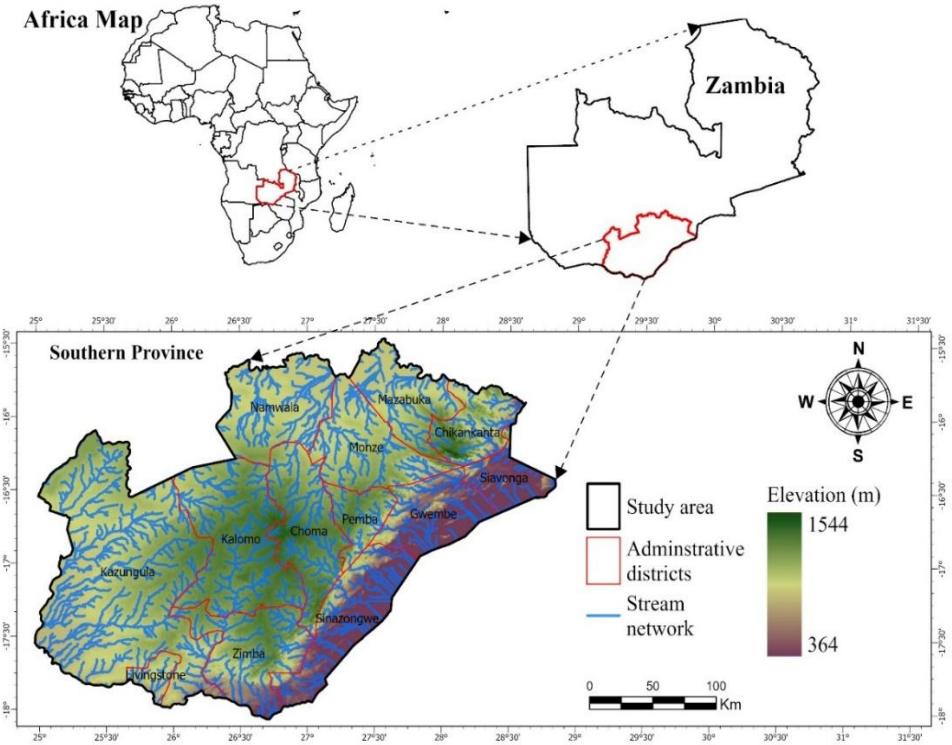

Figure 1: Study area

doi:10.6342/NTU202503692

This research focuses on the Southern Province of Zambia, as depicted in Figure 1, which is the third-largest province, covering approximately 67,517 square kilometers. This province is divided into 15 administrative districts: Chirundu, Chikankata, Choma, Gwembe, Kalomo, Itezhi-Tezhi, Kazungula, Monze, Mazabuka, Namwala, Livingstone, Pemba, Sinazongwe, Siavonga, and Zimba. The Central and Southern Provinces are the largest areas of commercial farmland in Zambia, contributing significantly to maize production. Nevertheless, the semi-arid climate and reliance on seasonal rainfall make these regions extremely vulnerable to drought, which is intensified by rainfall variability and broader climate fluctuations. The prevailing conditions significantly limit agricultural productivity and availability of water resources, resulting in diminished crop yields, heightened food insecurity, and economic losses, particularly among smallholder farmers who lack access to irrigation infrastructure. Furthermore, prolonged dry spells exacerbate the strain on limited water resources, jeopardizing rural livelihoods that rely heavily on rain-fed agriculture for both sustenance and income.

3.2 Data Source

This study utilized a variety of satellite-based datasets with a strong focus on the Climate Hazards Group InfraRed Precipitation with Station (CHIRPS) product. CHIRPS is widely acknowledged and used throughout Africa, especially in Southern Africa, including Zambia, for purposes such as monitoring droughts, analyzing rainfall trends, and conducting hydrological modeling. The integration of satellite imagery with data from ground-based stations, coupled with its high spatial and temporal resolution, makes it particularly valuable in areas where data are scarce. CHIRPS has been utilized to examine the temporal and spatial distribution of rainfall in South Kivu, Democratic Republic of Congo(Ahana et al., 2024), as well as to evaluate drought characteristics in Zambia through the use of the SPI (Chisanga et al., 2025). Furthermore, Chisanga et

doi:10.6342/NTU202503692

al.(2023) demonstrated that CHIRPS Version2 reliably estimates rainfall data using gauges for daily, monthly, and annual periods. Table 1 presents a concise summary of the datasets that were used in this research.

Table 1: Description of data sources

SN	Dataset	Source	Feature
1	Shapefile for Study area	Global Administrative Areas: https://gadm.org	Shapefile
2	Digital Elevation Model (DEM)	USGS Earth Explorer datasets portal: http://earthexplorer.usgs.gov/	30m x 30m
3	Land Use/Land cover (LULC)	Esri land use land cover 2023: https://livingatlas.arcgis.com/landcover	10m x 10m
4	Curve Number (CN)	global curve number datasets: https://doi.org/10.6084/m9.figshare.7756202	250m
5	Soil Texture	FAO: http://www.fao.org/soils-portal/soil-survey/soil-maps-and-databases	1:5.000.000
6	Rainfall spatial Data	CHIRPS Rainfall data: CHRS Data Portal (uci.edu)	0.05° x 0.05°
7	SPI data	CHIRPS:https://developers.google.com/earth-engine/datasets/catalog/UCSB-CHG_CHIRPS_PENTAD	0.05° x 0.05°
8	Road data	OpenStreetMap: https://www.openstreetmap.org	
9	Settlement	Open Buildings: https://sites.research.google/gr/open-buildings	Csv points

doi:10.6342/NTU202503692

3.3 Design of Expert-Based Pairwise Comparison Framework

Table 2 summarizes the backgrounds of the seven experts involved in the pairwise comparison process. The experts were chosen based on their academic qualifications and professional backgrounds in fields pertinent to the study, such as civil engineering, hydraulic engineering, environmental engineering, and water resources. Their educational backgrounds range from master's to doctoral degrees, with professional experience varying from less than five years to more than fifteen years.

Table 2: Profiles of Experts Involved in the Pairwise Comparison

No. of Ex	Expert ID	Background	Level of Education	Experience (Yrs)
1	Ex1	Civil Engineering	PhD	10~15
2	Ex2	Business Management	PhD	> 15
3	Ex3	Environmental Engineering	MSc	0~5
4	Ex4	Hydraulic Engineering	PhD	0~5
5	Ex5	Hydraulic Engineering	PhD	5~10
6	Ex6	Water Resources engineering	MSc	0~5
7	Ex7	Hydraulic Engineering	PhD	0~5

Table 3 displays Saaty’s essential scale for assessing relative importance, which was employed to create the pairwise comparison matrices. This scale, which spans from 1 (indicating equal importance) to 9 (indicating extreme importance), enables experts to quantitatively evaluate how one criterion compares in importance to another within the context of multi-criteria decision analysis (MCDA).

doi:10.6342/NTU202503692

Table 3: Saaty's Scale of relative importance

Linguistic Term	Scale of Importance
Equal importance	1
Equal to moderate importance	2
Moderately important	3
Moderate to strong importance	4
Important	5
Strong to very strong importance	6
Very strong importance	7
Very strong to the extreme importance	8
Extreme important	9

Table 4 to 10 present the individual pairwise comparison matrices provided by the seven experts. These matrices capture the experts' subjective evaluations of the relative importance of the selected criteria for rainwater harvesting site suitability. Each expert independently compared the criteria using Saaty's fundamental scale of relative importance, as outlined in Table 3. The resulting matrices form the basis for calculating both individual and aggregated criterion weights through the Fuzzy Analytic Hierarchy Process (FAHP), which is applied within the broader multi-criteria decision-making (MCDM) framework.

Table 4: Pairwise Comparison Matrix by Expert 1

Criteria	RF	CN	SL	El	DD	ST	LULC	PR	DSO	DS	PA	SPI
RF	1	2	2	2	1	3	4	8	7	6	6	9
CN	0.5	1	2	1	3	4	3	5	5	6	1	9
SL	0.5	0.5	1	3	1	2	1	3	2	7	7	8
El	0.5	1	0.33	1	2	1	4	4	2	7	7	7
DD	1	0.33	1	1	1	1	2	4	3	5	3	9
ST	0.33	0.25	0.5	1	1	1	2	3	2	2	5	5
LULC	0.25	0.33	1	0.25	0.5	0.5	1	3	2	2	3	8
PR	0.13	0.20	0.33	0.25	0.3	0.33	0.33	1	1	1	2	2
DSO	0.14	0.20	0.5	0.5	0.33	0.5	0.5	1	1	7	3	5
DS	0.17	0.17	0.14	0.14	0.2	0.5	0.5	1	0.14	1	2	2
PA	0.17	1.00	0.14	0.14	0.33	0.2	0.333	1	0.33	0.5	1	2
SPI	0.11	0.11	0.13	0.14	0.11	0.13	0.13	0.2	0.2	0.5	1	1

doi:10.6342/NTU202503692

Table 5: Pairwise Comparison Matrix by Expert 2

Criteria	RF	CN	SL	El	DD	ST	LU LC	PR	DSO	DS	PA	SPI
RF	1	3	5	6	6	4	5	7	6	8	9	7
CN	0.33	1	4	3	6	5	5	5	4	7	8	6
SL	0.20	0.25	1	0.33	5	4	4	4	3	6	7	5
El	0.17	0.33	3	1	4	3	3	3	2	5	6	4
DD	0.17	0.17	0.20	0.25	1	3	3	3	2	5	4	3
ST	0.25	0.20	0.25	0.33	0.33	1	3	2	2	4	5	3
LULC	0.20	0.20	0.25	0.33	0.33	0.33	1	2	2	4	5	3
PR	0.14	0.20	0.25	0.33	0.33	0.5	0.5	1	0.5	4	4	0.5
DSO	0.17	0.25	0.33	0.50	0.5	0.5	0.5	2	1	3	4	2
DS	0.13	0.14	0.17	0.20	0.2	0.25	0.25	0.3	0.33	1	3	0.33
PA	0.11	0.13	0.14	0.17	0.25	0.2	0.2	0.3	0.25	0.33	1	0.33
SPI	0.14	0.17	0.2	0.25	0.33	0.33	0.33	0.5	0.5	3	3	1

Table 6: Pairwise Comparison Matrix by Expert 3

Criteria	RF	CN	SL	El	DD	ST	LULC	PR	DSO	DS	PA	SPI
RF	1	3	5	3	5	7	7	7	7	7	7	1
CN	0.33	1	3	3	5	5	3	5	5	5	5	1
SL	0.2	0.33	1	1	1	3	1	3	5	3	3	0.33
El	0.33	0.33	1	1	3	5	3	3	5	5	3	0.33
DD	0.2	0.2	1	0.33	1	0.33	1	1	1	1	1	0.14
ST	0.14	0.2	0.33	0.2	3	1	3	1	1	1	1	0.2
LULC	0.14	0.33	1	0.33	1	0.33	1	3	1	0.33	3	0.2
PR	0.14	0.2	0.3	0.3	1	1	0.33	1	3	3	1	0.2
DSO	0.14	0.2	0.2	0.2	1	1	1	0.33	1	0.33	1	0.20
DS	0.14	0.2	0.3	0.2	1	1	3	0.3	3	1	3	0.2
PA	0.14	0.2	0.3	0.3	1	1	0.33	1	1	0.3	1	0.2
SPI	1	1	3	3	7	5	5	5	5	5	5	1

Table 7: Pairwise Comparison Matrix by Expert 4

Factors	Rf	CN	SL	El	DD	ST	LULC	PR	DR	DS	PA	SPI
Rf	1	3.00	3.00	3.00	3.00	3.00	4.00	4.00	3.00	4.00	4.00	2.00
CN	0.33	1.00	0.33	0.50	0.25	2.00	2.00	3.00	0.50	3.00	3.00	0.33
SL	0.33	3.00	1.00	2.00	0.33	2.00	3.00	4.00	0.50	4.00	4.00	0.50
El	0.33	2.00	0.50	1.00	0.33	0.33	2.00	2.00	0.33	3.00	3.00	0.50
DD	0.33	4.00	3.00	3.00	1.00	2.00	3.00	4.00	2.00	4.00	3.00	0.50
ST	0.33	0.50	0.50	3.00	0.50	1.00	2.00	3.00	0.50	2.00	0.25	0.50
LULC	0.25	0.50	0.33	0.50	0.33	0.50	1.00	3.00	0.50	2.00	0.50	0.33

doi:10.6342/NTU202503692

PR	0.25	0.33	0.25	0.50	0.25	0.33	0.33	1.00	0.25	0.50	0.50	0.33
DSO	0.33	2.00	2.00	3.00	0.50	2.00	2.00	4.00	1.00	2.00	3.00	0.50
DS	0.25	0.33	0.25	0.33	0.25	0.50	0.50	2.00	0.50	1.00	2.00	0.50
PA	0.25	0.33	0.25	0.33	0.33	4.00	2.00	2.00	0.33	0.50	1.00	0.25
SPI	0.5	3	2	2	2	3	3	2	2	2	4	1

Table 8: Pairwise Comparison Matrix by Expert 5

Criteria	RF	CN	SL	El	DD	ST	LULC	PR	DSO	DS	PA	SPI
RF	1	3.00	3	5	3	3	3	7	5	7	5	3
CN	0.33	1	3	3	1	1	1	5	3	5	3	1
SL	0.33	0.33	1	3	1	1	0.33	3	1	3	1	0.33
El	0.2	0.33	0.33	1	0.33	0.22	0.33	1	0.33	1	0.33	0.22
DD	0.33	1	1	3	1	1	1	3	5	3	3	1
ST	0.33	1	1	5	1	1	3	5	3	5	3	3
LULC	0.33	1	3	3	1	0.33	1	5	3	5	1	0.33
PR	0.14	0.22	0.33	1	0.33	0.2	0.2	1	0.33	1	0.3	0.33
DSO	0.14	0.33	1	3	0.2	0.33	0.33	3	1	3	1	0.33
DS	0.14	0.22	0.33	1	0.33	0.2	0.2	1	0.33	1	0.3	0.2
PA	0.2	0.33	1	3	0.33	0.33	1	3	1	3	1	0.33
SPI	0.33	1	3	5	1	0.33	3	3	3	5	3	1

Table 9: Pairwise Comparison Matrix by Expert 6

Criteria	RF	CN	SL	El	DD	ST	LULC	PR	DSO	DS	PA	SPI
RF	1	2	4	3	2	3	4	5	4	6	5	3
CN	0.5	1	2	3	2	3	2	6	5	6	4	3
SL	0.25	0.50	1	2	2	2	2	4	4	3	5	4
El	0.33	0.33	0.50	1	0.5	0.3	0.5	2	3	4	3	2
DD	0.5	0.50	0.50	2.00	1	0.5	2	3	4	3	2	5
ST	0.33	0.33	0.50	3.03	2.00	1	3	4	3	5	5	3
LULC	0.25	0.50	0.50	2.00	0.50	0.33	1	4	3	4	3	4
PR	0.2	0.17	0.25	0.50	0.33	0.25	0.25	1	0.33	3	0.3	0.5
DSO	0.25	0.20	0.25	0.33	0.25	0.33	0.33	3.00	1	2	3	0.5
DS	0.17	0.17	0.33	0.25	0.33	0.20	0.25	0.33	0.50	1	1	0.5
PA	0.2	0.25	0.20	0.33	0.50	0.20	0.33	3.00	0.33	2.00	1	0.33
SPI	0.33	0.33	0.25	0.5	0.2	0.3	0.25	2	2	2	3	1

doi:10.6342/NTU202503692

Table 10: Pairwise Comparison Matrix by Expert 7

Criteria	RF	CN	SL	EL	DD	ST	LULC	PR	DSO	DS	PA	SPI
RF	1	5	3	9	7	6	8	8	8	9	9	4
CN	0.2	1	0.33	8	5	4	6	6	6	7	7	0.33
SL	0.3	3	1	9	6	5	7	7	7	8	8	0.5
El	0.1	0.13	0.11	1	0.2	0.17	0.25	0.25	0.25	0.33	0.33	0.14
DD	0.1	0.2	0.17	5	1	0.5	3	3	3	4	4	0.25
ST	0.2	0.25	0.2	6	2	1	4	4	4	5	5	0.33
LULC	0.1	0.17	0.14	4	0.3	0.25	1	2	2	3	3	0.2
PR	0.1	0.17	0.14	4	0.3	0.25	0.5	1	1	2	2	0.17
DSO	0.1	0.17	0.14	4	0.3	0.25	0.5	1	1	2	2	0.17
DS	0.1	0.14	0.13	3	0.3	0.2	0.33	0.5	0.5	1	1	0.14
PA	0.1	0.14	0.13	3	0.3	0.2	0.33	0.5	0.5	1	1	0.14
SPI	0.3	3	2	7	4	3	5	6	6	7	7	1

3.3 Preparation of Thematic Layers

As indicated in Table 11, 12 criteria were employed to identify ideal RWH locations. Eleven of these factors were determined through a comprehensive assessment of relevant studies, while the remaining factor, The Standardized Precipitation Index (SPI) was included due to its crucial function in evaluating rainfall shortages, determining drought intensity, and pinpointing regions prone to drought conditions. The inclusion of SPI enhances the analytical rigor of this study by integrating a climatic indicator that facilitates sustainable site identification.

These 12 criteria were categorized into three main categories: physical, environmental, and socioeconomic factors. Physical criteria including elevation, slope, LULC, drainage density, soil texture, and Environmental factors are rainfall, curve number, and the Standardized Precipitation Index (SPI). Socioeconomic factors include proximity to farming regions, distance from populated areas, proximity to roads, and proximity to rivers. The subsequent sections offer an in-depth analysis of each parameter.

doi:10.6342/NTU202503692

Table 11: Selected Criteria for RWH Site Selection with References

Cluster	Criteria	ID	Stand-Function	Membership Bound		Reference
				Low	High	
1	Drainage Density	DD	ILFM	0	0.51	(Mouhoumed et al., 2023), (Matomela et al., 2020), (Adham et al., 2016), (Karakuş & Yıldız, 2022), (Ahmed et al., 2023), (Moumane et al., 2024), (Meghanadh et al., 2022), (R. Ahmad et al., 2024), (Al-Hasani et al., 2023).
2	Curve Number	CN	ILFM	60	94.0	(Mouhoumed et al., 2023), (Mahmoud et al., 2016), (de Winnaar et al., 2007), (Meghanadh et al., 2022)
3	Rainfall	RF	ILFM	887	2029	(Al-Adamat, 2008), (Mouhoumed et al., 2023), (Al-adamat et al., 2012), (Al-Adamat et al., 2010), (Mahmoud et al., 2016), (Mouhoumed et al., 2024b), (Adham et al., 2016), (Faisal & Abdaki, 2021), (Karakuş & Yıldız, 2022), (Ahmed et al., 2023), (Mahmoud & Alazba, 2015), (Moumane et al., 2024), (R. Ahmad et al., 2024), (Al-Hasani et al., 2023).
4	Land Use Land Cover	LULC	SW	-	-	(Al-Adamat, 2008), (Wu et al., 2018), (Mahmoud et al., 2016), (Mouhoumed et al., 2024b), (Faisal & Abdaki, 2021), (Karakuş & Yıldız, 2022), (Ahmed et al., 2023), (Mahmoud & Alazba, 2015), (Moumane et al., 2024), (Meghanadh et al., 2022), (Maina & Raude, 2016), (R. Ahmad et al., 2024), (Al-Hasani et al., 2023).
5	Slope	SP	DLFM	67.96	0.0	(Mouhoumed et al., 2023), (Wu et al., 2018), (Matomela et al., 2020), (Al-Adamat et al., 2010), (Mahmoud et al., 2016), (Mouhoumed et al., 2024b), (de Winnaar et al., 2007), (Ramya & Devadas, 2019), (Adham et al., 2016), (Faisal & Abdaki, 2021), (Karakuş & Yıldız, 2022), (Ahmed et al., 2023), (Mahmoud & Alazba, 2015), (Moumane et al., 2024), (Meghanadh et al., 2022), (Maina & Raude, 2016), (R. Ahmad et al., 2024), (Al-Hasani et al., 2023).
6	Elevation	EL	DLFM	1544	365	(Al-adamat et al., 2012), (Ramya & Devadas, 2019), (Faisal & Abdaki, 2021), (Karakuş & Yıldız, 2022)
7	Distance to stream Or	DR	DLFM	10481	0	(Al-Adamat, 2008) (Ramya & Devadas, 2019)
8	Proximity to Agriculture	PA	DLFM	45221.8	250	(Wu et al., 2018), (Mouhoumed et al., 2024b), (de Winnaar et al., 2007), (Ramya & Devadas, 2019), (Faisal & Abdaki, 2021), (Ahmed et al., 2023).
9	Distance to Settlement	DS	DLFM	62219.9	250	(Matomela et al., 2020), (Al-Adamat et al., 2010), (Mouhoumed et al., 2024b), (de Winnaar et al., 2007), (Ramya & Devadas, 2019), (Adham et al., 2016), (Faisal & Abdaki, 2021), (Karakuş & Yıldız, 2022), (Ahmed et al., 2023).
10	Proximity to Roads	PR	DLFM	60651.3	250	(Wu et al., 2018), (Matomela et al., 2020), (Mouhoumed et al., 2024b), (Ramya & Devadas, 2019), (Faisal & Abdaki, 2021), (Karakuş & Yıldız, 2022), (Ahmed et al., 2023).
11	Soil Texture	ST	SW	-	-	(Al-Adamat, 2008), (Mouhoumed et al., 2023),(Wu et al., 2018), (Al-adamat et al., 2012), (Al-Adamat et al., 2010), (Mahmoud et al., 2016), (Mouhoumed et al., 2024b), (Ramya & Devadas, 2019), (Adham et al., 2016), (Faisal & Abdaki, 2021), (Karakuş & Yıldız, 2022), (Ahmed et al., 2023), (Mahmoud & Alazba, 2015), (Moumane et al., 2024), (Meghanadh et al., 2022), (Maina & Raude, 2016), (R. Ahmad et al., 2024), (Al-Hasani et al., 2023).
12	Standard Precipitation Index	SPI	DLFM	2.22	-1.63	This study introduces a novel criterion that has not been utilized in previous research on RWH site selection

doi:10.6342/NTU202503692

Where ILFM represents increasing linear fuzzy membership, DLFM is abbreviated decreasing linear fuzzy membership and SW is stepwise function for presenting ST and LULC scores.

3.3.1 Physical Factors

3.3.1.1 Elevation

The Digital Elevation Model (DEM) represents a raster dataset that conveys the Earth's surface elevation, typically derived from topographic maps, satellite imagery, or aerial photographs (Al-Hasani, 2023). In this study, the DEM was sourced from the NASA Shuttle Radar Topography Mission (SRTM) with a resolution of 30 m, offering elevation information for the study region, as illustrated in Figure 2. Elevation is crucial in choosing locations for RWH, as it greatly influences the rate of surface runoff, the flow's direction, and the regions where water accumulates. Areas at lower elevations are generally more advantageous for RWH because they promote the accumulation of runoff, making them ideal for installing RWH structures. In contrast, regions at higher elevations tend to produce quicker runoff and have lower storage capacity. Consequently, lower elevation areas usually receive higher suitability ratings because of their enhanced ability to capture surface runoff and reduce the flow speed.

doi:10.6342/NTU202503692

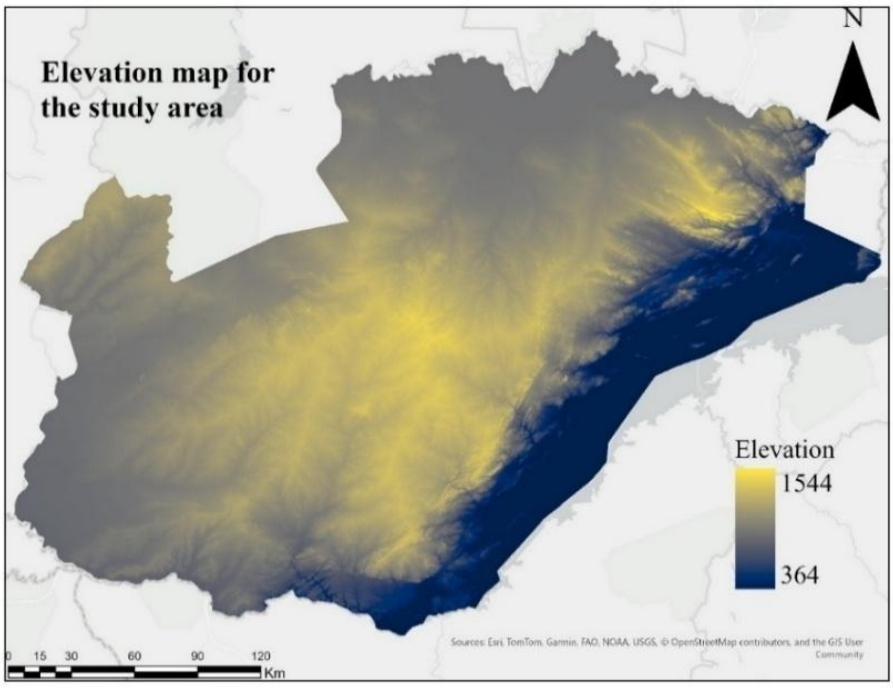

Figure 2: Elevation map

3.3.1.2 Slope

The slope is an essential physical factor that greatly influences the effectiveness of RWH systems. This affects the speed of surface runoff, the ability to retain water, and the feasibility of constructing RWH infrastructure. Gently to moderately sloped areas are typically more favorable for rainwater harvesting (RWH) because they slow runoff, improve groundwater absorption, and reduce soil erosion. In contrast, steep slopes increase the speed of surface runoff, decrease water retention, and pose construction difficulties owing to their higher gradient and erosion risk. This study involved acquiring slope information from the DEM using raster-based spatial analysis performed in ArcGIS Pro. As shown in Figure 3, the spatial arrangement of the slopes varied throughout the study area. Regions with gentler slopes are more favorable for RWH than steeper areas, as they provide optimal conditions for capturing runoff and enhancing water infiltration.

doi:10.6342/NTU202503692

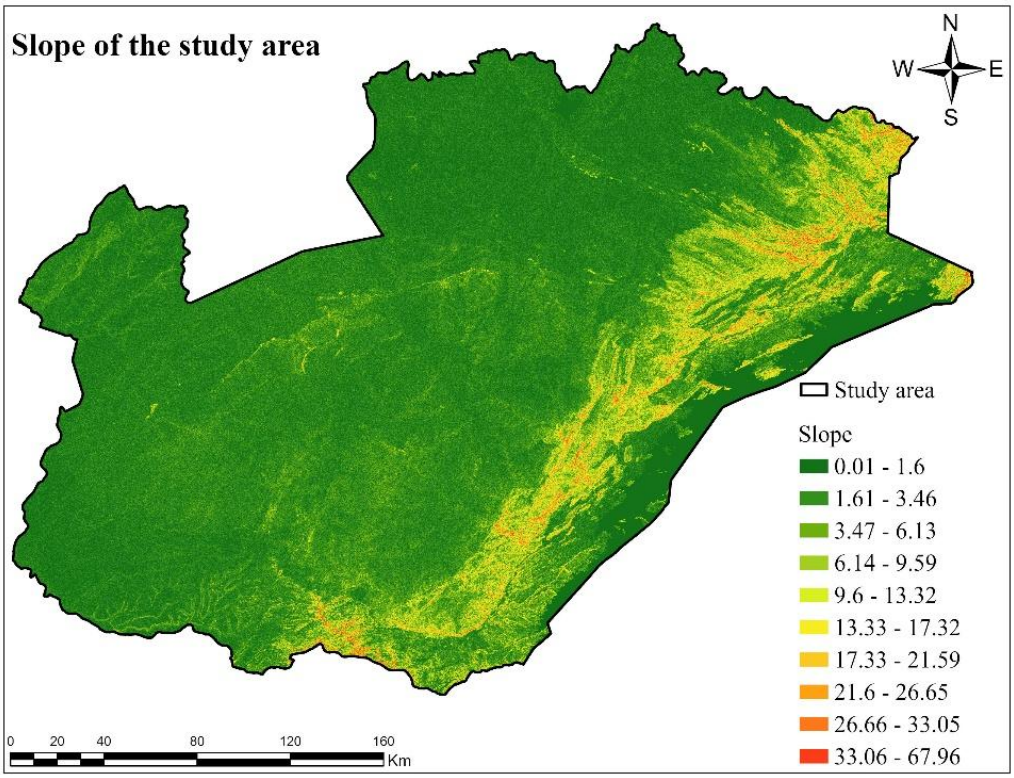

Figure 3: Slope map of the study area

3.3.1.3 Soil texture

Soil texture is essential in determining appropriate locations for rainwater harvesting (RWH) because it affects infiltration rates, the ability to retain water, and the generation of runoff. As noted by Al-Hasani et al. (2023) and Sayl et al. (2022), soils that possess a high capacity for retaining water, such as those rich in clay, are typically more suitable for RWH due to their low porosity and slow drainage characteristics. In contrast, sandy soil, which is known for its high permeability and rapid drainage, is generally less capable of holding water.

doi:10.6342/NTU202503692

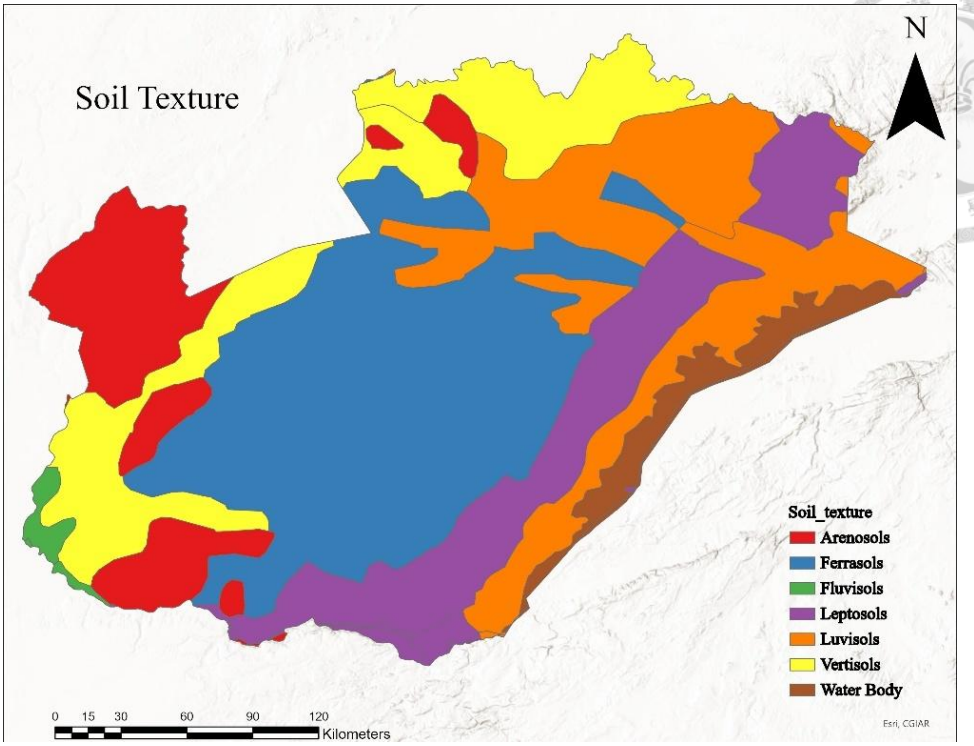

Figure 4: Soil texture map

Figure 4 illustrates the spatial arrangement of soil texture across the study region, as categorized by the FAO Harmonized World Soil Database. According to this classification, Ferrasols, Luvisols, and Fluvisols are deemed to have moderate drainage, while Arenosols are categorized as having excessive drainage. In contrast, Vertisols and Leptosols are recognized as having poor and imperfect drainage, respectively. Suitability scores were determined based on these hydrological characteristics, with the highest scores given to imperfectly drained soils due to their excellent water retention ability as shown in Figure *5*.

doi:10.6342/NTU202503692

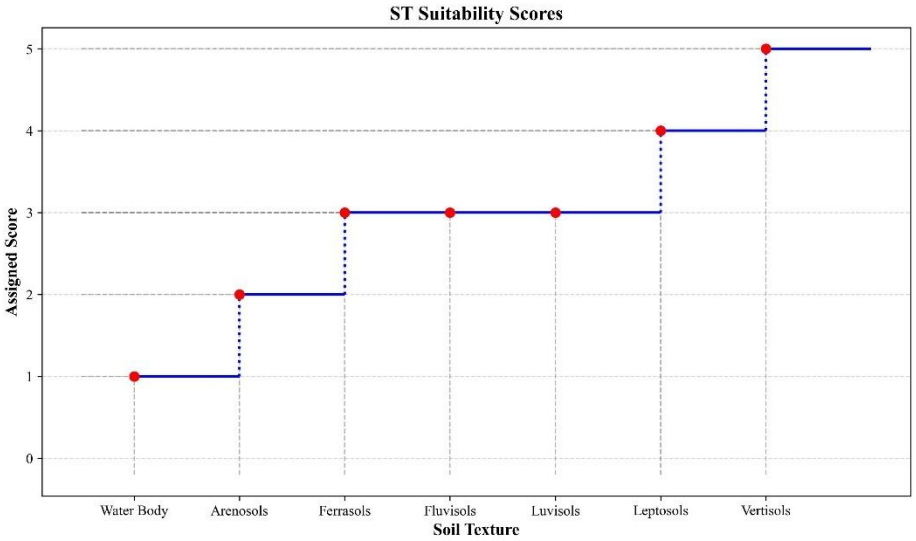

Figure 5: Assigned RWH suitability scores based on soil texture

3.3.1.4 Drainage Density

Drainage density (DD) is characterized by the cumulative length of stream channels within a given watershed area, reflecting the extent to which the landscape is dissected and how efficiently the surface runoff is directed to the basin outlet. Within the realm of RWH, DD acts as a crucial physical factor that affects the concentration of runoff and hydrological response of the catchment area. Areas with a high density of drainage systems are often considered ideal for rainwater harvesting (RWH) site selection. This is because their extensive stream networks enable efficient collection and storage of concentrated surface runoff. Conversely, Regions with a high concentration of drainage systems are often considered optimal for selecting rainwater harvesting (RWH) sites. This is because of their extensive network of streams, which facilitates the effective collection and storage of concentrated surface runoff (Ahmed et al., 2023; Matomela et al., 2020).

doi:10.6342/NTU202503692

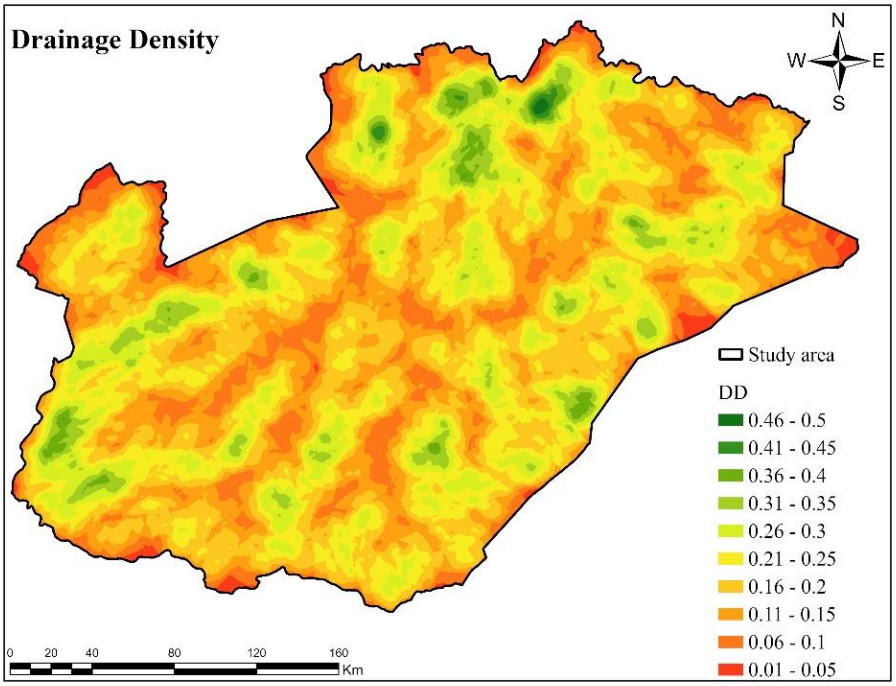

Figure 6:Drainage density map

Figure 6 illustrates the drainage density obtained from the stream networks, which were identified using a DEM by utilizing the line density in ArcGIS Pro. For the suitability analysis, drainage density was categorized according to its relative suitability for RWH. Areas with a highly dense network are considered more suitable, indicating their greater potential for effective surface runoff collection, whereas areas with a low stream network density are less preferable.

3.3.1.5 Land Use Land Cover (LULC)

Land surface conditions significantly affect surface runoff, infiltration, and water retention, with LULC being a key factor in these processes. LULC focuses on how water interacts with the surface. Natural vegetation, such as forest areas or grasslands, promotes water infiltration and reduces runoff velocity, trapping water streams due to the high permeability of the soil and the capacity for water retention of vegetation. However, land use related to human activities that influence landscape conditions, such as urban areas,

doi:10.6342/NTU202503692

impervious surfaces such as roads, and buildings, increase surface runoff, making them ideal places for rooftop water harvesting systems.

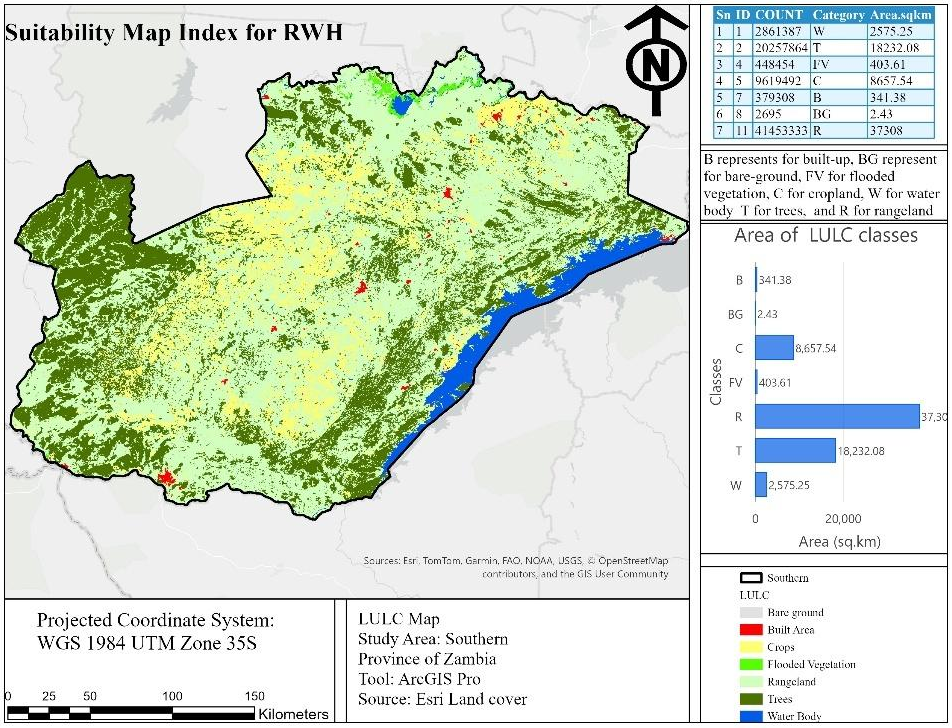

Figure 7: LULC classification map

According to the current study, the Esri Land Cover 2023 dataset was utilized to provide spatial LULC at a 10-meter resolution that contains seven classes, as illustrated in Figure *7*. For runoff harvesting, areas characterized by high surface runoff, such as bare ground, built-up, and rangelands zones, were considered more suitable, owing to their potential for efficient runoff collection. Forested areas, which exhibited lower runoff but higher infiltration capacity, were considered moderately suitable and assigned intermediate scores. Conversely, water bodies were considered inappropriate for runoff harvesting because they already possess ample water resources, as shown in Figure *8*.

doi:10.6342/NTU202503692

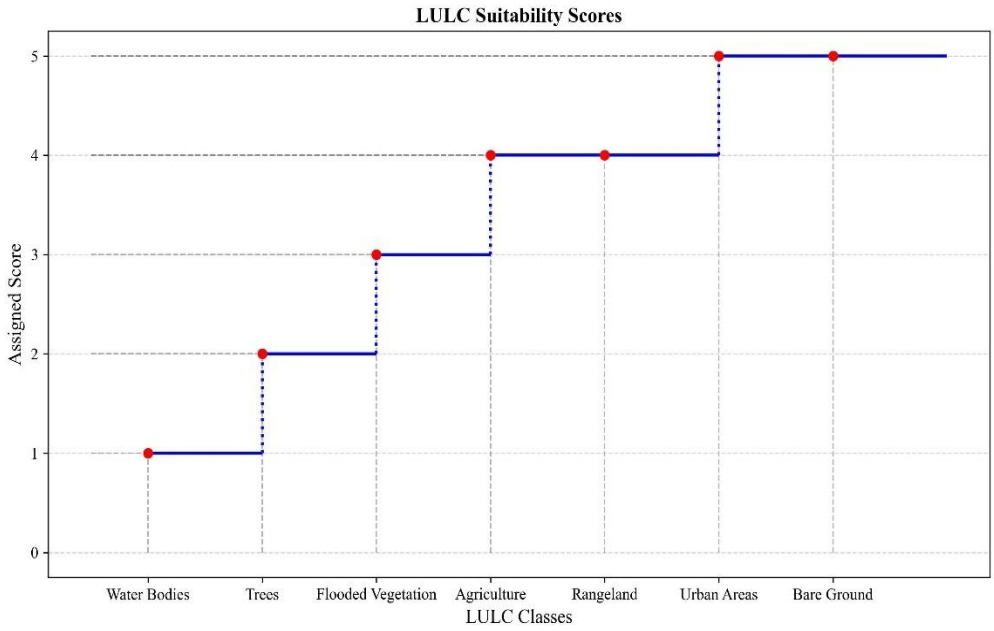

Figure 8: Stepwise function for LULC

3.3.2 Environmental Factors

3.3.2.1 Rainfall

Rainfall serves a crucial role in determining the best sites for RWH, as it is the main factor influencing runoff and greatly affects the volume of water that can be gathered in a specific location. The study utilized rainfall data obtained from CHIRPS, a high-resolution satellite dataset with a spatial resolution of 0.05°, which is available in raster format 2023, as depicted in Figure 9. The rainfall raster data were sorted into separate categories according to the spatial differences in the distribution of rainfall. Areas receiving higher rainfall were considered more suitable for RWH, whereas regions with lower rainfall were deemed less favorable.

doi:10.6342/NTU202503692

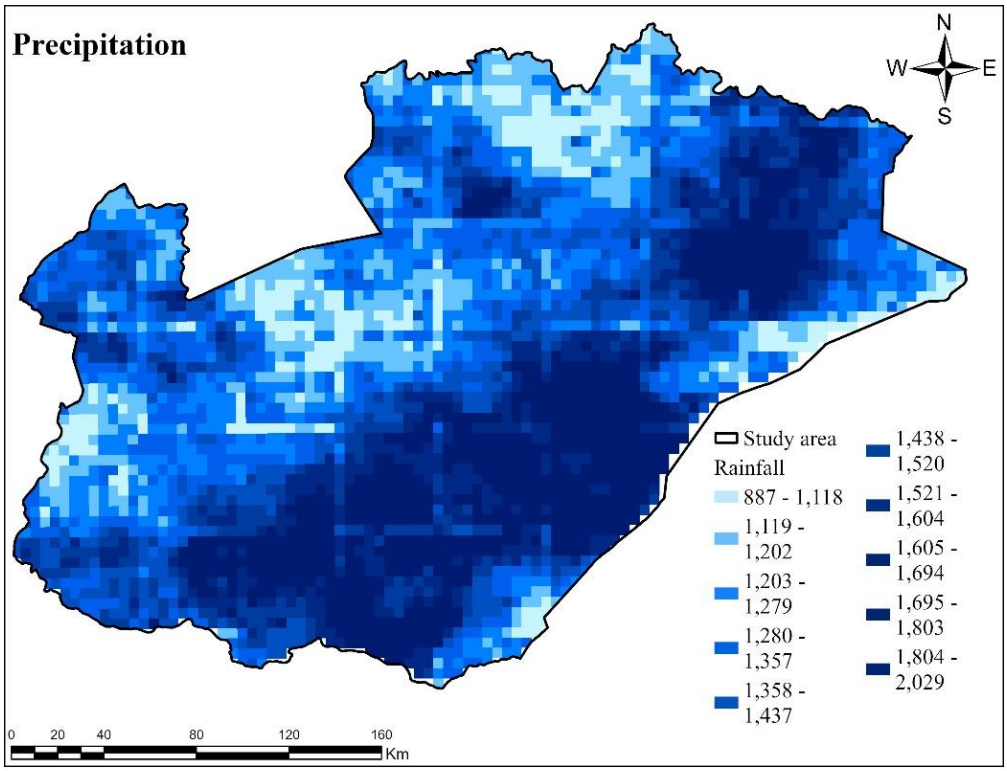

Figure 9: Map of the rainfall 2023

3.3.2.2 Curve Number (CN)

The CN serves as an indicator to assess the portion of rainfall expected to be converted into surface runoff, considering elements such as land utilization, soil attributes, and prevailing ground conditions. This serves as a crucial criterion for identifying regions with a greater likelihood of runoff, which is essential for selecting appropriate locations for RWH. In this study, CN values were obtained from a high-resolution (250-meter) global gridded dataset developed by Jaafar et al. (2019), as presented in Figure 10, which integrated land cover and soil data to generate spatially detailed runoff estimates. These values were subsequently classified into suitability categories, with higher CN values indicating greater surface runoff potential and thus considered more favorable for RWH. Conversely, areas with lower CN values, which were more likely to absorb water than generate runoff, were deemed less suitable for harvesting purposes.

doi:10.6342/NTU202503692

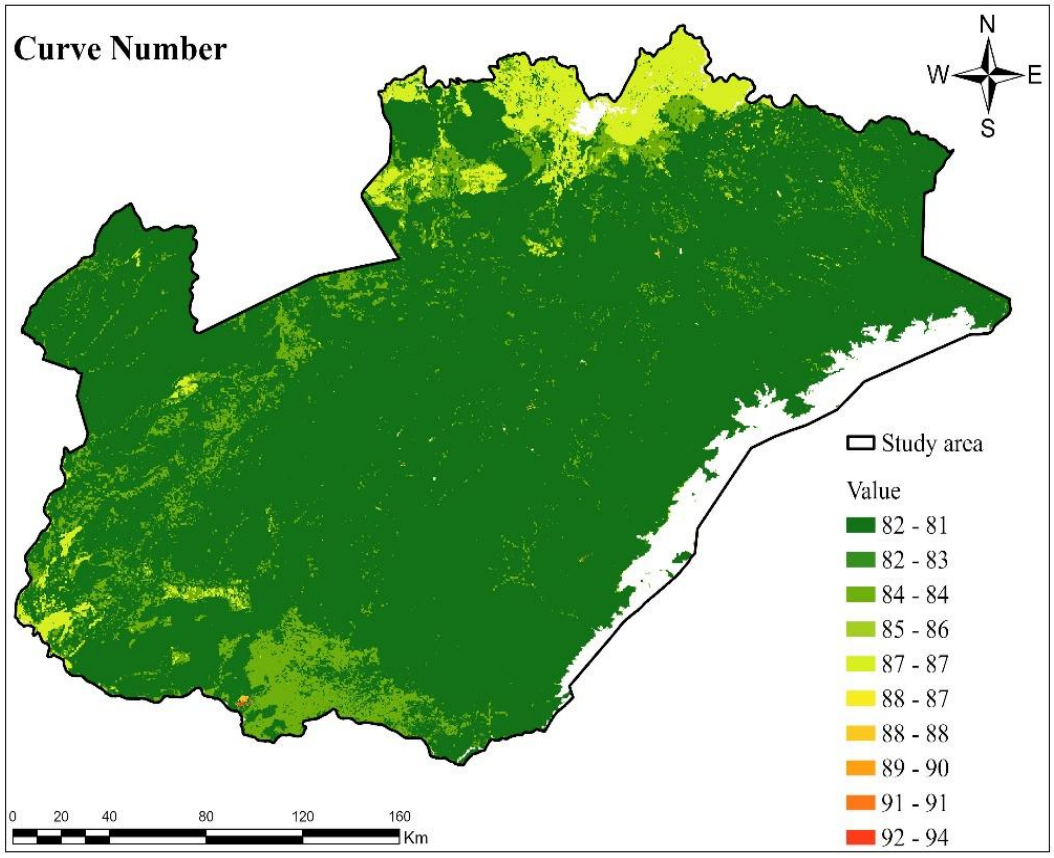

Figure 10: Curve number map

3.3.2.3 Standardized Precipitation Index (SPI)

SPI was determined using the approach outlined by McKee et al. (1993), which involves the normalization of precipitation data over a defined time period, as described in Equation (1). The SPI was calculated at a one-month scale (SPI-1) using 27 data points downloaded from CHIRPS rainfall across the study area, spanning from January 1990 to December 2023. SPI values can be either positive or negative, reflecting current climatic conditions, with positive values indicating better-than-normal conditions and negative values indicating the presence of dry or drought conditions. The classifications of drought and wetness intensity based on SPI values are summarized in Table 12. Subsequently, the

doi:10.6342/NTU202503692

obtained values were converted into spatial maps using ArcGIS Pro as shown in Figure 11. This was calculated using the following equation:

$$SPI = \frac{X-\bar{X}}{\sigma} \quad (1)$$

$$\sigma = \sqrt{\frac{\sum_{i=1}^{n}(x_i-\bar{x})^2}{n-1}} \quad (2)$$

where X is precipitation, $\overline{X}$ is the average precipitation, σ is the standard deviation of the precipitation and n is the number of data points

Table 12: Classification of drought conditions based on SPI ranges

SN	SPI values	Classification
1	2 and above	Extremely wet
2	1.5 to 1.99	Very wet
3	1.0 to 1.49	Moderately wet
4	-0.9 to 0.99	Nearly normal
5	-1.0 to -1.49	Moderately dry
6	-1.50 to -1.99	Severely dry
7	-2 and less	Extremely dry

doi:10.6342/NTU202503692

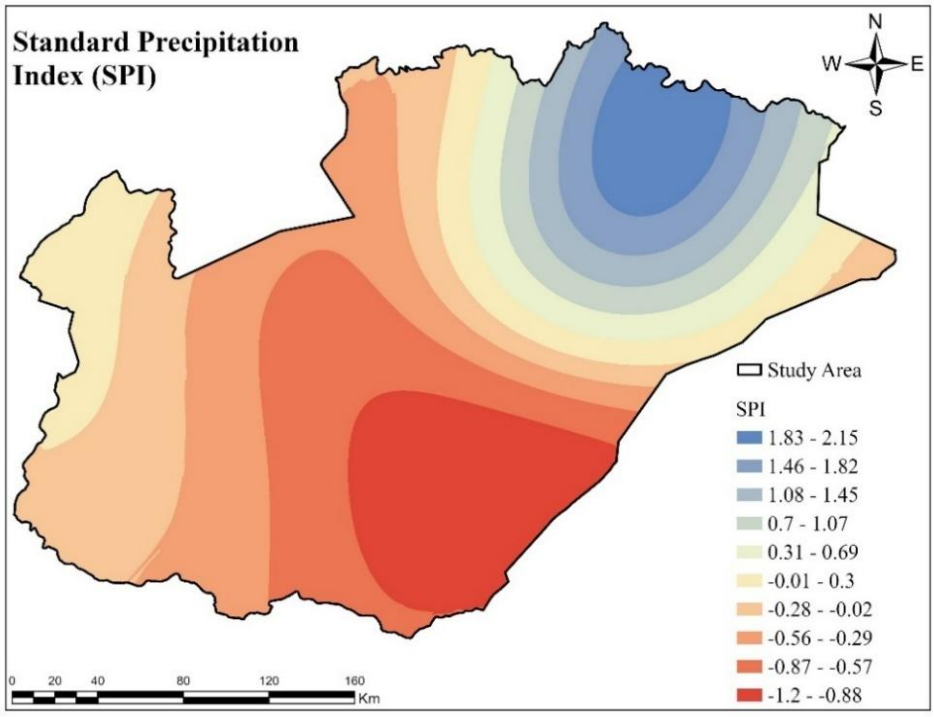

Figure 11: Standard precipitation index (SPI) map

3.3.3 Socioeconomic Factors

3.3.3.1 Proximity to Roads (PR)

This study employed road network data from OpenStreetMap to develop a proximity map through spatial analysis. The vector-based road data was buffered by 250 m to allow for potential future road development and prevent conflicts with the RWH infrastructure. was subsequently converted into a continuous raster surface using the Euclidean distance function to generate a proximity road (PR) raster, as shown in Figure 12. The generated raster was then reclassified into suitability classes, with areas in close proximity to roads considered more suitable for RWH implementation. Conversely, far-distance regions were considered less suitable.

doi:10.6342/NTU202503692

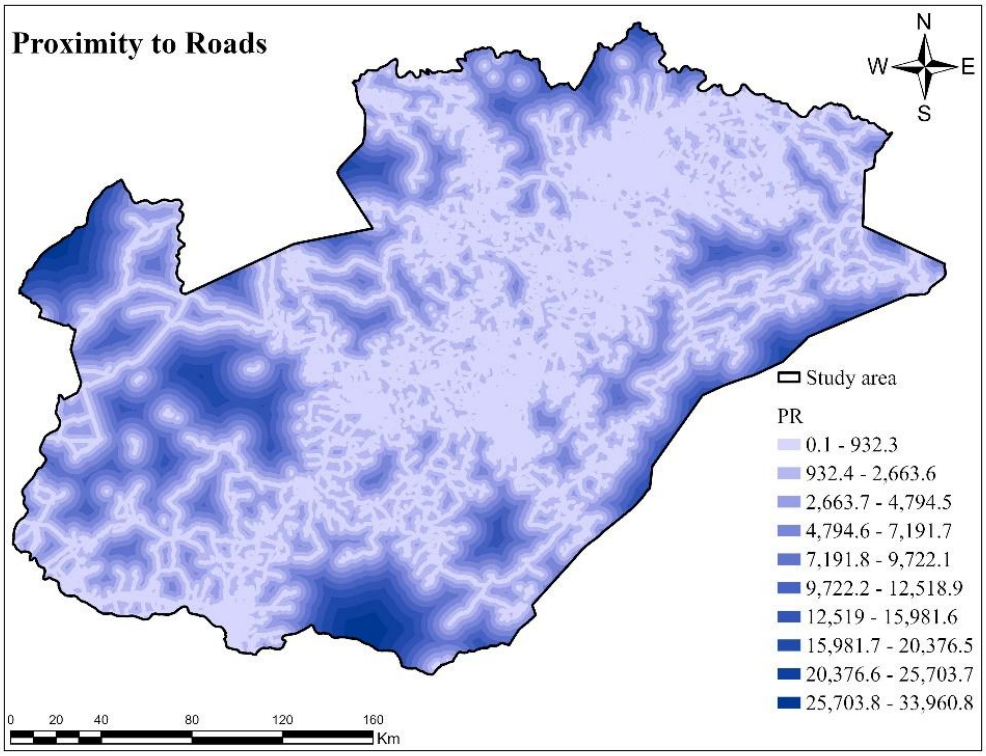

Figure 12: Proximity to roads map

3.3.3.2 Proximity to Agriculture (PA)

Proximity to agriculture (PA) refers to the distance between a given location and cultivated areas. This layer is derived from Esri Land Use/Land Cover (LULC) data by clipping agricultural areas as a separate layer and applying the Euclidean Distance tool, as shown in Figure 13. The output obtained was refined by using the study area's boundary shapefile to define the area of interest. The generated raster layer was subsequently reclassified into suitability classes based on its relative accessibility to the agricultural land. Locations closer to cultivated areas were considered more suitable for RWH implementation than those farther from croplands.

doi:10.6342/NTU202503692

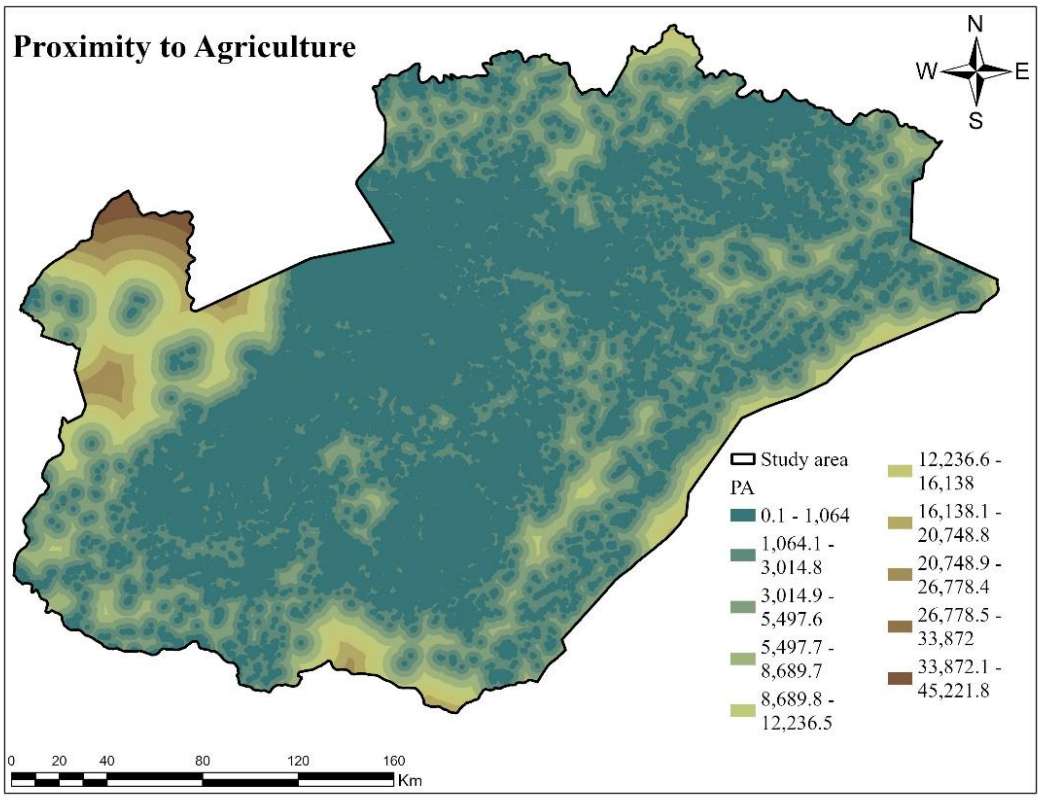

Figure 13:Proximity to agriculture map

3.3.3.3 Distance to Settlement (DS)

Distance to settlements (DS) layer is obtained from Open Buildings data in CSV point format (https://sites.research.google/gr/open-buildings/). In ArcGIS Pro 3.3, the Euclidean Distance tool was utilized to create a raster layer that indicated the distance from each pixel to the closest settlement. The raster was subsequently trimmed using the boundary shape file of the study area to delineate the area of interest, as illustrated in Figure 14. The resulting distance layer was classified into five suitability classes, with areas closer to settlements considered more favorable for rainwater harvesting (RWH) site selection. Conversely, areas located farther from the settlements were considered less suitable.

doi:10.6342/NTU202503692

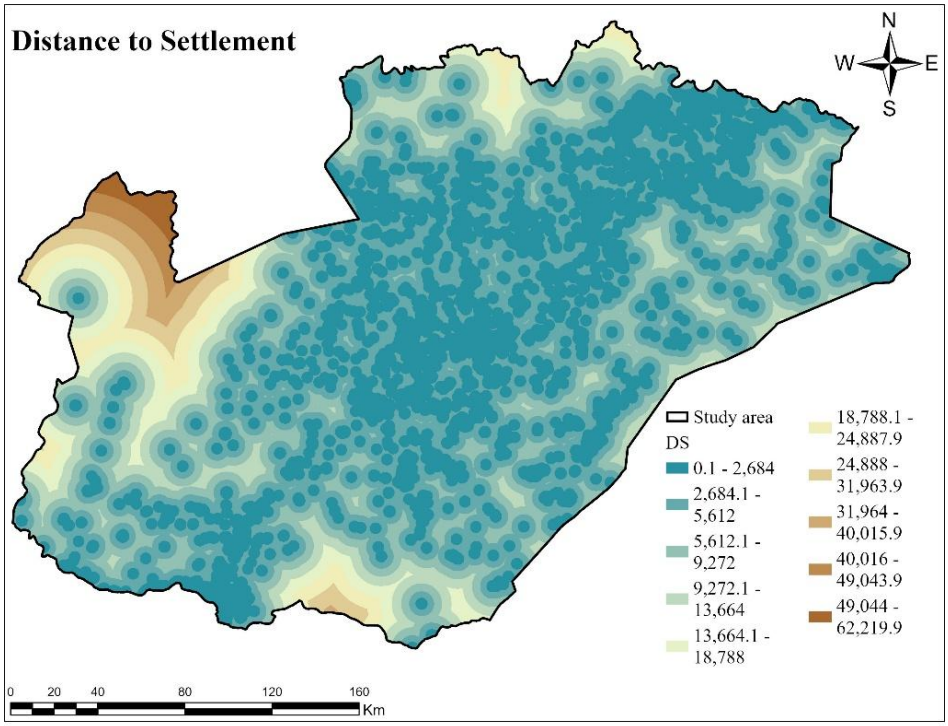

Figure 14:Distance to settlement map

3.3.3.4 Distance to Stream Order (DSO)

Distance to rivers (DR) is a crucial criterion in the selection of potential RWH locations, as it helps in identifying areas that are either favorable for capturing surface runoff or potentially vulnerable to erosion and flooding. Locations close to river channels often exhibit higher runoff accumulation, thereby increasing their hydrological viability for RWH. As illustrated in Figure 15, the DSO layer was created from a DEM by employing the Euclidean Distance tool to map a raster surface that indicates the closeness to the river network. Higher network areas are preferable for harvesting because of their high runoff potential, whereas lower network areas are less favorable.

doi:10.6342/NTU202503692

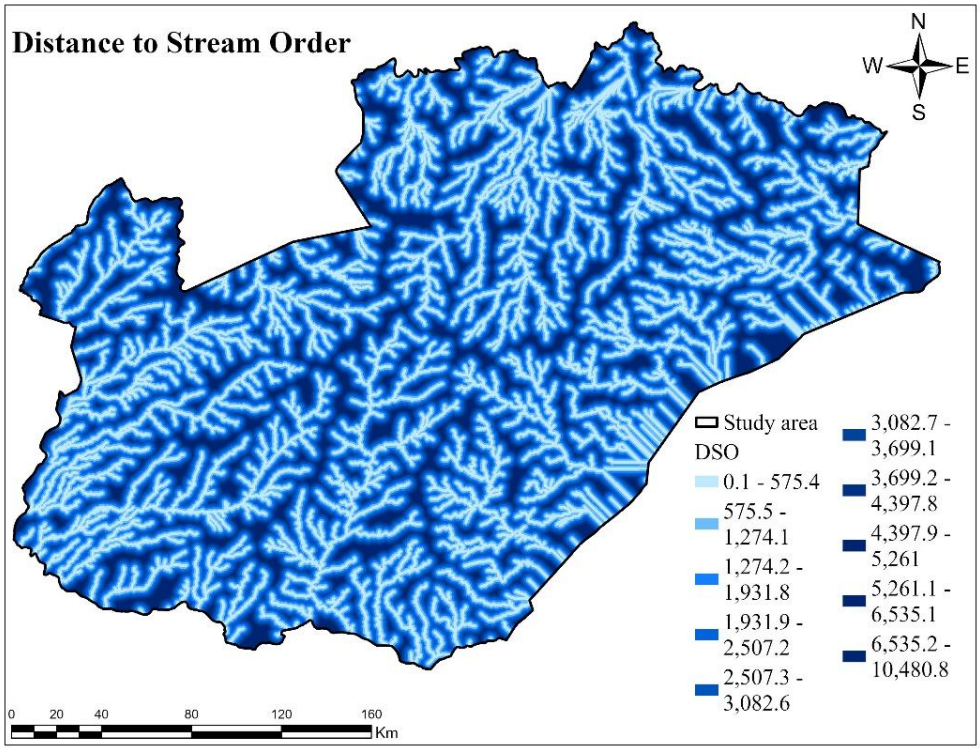

Figure 15:Distance to streams orders

3.4 Standardizing Decision Criteria

Standardization involves adjusting all parameters to a uniform scale to ensure that they are compatible with integration within GIS systems. In this study, a standardization technique was applied using a linear fuzzy membership function to represent both the increasing and decreasing relationships, as shown in Table 11. The normalized values were categorized into five suitability levels: unsuitable, low, moderate, high, and optimal, with corresponding scores ranging from 1 to 5 (Mouhoumed et al., 2023). Additionally, they were classified into 10 scales ranging from 1 to 10 (Wu et al., 2018). This study adopted a 1 to 5 scale as shown in Figure 16, where higher values were indicative of more favorable conditions, while lower values denoted less suitable areas. For instance, the most appropriate areas were given a score of 5, while highly appropriate areas received

doi:10.6342/NTU202503692

4, moderately appropriate areas of 3, less appropriate areas of 2, and inappropriate areas of 1.

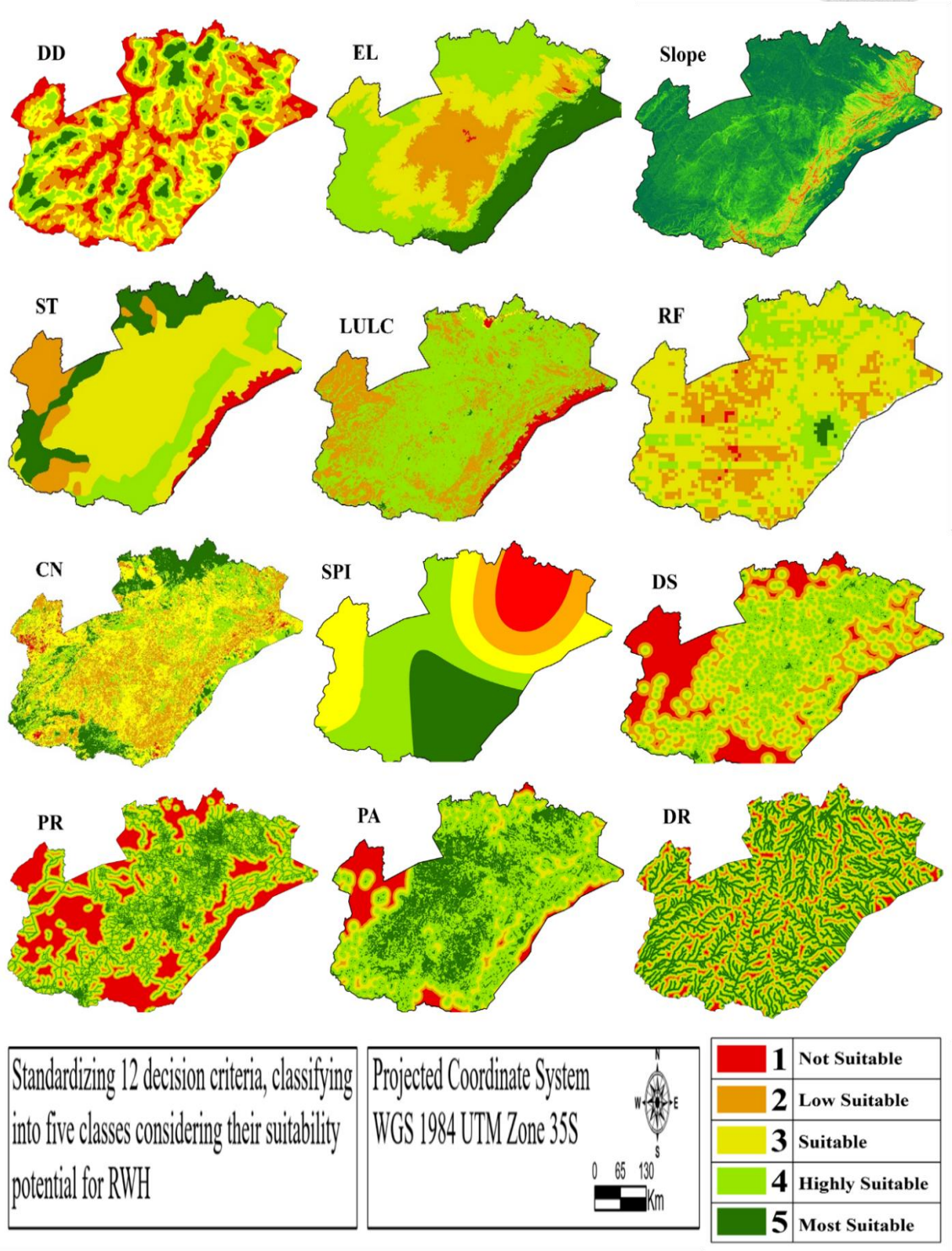

Figure 16: Standardizing decision criteria map

doi:10.6342/NTU202503692

Chapter 4: Methodology

4.1 Fuzzy Analytical Hierarchy Process (Fuzzy-AHP)

Fuzzy AHP was originally developed by ZADEH (1965), which incorporates fuzzy set theory to efficiently tackle the complexity and uncertainty found in environmental conditions and expert evaluations (Mouhoumed et al., 2023). Fuzzy AHP involves four fundamental steps: fuzzification of crisp or linguistic values, standardization and geometric mean calculations, normalization of weights, and defuzzification of fuzzy numbers. Each step is explained in the subsequent sections.

4.1.1 Constructing Fuzzy Pairwise Matrix

The initial step in applying Fuzzy-AHP involves constructing a fuzzy pairwise matrix, which facilitates the creation of a decision matrix that includes all pertinent parameters. As shown in Table 4~10, a group of seven experts participated in the pairwise comparison process, utilizing Saaty's scale of relative importance, as depicted Table 3.

$$\tilde{A} = \begin{bmatrix} C_{11} & C_{12} & \cdots & \dots & C_{1n} \\ C_{21} & C_{22} & \cdots & \dots & C_{2n} \\ \vdots & \vdots & \ddots & \cdots & \vdots \\ \vdots & \vdots & \cdots & \ddots & \vdots \\ C_{n1} & C_{n2} & \cdots & \dots & C_{nn} \end{bmatrix} \quad (3)$$

Where $\tilde{A}$ is a fuzzy pairwise comparison matrix, C_{ij} is the fuzzy comparison value between criterion i and criterion j and n is the total number of criteria (where $n = 12$ for this study)

doi:10.6342/NTU202503692

4.1.2 Consistency Ratio

To evaluate the reliability of expert assessments within the Fuzzy-AHP, an extra step was added to determine the Consistency Ratio (CR), as proposed by Saaty (1980) and detailed in Equation (4). This step was utilized to verify the uniformity of the weights assigned in pairwise comparisons, ensuring that the criteria weights were determined through a systematic process rather than arbitrarily.

$$CR = \frac{\lambda max - n}{RI(n-1)} \tag{4}$$

Where CR is for the consistency ratio, λmax is the maximum eigenvalue of the pairwise comparison matrix, n is the number of decision parameters, and RI is the random index (Table 13) (Velmurugan et al., 2011).

Table 13: RI of AHP

RI	0.58	0.9	1.12	1.24	1.32	1.41	1.45	1.49	1.51	1.58
Size of Matrix	3	4	5	6	7	8	9	10	11	12

If the calculated CR exceeds 0.1, it is necessary to reevaluate the assigned weights to ensure an acceptable level of consistency. Moreover, the AHP method was used to determine the CR. When the CR is within the acceptable range, the fuzzy AHP approach is applied.

4.1.3 Fuzzification of Crip Value of AHP

The procedure involves converting the crisp values in the AHP pairwise matrix into fuzzy numbers by determining the lower bound (l_{ij}), middle value (m_{ij}), and upper bound (u_{ij}), which represent the comparison of criterion i to criterion j. The crisp values and their

doi:10.6342/NTU202503692

reciprocals (Table 14), which are derived from linguistic terms, were established based on expert assessments of the criteria's relative importance.

Table 14: Saaty's Scale Used in AHP and Fuzzy-AHP Judgments

Linguistic Term	AHP Scale of Importance	Reciprocal AHP	Fuzzy-AHP Fuzzy-AHP TFN (l_{ij}, m_{ij}, u_{ij})	Reciprocal TFN $\left(1/u_{ij}, 1/m_{ij}, 1/l_{ij}\right)$
Equal importance	1	(1)	(1, 1, 1)	(1, 1, 1)
Equal to moderate importance	2	(1/2)	(1, 2, 3)	(1/3, 1/2, 1)
Moderately important	3	(1/3)	(2, 3, 4)	(1/4, 1/3, 1/2)
Moderate to strong importance	4	(1/4)	(3, 4, 5)	(1/5, 1/4, 1/3)
Important	5	(1/5)	(4, 5, 6)	(1/6, 1/5, 1/4)
Strong to very strong importance	6	(1/6)	(5, 6, 7)	(1/7, 1/6, 1/5)
Very strong importance	7	(1/7)	(6, 7, 8)	(1/8, 1/7, 1/6)
Very strong to the extreme importance	8	(1/8)	(7, 8, 9)	(1/9, 1/8, 1/7)
Extreme important	9	(1/9)	(9, 9, 9)	(1/9, 1/9, 1/9)

Where TFN is a triangular fuzzy number

4.1.4 Geometric Mean Calculation

Geometric means is frequently utilized to aggregate the pairwise comparisons provided by multiple experts, resulting in the values l_{ij}, m_{ij}, and lu_{ij}, facilitating normalization, maintaining proportionality, and reducing the impact of extreme values

doi:10.6342/NTU202503692

that are particularly crucial in decision-making processes. The l_{ij} represents the lower bound, which reflects the most optimistic evaluation, the m_{ij} is the middle value, which serves as the representative estimate of the fuzzy number and the u_{ij} is the upper bound value, which denotes the most pessimistic evaluation. This method ensures balanced and reliable synthesis of expert judgments within a pairwise comparison matrix.

$$l_{ij} = \left(\prod_{j=1}^{n} l_{ij}\right)^{\frac{1}{k}}, \quad m_{ij} = \left(\prod_{j=1}^{n} mij\right)^{\frac{1}{k}}, \; u_{ij} = \left(\prod_{j=1}^{n} uij\right)^{\frac{1}{k}} \tag{5}$$

Where k is the total number of experts (k=7 in this study) participating in the pairwise comparison evaluation process.

4.1.5 Degree of Possibility and Weight Calculations

In the extent analysis method introduced by Chang (1996), the aggregate extent value Si for each criterion was calculated by combining and standardizing the fuzzy extent values. This approach addresses the uncertainties in expert judgments by transforming crisp values into fuzzy numbers. In this approach, an object X is defined to represent a set $(x_1,\ x_2\ , \ldots\ldots x_n)$ with a corresponding goal set U containing $(u_1,\ u_2\ , \ldots\ldots u_n)$ where extent analysis is applied to each goal individually.

$$S_i = \sum_{j=1}^{m} M_{gi}^{j} * \left(\sum_{i=1}^{n}\sum_{j=1}^{m} M_{gi}^{j}\right)^{-1} \tag{6}$$

Where $j = 1, 2, \ldots . m$, m is number of criteria $i = 1, 2, \ldots . . n$, n is number of alternatives

S_i is a synthetic extent value for criterion i, M_{gi}^{j} is Fuzzy extent value for goal j with respect to criterion i, based on the j^{th} alternative,

doi:10.6342/NTU202503692

The calculation of the M value for fuzzy extent analysis involves summing each triangular fuzzy number (TFN) across the rows of the matrix, as described by the following equation:

$$\sum_{j=1}^{m} M_{gi}^{j} = (\sum_{j=1}^{m} l_j,\ \sum_{j=1}^{m} m_j,\ \sum_{j=1}^{m} u_j) \tag{7}$$

Similarly, the aggregated fuzzy extent value across all the alternatives is.

$$\left[\sum_{i=1}^{n}\sum_{j=1}^{m} M_{gi}^{j}\right] = \left[\sum_{i=1}^{n}\sum_{j=1}^{m} l_j\ ,\ \sum_{i=1}^{n}\sum_{j=1}^{m} m_j\ ,\ \sum_{i=1}^{n}\sum_{j=1}^{m} u_j\right] \tag{8}$$

The inverse of the aggregated fuzzy extent value was calculated to normalize the fuzzy numbers using Equation 8.

$$\left[\sum_{i=1}^{n}\sum_{j=1}^{m} M_{gi}^{j}\right]^{-1} = \left(\frac{1}{\sum_{i=1}^{n} u_{ij}},\ \frac{1}{\sum_{i=1}^{n} m_{ij}}\ ,\frac{1}{\sum_{i=1}^{n} l_{ij}}\right) \tag{9}$$

To evaluate the extent to which one triangular fuzzy number is at least as large as another, the possibility degree between them was determined. Let $M_1 = (l_1,\ m_1,\ u_1)$ and $M_2 = (l_2,\ m_2,\ u_2)$ is two triangular fuzzy membership functions. The degree of probability that $M_2 \geq M_1$ is defined as:

$$M_2 \geq M_1 = \begin{cases} 1,\ if\ m_2 \geq m_1 \\ 0,\quad if\ l_1 \geq u_2 \\ \dfrac{(l_1 - u_2)}{(m_2 - u_2) - (m_1 - l_1)},\ otherwise \end{cases} \tag{10}$$

doi:10.6342/NTU202503692

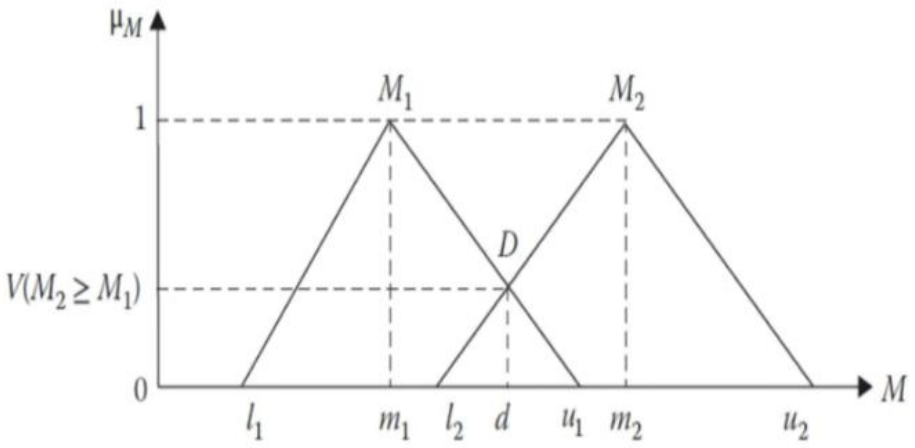

Figure 17:Possibility of $M2 \geq M1$ for Triangular Fuzzy Numbers (Chang, 1996)

Determining the minimum value for the comparison of M_1 and M_2 it is calculated the value of $V(M_2 \geq M_1)$ using equation 10

$$d'(A_i) = minV(S_i \geq S_k \tag{11}$$

Where k is $1,, 2, \ldots n$; but $k \neq i$, the weight vector is subsequently calculated using the following expression:

$$W' = \left(d'(A_1), d'(A_2), \ldots \ldots, d'(A_n)\right)^T \tag{12}$$

Where $A_i (i = 1, 2, \ldots . n)$ are n components, and $d'(A_i)$ represents the priority degree quantifying the evaluation of each alternative.

4.1.6 Normalizing Weights of Criteria

To obtain crisp values from the fuzzy weights, a defuzzification process was performed by normalizing the weights using Equation (12).

$$W = \left(\frac{d'(A_i)}{\sum_{i=1}^{n}(d'(A_i))}\right) \tag{13}$$

Where W represents the normalized non-fuzzy weight, with $i = 1, 2, \ldots ., n$.

doi:10.6342/NTU202503692

4.2 Sensitivity Analysis

The concluding phase of Fuzzy-AHP involves conducting a sensitivity analysis, which is crucial for examining how changes in the level of fuzziness influence criteria weights and rankings, thereby evaluating the model's stability. The baseline scenario for fuzziness degrees is set to 1, representing the original fuzzy weight results, whereas the additional fuzziness degrees range from 0.85 to 1.75 with increments of 0.15. Changes in ranking order indicate that the criteria are sensitive to variations in the fuzziness degree, whereas criteria that remain unchanged demonstrate the stability of the proposed model (Ekmekcioğlu et al., 2021; Ishizaka and Labib, 2011).

4.3 Mapping of RWH Suitability

To create the RWH feasibility map, the weights calculated from the Fuzzy-AHP process were incorporated with GIS by utilizing the raster calculator tool. The normalized raster layer for each criterion is multiplied by its respective weight, and these weighted layers are then combined to create a composite raster that represents the RWH Suitability Index (RWHSI). The equation used is as follows:

$$RWHSI = \sum_{j=1}^{n} W_j C_j \tag{14}$$

Where RWHSI is RWH suitable map Index, W_j is a weight assigned to the j^{th} criterion, obtained through Fuzzy-AHP analysis, C_j is normalized raster value of the j^{th} criterion, n is a total number of criteria.

doi:10.6342/NTU202503692

4.4 TOPSIS

The Technique for Order of Preference by Similarity to Ideal Solution (TOPSIS) developed by Hwang and Yoon (1981) is both logically sound and operationally effective, choosing options considered on their distance to the ideal positive solution and their remoteness from the ideal negative solution. As outlined by Behzadian et al. (2012), the TOPSIS method follows a structured six-step procedure: (1) creating the pairwise matrix, (2) standardizing the pairwise matrix, (3) allocating weights to the criteria, (4) calculating ideal positive and negative solutions, (5) computing the Euclidean distance, and (6) assessing the relative distance to the ideal solution. These steps are described in the following sections.

4.4.1 Developing the Decision Matrix

The determination matrix encompasses all attainable alternatives and integrates values across multiple criteria. As illustrated in figure 18, the decision matrix was developed through multiple steps, which included forming 1000m x 1000m grids by using the Fishnet tool in ArcGIS Pro to clip the study area. Following this, the Zonal Statistics as Table tool was utilized to calculate the average value for each pixel across the 12 input criteria raster datasets, as shown in Figure 18. The outcome of this process was a decision matrix consisting of 68,454 rows and 12 columns. This matrix is structured in an m × n format, where m signifies the number of choices and n represents the number of parameters, as indicated in Equation (14).

$$\widetilde{D} = \begin{bmatrix} C_1 & C_2 & C_n \\ a_{11} & a_{12} & a_{1n} \\ a_{21} & \dots & \vdots \\ a_{m2} & \dots & a_{mn} \end{bmatrix} \tag{15}$$

doi:10.6342/NTU202503692

Where $\widetilde{D}$ is a decision matrix, C_i is criteria, a_i is alternatives, $i = 1, 2, 3, .. n; and\ j = 1,2,3, .. m$.

4.4.2 Normalizing the Decision Matrix

Normalization was performed to bring all criteria to a comparable scale, thereby ensuring a fair evaluation. The normalized pairwise matrix is calculated using Equation 15 as follows:

$$D_{ij} = \frac{a_{ij}}{\sqrt{\sum_{i=1}^{m} Xij}} \tag{16}$$

Where D_{ij} is a normalized decision matrix, $i = 1, 2, \ldots . m$; and $j = 1, 2, \ldots . n$.

4.4.3 Assigning Weights to Criteria

Expert judgment was applied to assign weights to each criterion, and the Fuzzy-AHP method was used to compute the normalized weights of the decision matrix by multiplying each normalized value with its corresponding criterion weight.

$$V_{ij} = W_j D_{ij} \tag{17}$$

Where V_{ij} is a weighted normalized decision matrix, W_j is a criterion weight obtained through Fuzzy AHP analysis

4.4.4 Identifying the Ideal Solution

The Positive Ideal Solution (PIS) represents the most advantageous choice, characterized by attaining the maximum possible values for all criteria. For criteria that are beneficial, the highest values are selected, while for those that are not beneficial, the lowest values are taken into account. In contrast, the Negative Ideal Solution (NIS)

doi:10.6342/NTU202503692

represents the least desirable choice, identified by selecting the minimum values for beneficial criteria and the maximum values for detrimental criteria.

i. Positive ideal solution (A^+)

$$A^+ = \{v1^+ \dots \dots \dots \dots vn^+\} \quad (18)$$

$$\text{Where } v_j^+ = \begin{cases} max(V_{ij}), if\ j\ is\ benefit\ criterion \\ min(V_{ij}), if\ j\ is\ cost\ criterion \end{cases}$$

ii. negative ideal solution (A^-)

$$A^- = \{v1^- \dots \dots \dots \dots vn^-\} \quad (19)$$

$$\text{Where } v_j^- = \begin{cases} min(V_{ij}), if\ j\ is\ benefit\ criterion \\ max(V_{ij}), if\ j\ is\ cost\ criterion \end{cases}$$

4.4.5 Determination of the Euclidean Distance

To identify the proximity of each alternative to the Positive Ideal Solution (PIS) and the Negative Ideal Solution (NIS), Euclidean distance is utilized. The proximity to the PIS indicates how close an option is to being the best choice, whereas the distance from the NIS shows how far it is from the least desirable option.

- Separation from the most preferred (ideal) alternative (D_i^+):

$$D_i^+ = \sqrt{\sum_{j=1}^{n}\left(V_{ij} - V_{ij}^+\right)^2} \quad (20)$$

- Separation from the least preferred (worst) alternative (D_i^-):

$$D_i^- = \sqrt{\sum_{j=1}^{n}\left(V_{ij} - V_{ij}^-\right)^2} \quad (21)$$

doi:10.6342/NTU202503692

4.4.6 Calculating Relative Closeness (CR)

The relative closeness coefficient (RC) evaluates how near each option is to the Positive Ideal Solution while also taking into account its distance from the Negative Ideal Solution.

$$RC_i = \frac{D_i^-}{D_i^+ + D_i^-} \tag{22}$$

The RC value is expected to fall within the range of 0 to 1, where a value approaching 1 suggests closer alignment with the ideal solution. and a value closer to zero indicates proximity to the negative ideal solution. Choices are arranged from highest to lowest based on their values, with higher values indicating more desirable options. Moreover, the obtained result was imported into GIS and joined with the sampling grid created in Section 3.2.1 and subsequently converted into a raster map as described in Figure *18*.

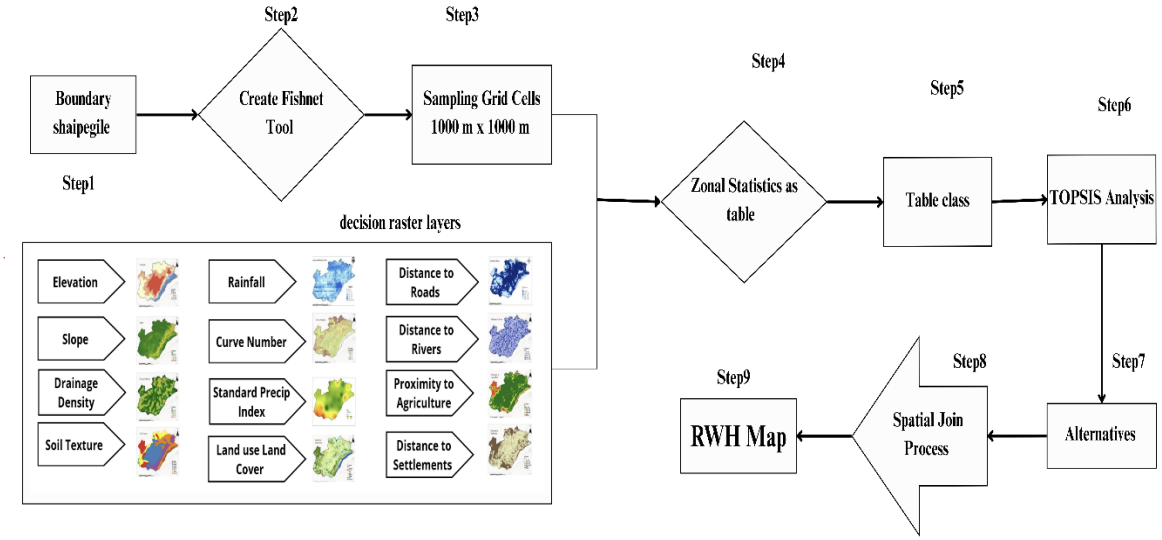

Figure 18: Spatial Mapping Workflow of TOPSIS Results

doi:10.6342/NTU202503692

4.5 Comparing Fuzzy-AHP and TOPSIS for Suitability Raster Maps

4.5.1 Change Detection Analysis

The Compute Change Raster tool was utilized to conduct a change detection analysis using the Categorical Difference approach. The Filter Method was set to change pixels only, ensuring that the analysis focused exclusively on category transitions by excluding unchanged pixels from the classification results. Table *15* summarizes the input parameters used in the change-detection process, including their labels, definitions, and data types.

Table 15: Input parameters for compute change raster

Label	Definition	Data Type
From Raster	Old Raster (Fuzzy-AHP raster)	Raster Dataset
To Raster	New/latter Raster (TOPSIS raster)	Raster Dataset
Computer Change Method	Categorical difference	String
Filter Method	Changed Pixels Only	String

4.5.2 Confusion Matrix Analysis

In the confusion matrix analysis, certain suitable RWH classes occupied very small areas, leading to a class imbalance when selecting random sampling points. To address this issue, the suitability map was reclassified into a binary format. Specifically, moderate, high, and optimal suitability of zones were merged into a single class labeled as suitable (assigned a value of 1), while the low suitability and unsuitable categories were grouped into an unsuitable class (assigned a value of 0). This reclassification enabled stratified random sampling with balanced representation across classes. In this procedure, the user's accuracy was calculated using Equation (23), producer's accuracy was used for Equation

doi:10.6342/NTU202503692

(24), and Overall Accuracy was determined using Equation (25) to assess the effectiveness of the classification.

$$U_A = \frac{P_{CCC}}{P_{Tc}} \quad (23)$$

Where U_A is user's Accuracy, P_{CCC} is correctly classified pixels for a class, and P_{Tcc} is total pixels classified into that class.

$$P_A = \frac{P_{CCC}}{P_{Trc}} \quad (24)$$

Where P_{RA} is producer's accuracy, P_{CCC} is correctly classified as pixels for a class and P_{Trc} is total reference pixels for that class.

$$O_A = \frac{P_{ncc}}{P_{Tnr}} \quad (25)$$

Where O_A is overall accuracy, P_{ncc} is a number of correctly classified pixels and P_{Tnr} is a total number of reference pixels.

4.5.3 Correlation Analysis of Fuzzy-AHP and TOPSIS

4.5.3.1 Sample Size Determination

To ensure a statistically valid comparison between the raster maps of Fuzzy-AHP and TOPSIS, Cochran's sample size formula was employed to determine the necessary sample size (Olofsson et al., 2014). The observed overall accuracy, derived from the confusion matrix comparing the agreement between the TOPSIS and Fuzzy-AHP raster maps, was used as the input parameter. A confidence level of 95% and a margin of error of 5% were utilized. The formula is as follows:

$$n = \frac{Z^2 O(1-O)}{d^2} \quad (26)$$

doi:10.6342/NTU202503692

In this scenario, n is the required sample size, O represents the observed overall accuracy, Z is the standard normal deviation for a 95% confidence level, and d indicates the margin of error, which was set at 0.05.

4.5.3.2 Descriptive Statistical Analysis and Normality Test

After determining the sample size, the corresponding suitability scores at each sampled location were extracted from the Fuzzy-AHP and TOPSIS raster layers. These paired values served as inputs for the correlation analysis. Descriptive statistical measures include the average, middle value, variability, asymmetry, and peakedness (Joanes & Gill, 1998; Murray et al., 2009), were computed to evaluate the distributional characteristics and normality of the samples extracted from the Fuzzy-AHP and TOPSIS raster datasets.

Measurement of Central Tendency and dispersion

$$\bar{x} = \sum_{i=1}^{n} x_i; \quad and \quad S = \sqrt{\frac{\sum_{i=1}^{n}(x_i - \bar{x})^2}{n-1}} \tag{27}$$

Where x_i represents an extracted data from datasets, n is a sample size, $\bar{x}$ is sample mean, and S is a standard deviation of the sample data.

Measure of Symmetry:

$$C_s = \frac{n\sum_{i=1}^{n}(x_i - \bar{x})^3}{(n-1)(n-2)S^3} \tag{28}$$

Where C_s is coefficient of skewness.

Measure of Kurtosis:

$$K = \frac{n^2\sum_{i=1}^{n}(x_i - \bar{x})^4}{(n-1)(n-2)(n-3)S^4} \tag{29}$$

doi:10.6342/NTU202503692

Where K is coefficient of Kurtosis.

The Anderson–Darling (AD) test, as represented in equation (29), was used to assess the normality of the extracted sample data. This statistical technique evaluates how well the empirical data distribution aligns with a theoretical normal distribution with heightened sensitivity to variations in the distribution tails(Stephens, 1974).

$$AD = -N - \frac{1}{N}\sum_{i=1}^{N}(2i-1)[ln\,(F(X_i)) + ln\big(1 - F(X_{N+1-i})\big)] \quad (30)$$

Where AD is Anderson Darling test, N is number of samples, F (X_i) the cumulative distribution function (CDF) evaluated at the i^{th} ordered sample X_i , and $X_{(N+1-i)}$ is an i^{th} value in descending order.

4.5.3.3 Spearman's Rho Analysis

Spearman's rho coefficient, as introduced by Spearman (1904), is a non-parametric statistical tool used to evaluate the strength and direction of a monotonic relationship between two variables. This study utilized a technique to evaluate the relationship between the suitability scores obtained from Fuzzy-AHP and TOPSIS. The coefficient was determined using the following formula:

$$\rho = 1 - \frac{6*\sum di^2}{n(n^2-1)} \quad (31)$$

where ρ is Spearman's rho coefficient and d is the ranking difference.

$$t = \frac{\rho*\sqrt{n-2}}{\sqrt{1-\rho^2}} \quad (32)$$

Where t is a t-statistic, $n-2$ is degree of freedom.

doi:10.6342/NTU202503692

At a 95% confidence level, the calculated t-statistics and corresponding p-values indicate that a p-value below 0.05 indicates a statistically significant connection between the two sets of scores.

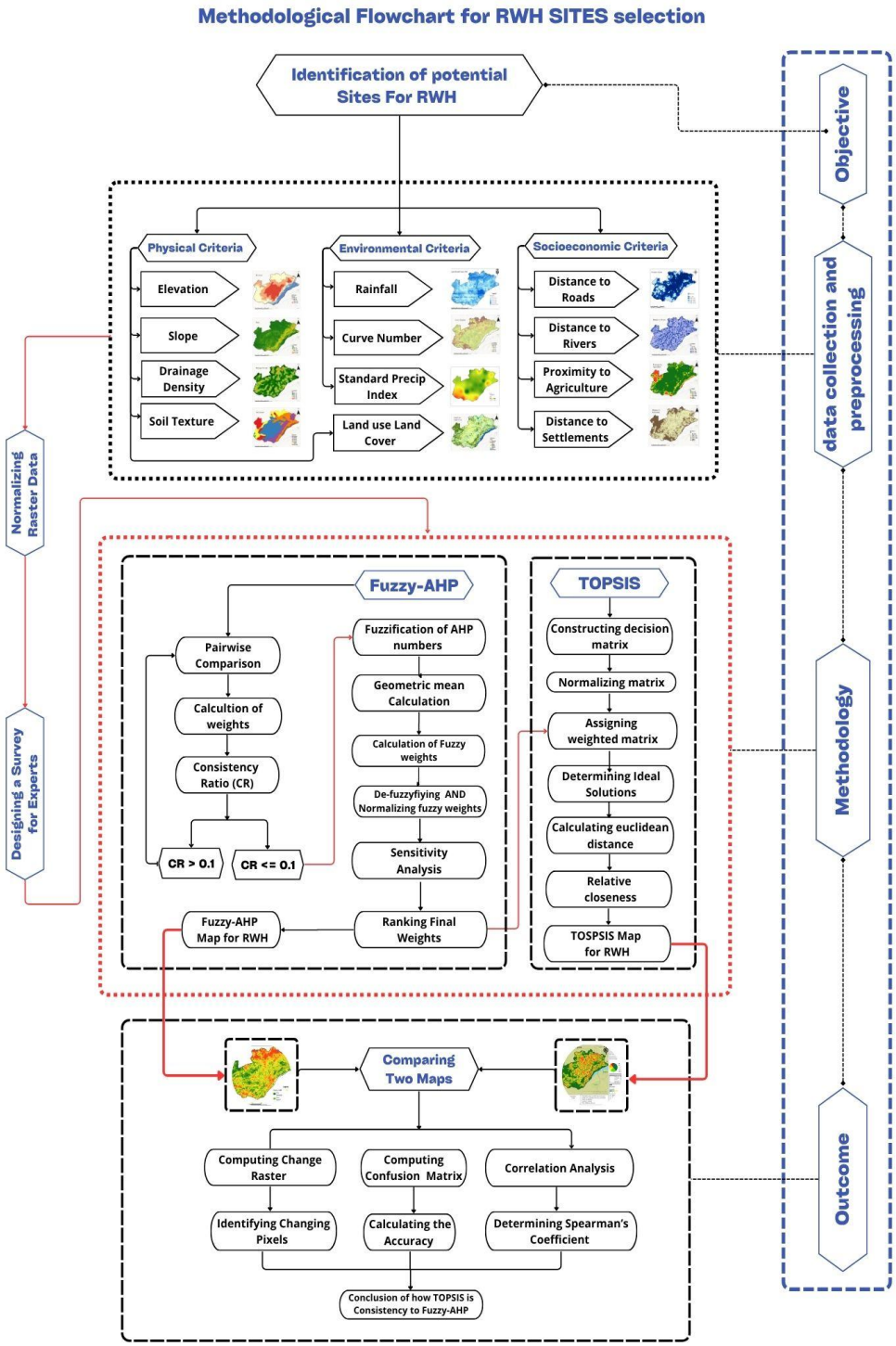

Figure 19: Flowchart of the Methodological Framework

doi:10.6342/NTU202503692

Chapter 5: Results and Discussions

5.1 Fuzzy-AHP Result

5.1.1 Determination of Relative Weights for Decision Criteria

This research evaluated the appropriateness of RWH locations using the Fuzzy-AHP method, considering 12 decision criteria. This study primarily aimed to evaluate how each criterion contributes to the RWH potential across the study area. To accomplish this, expert opinions were collected through pairwise comparison surveys involving seven experts, each independently assessing the relative significance of the criteria. These responses served as the basis for constructing individual matrices for pairwise comparisons, which served as the basis for calculating weights using Fuzzy-AHP, as displayed in Figure 20. This approach facilitates the incorporation of expert insights into the structured and systematic nature of a formal decision-making framework, effectively capturing the uncertainty and variability inherent in expert evaluations.

A crucial aspect of the Fuzzy-AHP approach is to verify the consistency of expert evaluations. To ensure the logical consistency of these assessments, the consistency ratio (CR) was determined for each expert comparison matrix. The CR values were subsequently evaluated against a standard limit of 0.1 (10%), which signifies an acceptable level of consistency. Figure 21 illustrates the CR values for all seven experts. As shown, all CR values remained below the threshold, indicating that pairwise comparisons were both consistent and methodologically sound. This validation process is essential for verifying the reliability of the calculated weights and reducing the impact of inconsistencies that might arise from subjective assessments.

doi:10.6342/NTU202503692

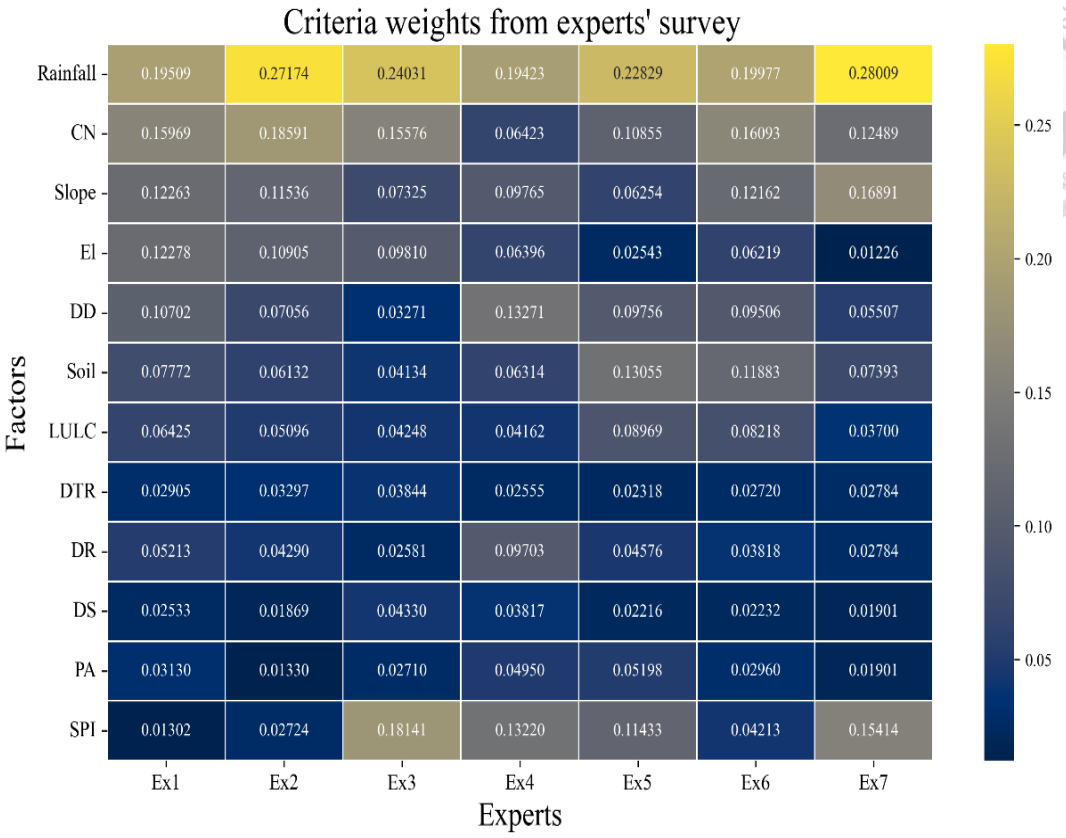

Figure 20: Criteria weights obtained from experts' survey

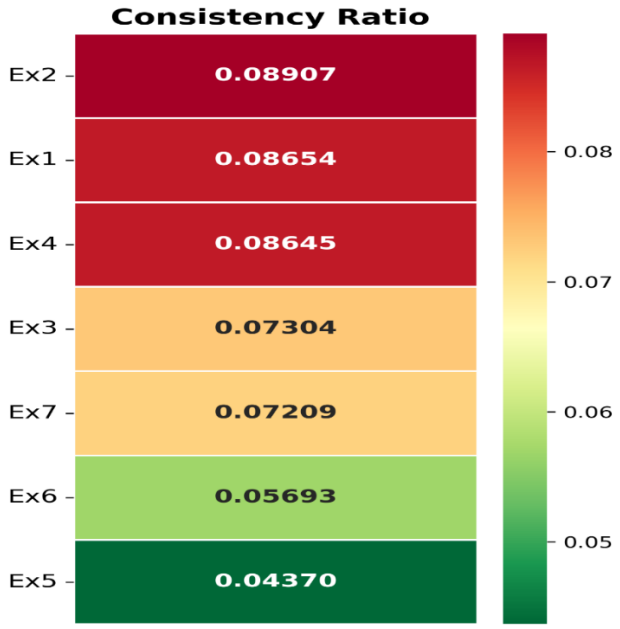

Figure 21: Consistency ratio of seven experts' survey

doi:10.6342/NTU202503692

After conducting a consistency check, the fuzzy weights for each criterion were determined and expressed as triangular fuzzy numbers that included the lower, middle, and upper bounds. These weights are detailed in Table *16*, offering a range-based representation that captures the uncertainty inherent in expert evaluations. To facilitate direct comparison and practical use, the fuzzy weights were defuzzified using a suitable method, transforming each triangular fuzzy number into a single representative value. Subsequently, the defuzzified weights were normalized so that their total equaled one, ensuring that they were interpretable and appropriate for further spatial analysis within the GIS framework. These procedures ensured that the resulting weights could be effectively utilized for spatial suitability mapping of the RWH sites.

Table 16: Fuzzy-AHP Output Weights

Criteria	Fuzzy Weight			De-fuzzifying	Normalizing Final Weight
RF	0.16011	0.26010	0.40325	0.27449	0.25311
CN	0.08729	0.14396	0.23397	0.15508	0.1430
SL	0.06772	0.11284	0.18714	0.12257	0.11302
EL	0.03635	0.05986	0.10425	0.06682	0.06162
DD	0.04956	0.08205	0.13416	0.08859	0.08169
ST	0.04588	0.07727	0.13006	0.08440	0.07783
LULC	0.03473	0.05703	0.09977	0.06385	0.05887
PR	0.01919	0.03044	0.05270	0.03411	0.03145
DSO	0.02692	0.04624	0.08048	0.05121	0.04722
DS	0.01685	0.02667	0.04509	0.02954	0.02724
PA	0.01843	0.02879	0.04774	0.03165	0.02919
SPI	0.04457	0.07476	0.12720	0.08217	0.07577

Table 17 displays the criteria weights and the rankings of decision factors determined using the Fuzzy-AHP method, categorized into three main areas: Physical, Environmental, and Socioeconomic parameters. The environmental category played the most significant role in the decision-making process, representing 47.19% of the total weight. This is followed by the physical category, which accounts for 39.30%, and the

doi:10.6342/NTU202503692

socioeconomic category, which contributes 13.51%. For each category, both local weights (reflecting the relative importance within each group) and global weights (representing the overall influence across all criteria) are provided, along with corresponding rankings to support comparative analysis.

Table 17: Computed weights and priority rankings of decision factors

				Weight %		Ranking	
Group	Weight	Criteria	ID	Local	Global	Local	Global
Physical	39.30	SL	SL	28.75	11.3	3	3
		ST	ST	19.8	7.78	10	5
		EL	EL	15.67	6.16	5	7
		DD	DD	20.79	8.17	7	4
		LULC	LULC	15.0	5.89	12	8
Environmental	47.19	RF	RF	53.63	25.31	1	1
		CN	CN	36.39	14.3	4	2
		SPI	SPI	19.29	7.58	11	6
Socioeconomic	13.51	DSO	DR	34.94	4.72	2	9
		PA	PA	20.13	2.92	9	11
		PR	PR	23.32	3.15	6	10
		DS	DS	21.61	2.72	8	12

A comprehensive assessment of the criteria revealed that rainfall (RF) holds the greatest significance, achieving a maximum local influence of 53.63% and a top global weight of 25.31%, thereby securing the first position overall. Curve number (CN) ranks second globally, with a global significance of 14.30% and a local significance of 36.39%. In terms of physical factors, slope (SL) ranks third globally, with a local weight of 28.75% and a global weight of 11.30%. Drainage density (DD) followed, with a local weight of 20.79% and a global ranking of fourth. The other important physical parameters were soil texture (ST) with a local weight of 19.80% and a global rank of fifth, elevation (EL) with a local weight of 15.67%, LULC with a local significance of 15.00%, and a global rank of eighth.

doi:10.6342/NTU202503692

On the other hand, the Socioeconomic category had a relatively low impact on the overall suitability evaluation. Within this group, distance-to-stream orders (DSO) stand out as the most significant factor locally, with a weight of 34.94%. However, on a global scale, it was ranked ninth, contributing only 4.72% of the total weight. Other socioeconomic factors, such as proximity to agriculture (PA), proximity to roads (PR), and distance to settlements (DS), had global weights of 2.92%, 3.15%, and 2.72%, respectively, placing them towards the bottom of the global rankings.

These results have important consequences for the planning and execution of RWH techniques. These findings suggested that environmental and hydrological elements, such as rainfall, curve number, and slope, highlight the necessity of focusing on these factors during the initial phases of site selection. The significant global weights suggest that the suitability of RWH is primarily influenced by the natural features of the landscape, which impact both runoff production and the capacity to retain water. This observation is in line with the body of research underscoring the pivotal influence of rainfall intensity and its spatial and temporal distribution in selecting optimal sites for rainwater harvesting (Tsubo et al., 2005).Therefore, planners should first focus on these parameters to determine technically viable sites before considering the social or infrastructural factors.

In semi-arid areas, such as Zambia's Southern Province, where water shortages are exacerbated by unpredictable rainfall, paying attention to hydrological and topographic suitability is particularly crucial. Even though socioeconomic aspects, such as proximity to roads, settlements, and agricultural zones, have a relatively minor global impact, they are vital for the practical application and long-term sustainability of systems. Although their lower positions in the model might indicate the study area's limited spatial variability, these criteria are crucial for effective operational planning. For instance, locations that

doi:10.6342/NTU202503692

are far from road systems might sustain increased costs for building and transportation, whereas remote communities could face challenges in terms of access, upkeep, and use.

These findings align with research from other semi-arid regions where environmental and physical factors have been recognized as the main influences on RWH suitability (Matomela et al., 2020; Mouhoumed et al., 2024b). The significant influence of rainfall and runoff-related factors underscores their essential role in determining effective site prioritization. This highlights the usefulness of hydrologically based spatial analyses, particularly in data-scarce conditions where field validation is resource-intensive. These insights lay the groundwork for refining spatial decision support models to achieve an optimal balance between environmental accuracy and practical feasibility in implementation.

5.1.2 Fuzzy-AHP-Based RWH Suitability Mapping

The spatial arrangement of the RWH suitability zones in Zambia's Southern Province was determined by combining the criterion weights from the Fuzzy-AHP method with their respective parameters in ArcGIS Pro. The classification framework was organized into five levels: very low, low, moderate, high, and optimal. As depicted in Figure 22, the resulting spatial pattern revealed varied distribution throughout the province. The high and most suitable zones are relatively continuous in northern Mazabuka and Monze, Namwala, central and northern parts of Sinazongwe, Livingstone, and southwestern Kazungula districts. In contrast, other areas exhibited a more fragmented layout, with scattered occurrences of moderate and optimal suitability patches.

doi:10.6342/NTU202503692

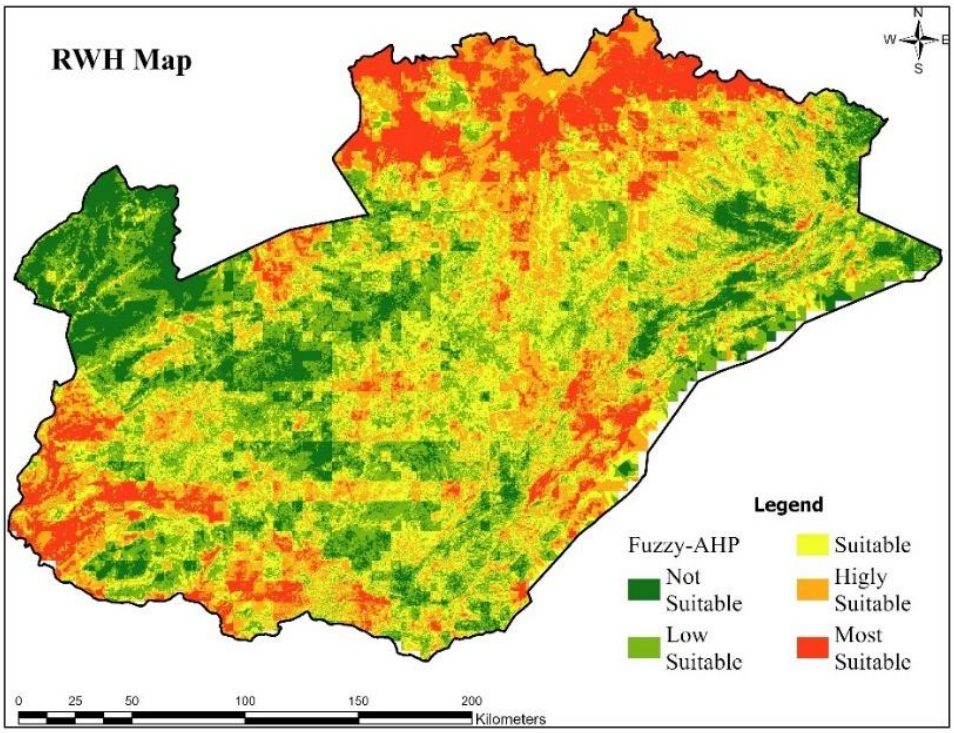

Figure 22: Spatial classification map obtained through Fuzzy-AHP

As depicted in Figure 23 (a) and (b), the suitable zone covers the largest area, approximately 18,676.4 km², accounting for 28% of the entire study region. This indicates that a considerable portion of the province offers moderately favorable conditions for selecting RWH sites. The Low Suitable zone, spanning 17,037.18 km² (26%), consists of areas that only satisfy a portion of the evaluation criteria.

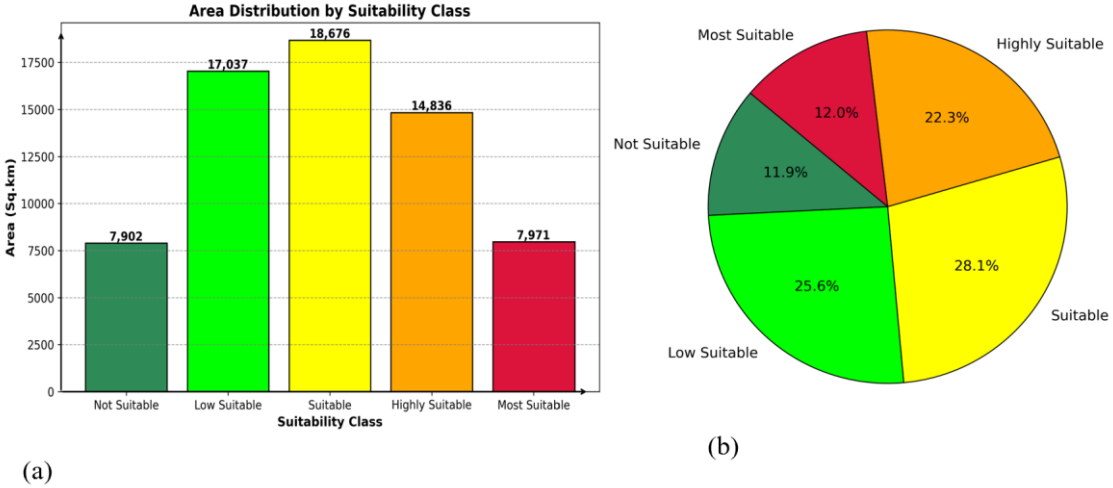

Figure 23: Suitability class distribution: (a) Area, (b) Proportion

doi:10.6342/NTU202503692

The high suitable and most suitable zones cover 14,835.77 km² (22%) and 7,971.42 km² (12%), respectively. These areas exhibit highly favorable conditions, including balanced decision criteria. Interestingly, the most advantageous areas were mainly situated in the northern, southeastern, and southwestern parts of the province. These zones are considered ideal for large-scale RWH interventions owing to their advantageous physical, environmental, and socioeconomic factors. On the other hand, the regions classified as Not Suitable, which also account for 12% of the area (7,901.66 km²), are predominantly located in the western and central parts of the region of interest. These zones are identified by multiple limiting factors, including poor accessibility, remoteness from settlements and agricultural fields, and unfavorable soil conditions with low water retention capacity, which reduce the feasibility of implementing RWH systems.

Approximately 62% of the provinces comprising the suitable, highly suitable, and most suitable zones were considered favorable for RWH development. These results offer an essential direction for policymakers and planners in determining priority areas. To enhance the process of selecting sites and enable a comparative ranking of choices based on their closeness to an ideal solution, the criteria weights derived from Fuzzy-AHP analysis were subsequently utilized in the TOPSIS method. By combining the unique advantages of both decision-making tools, this method enables a more comprehensive and detailed assessment of the potential RWH sites.

5.2 Sensitivity Analysis

To assess the stability and robustness of the proposed framework, a sensitivity analysis was performed by altering the fuzziness degree (FD). In this study, the focus was on how different degrees of uncertainty affected the significance assigned to decision criteria, thus evaluating the consistency of the findings. The fuzziness degrees varied from

doi:10.6342/NTU202503692

0.85 to 1.75, in increments of 0.15. Table 18 illustrates that as the FD values increased, the importance of the various criteria changed. Specifically, the significance of rainfall (RF), curve number (CN), and slope (SL) consistently increased with increasing FD values, enabling these criteria to maintain their rankings. By contrast, most other criteria experienced a decrease in weight, leading to changes in their rankings.

To better understand the stability of the rankings, when FD is set to 1, it acts as the standard scenario for comparison. At an FD of 0.85, seven criteria retained their original positions, whereas five others, EL, DD, ST, LULC, and SPI, underwent changes in their rankings. At FD values of 1.3 and 1.45, only elevation and SPI experienced shifts in ranking. As FD rose to 1.6 and 1.75, additional criteria, such as elevation (EL), distance to settlements (DS), proximity to agriculture (PA), and SPI, exhibited changes in their rankings. Interestingly, at FD = 1.15, the rankings of all criteria remained stable. Across all FD levels, the rankings for rainfall (RF), curve number (CN), slope (SL), proximity to roads (PR), and distance to rivers (DR) remained consistent, underscoring the reliability of these factors. Moreover, when FD surpassed 1.0, the eight criteria consistently maintained their rankings, demonstrating their stability under increased fuzziness.

Table 18: Sensitivity of criteria weights across varying fuzziness degrees

FD	$W_{0.85}$	$W_{Baseline}$	$W_{1.15}$	$W_{1.30}$	$W_{1.45}$	$W_{1.60}$	$W_{1.75}$
RF	0.22689	0.25311	0.27616	0.29650	0.314622	0.33089	0.34562
CN	0.13330	0.14300	0.15086	0.15727	0.16255	0.16696	0.17067
SL	0.10825	0.11302	0.11649	0.11897	0.12075	0.12201	0.12287
EL	0.06135	0.06162	0.06143	0.06093	0.06026	0.05947	0.05863
DD	0.08260	0.08169	0.08037	0.07879	0.07711	0.07540	0.07370
ST	0.08026	0.07783	0.07528	0.07272	0.07023	0.06785	0.06560
LULC	0.06240	0.05887	0.05539	0.05232	0.04953	0.04701	0.04471
PR	0.03480	0.03145	0.02851	0.02608	0.02398	0.02217	0.02060
DSO	0.05308	0.04722	0.04222	0.03814	0.03471	0.03178	0.02926
DS	0.03166	0.02724	0.02377	0.02098	0.01870	0.01680	0.01521
PA	0.03464	0.02919	0.02485	0.02156	0.01892	0.01677	0.01499
SPI	0.09081	0.07577	0.06467	0.05574	0.04863	0.04288	0.03815

doi:10.6342/NTU202503692

As depicted in Figure 24 (a), there is a steady upward trend in rainfall (RF), signifying a notable increase in its weight as FD escalates. This trend implies that RF becomes more influential in decision making when uncertainty is higher. CN and SL also showed upward trends, albeit at a slower pace than that of RF. Conversely, several criteria, including EL, ST, SPI, PA, and DS, exhibited decreasing weight trends, indicating a decline in their relative importance as FD increased. These findings suggest that greater uncertainty amplifies the influence of the most critical criteria, while reducing the impact of less significant ones. Furthermore, Figure 24 (b) supports this pattern by showing the variation of weights across all the criteria at different FD levels. The graph demonstrates that certain criteria, such as RF and CN, maintain consistent rankings, whereas others show small variation, as indicated by overlapping weight lines. The close overlap among the weight curves indicates the stability and robustness of the method, as only minor variations in criterion weights are observed across different fuzziness degrees (FDs).

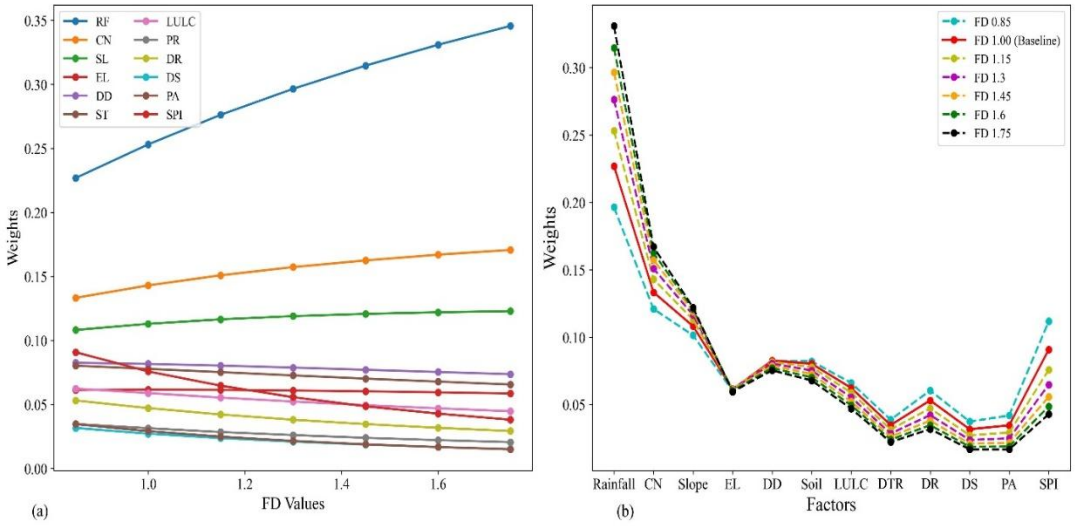

Figure 24: (a) Criteria Weight Trends, (b) Weight Variation Across FD Levels

To evaluate the influence of fuzziness on spatial decision-making, Figure 25 presents the spatial impact of different fuzziness degrees (FD) on RWH suitability classifications obtained through the Fuzzy-AHP method. Each map is associated with a

doi:10.6342/NTU202503692

specific FD value, ranging from 0.85 to 1.75 in 0.15 increments, and shows the spatial variation in RWH suitability zones across the study area. In a manner similar to the baseline scenario, each map was classified into five zones: not, low, moderate, high, and optimal suitability. As the FD value increased, the maps revealed a gradual transition from sharply defined boundaries to more generalized and spatially diffuse patterns. This suggests that lower FD values impose stricter classification thresholds, resulting in clearer delineations, whereas higher FD values allow for greater uncertainty, leading to broader and more adaptable suitability zones.

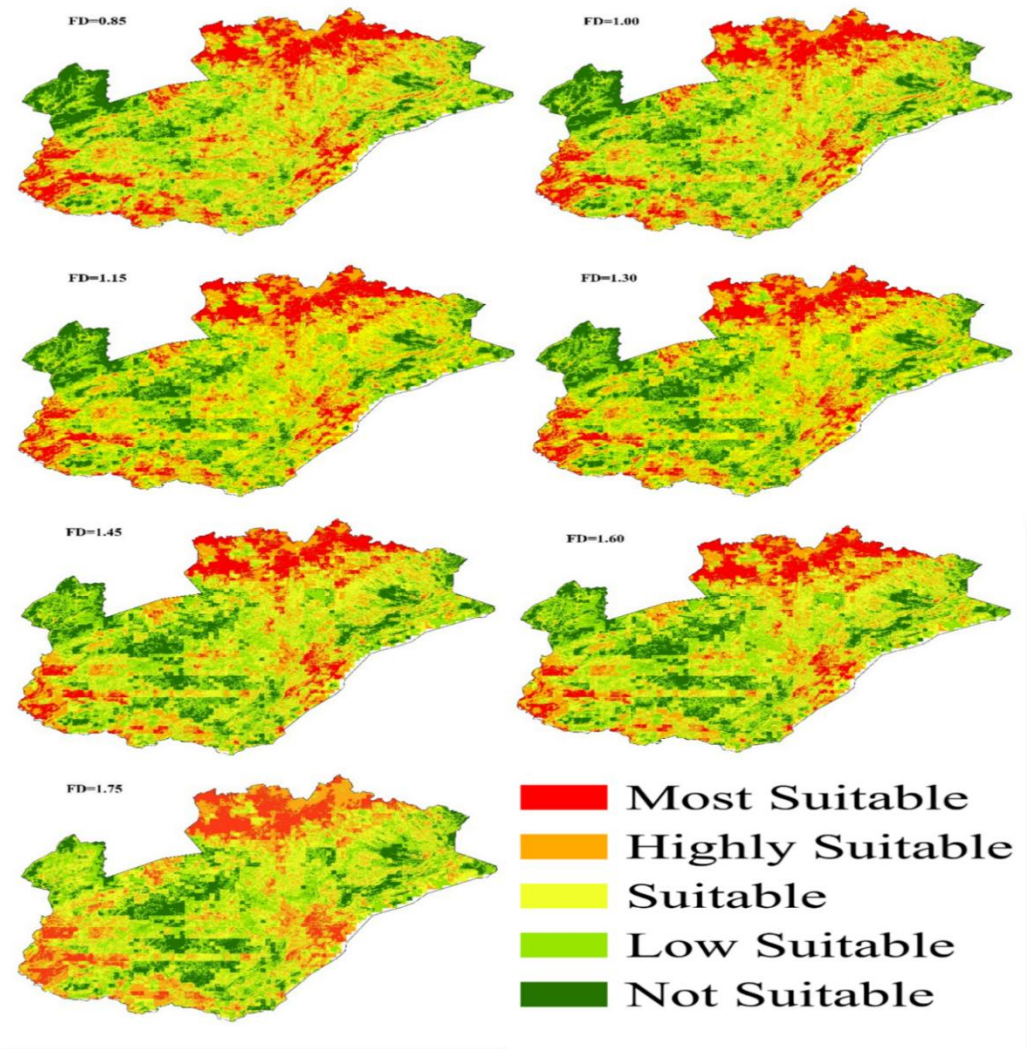

Figure 25: RWH Suitability Maps Generated Under Varying FD Levels

doi:10.6342/NTU202503692

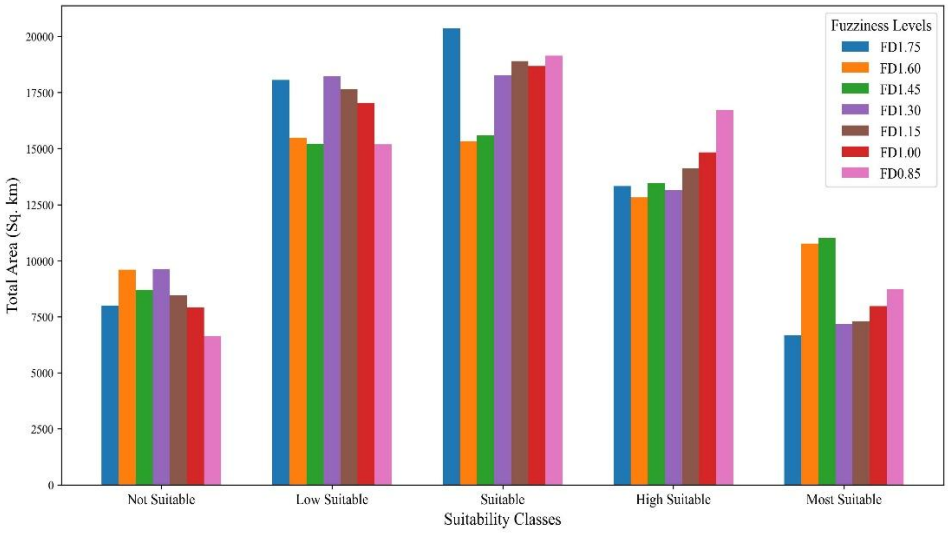

Figure 26: Variation in Suitability Class Areas Across Different FD

Figure 26 illustrates how the total area assigned to each RWH suitability category changes with varying FDs in the fuzzy-AHP framework. Despite experiencing slight variations as the FD increases, the Suitable category consistently occupies the largest segment of the study area. A noticeable trend is that the areas labeled as Most Suitable and Highly Suitable gradually shrink with higher FD values, suggesting a more cautious assessment, as the model becomes less decisive in pinpointing ideal locations. Conversely, the regions marked as low suitability and not suitable grow with increasing FD, indicating a heightened sensitivity to uncertainty and a broader classification of less favorable areas. These patterns imply that higher FD values result in smoother and more generalized suitability distributions, aligning with the theoretical notion that increased fuzziness introduces more ambiguity and diminishes the model's discrimination precision. Therefore, to supplement the Fuzzy-AHP analysis and facilitate a comparative assessment, TOPSIS was employed independently, as outlined in Section 5.4, using the same input parameters and criterion weights obtained from the Fuzzy-AHP method.

doi:10.6342/NTU202503692

5.3 TOPSIS Results and Alternative Rankings

5.3.1 Alternative Analysis

To utilize the TOPSIS technique for selecting locations for RWH, a sampling grid with cells measuring 1000 m x 1000 m was generated throughout the study region. Zonal statistics were employed to calculate the mean values of the 12 criteria used for decision-making for each grid cell. These input variables, sourced from thematic raster datasets, provided a uniform and spatially explicit foundation for the TOPSIS analysis. This approach produced a dataset comprising 68,454 alternatives, with each grid cell assigned a Relative Closeness (RC) value ranging from 0.046 to 0.998, as determined through TOPSIS analysis. The considerable number of alternatives generated is illustrated in Table 19.

Table 19: Obtained RC through TOPSIS analysis

Alternative	S+	S-	RC	Class
Alter1	0.000856	0.051193	0.983549431	Most Suitable
Alter2	0.045909	0.008531	0.156704124	Not Suitable
Alter3	0.005983	0.030451	0.835774173	Most Suitable
Alter4	0.026752	0.009342	0.258819117	Low Suitable
Alter5	0.041066	0.008371	0.16933419	Not Suitable
Alter6	0.043921	0.008761	0.166303124	Not Suitable
Alter7	0.00316	0.040599	0.927784698	Most Suitable
Alter8	0.026486	0.011127	0.295820562	Low Suitable
Alter9	0.008748	0.025054	0.741200205	High Suitable
Alter10	0.020312	0.013815	0.404819799	Suitable
…	…	…	…	…
…	…	…	…	…
…	…	…	…	…
Alter68454	0.049687	0.009207	0.156334046	Not Suitable

To enhance clarity and facilitate decision-making, RC scores were divided into five categories of suitability. Alternatives with RC values of 0.80 or higher were labeled as

doi:10.6342/NTU202503692

Most Suitable, indicating the greatest potential for RWH implementation. Values from 0.60 to 0.80 were deemed highly suitable, while those between 0.40 and 0.60 were considered suitable. RC values from 0.20 to 0.40 were classified as low suitable, and those below 0.20 were marked as unsuitable, representing the least favorable options for RWH development as illustrated Figure 27 (a). Figure 27 (b) presents the percentage distribution of alternatives across the five suitability categories, based on a total of 68,454 grid cells. It is crucial to understand that the figure represents the percentage of options allocated to each category rather than the physical area occupied by each class.

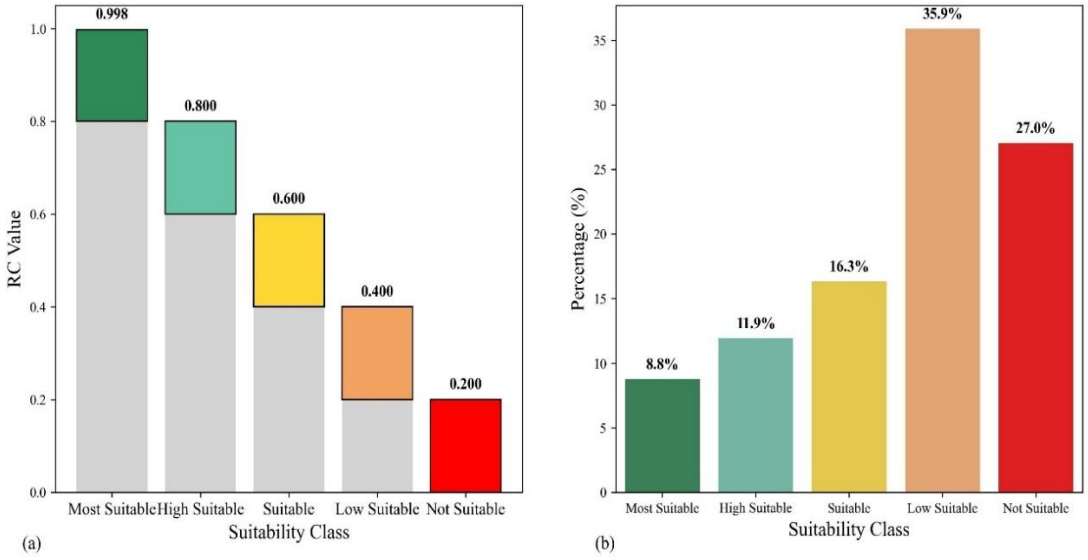

Figure 27: (a) Relative closeness values; (b) Percentage of categories in Alternatives

The results indicated that about 35.9% of the options were considered to have low suitability, while 27.0% were classified as unsuitable. In comparison, 16.3% were categorized as moderate, 11.9% as high, and only 8.8% as optimal, highlighting the limited availability of highly favorable sites for RWH within the study area. Collectively, this classification pattern illustrates the discriminatory power and internal consistency of the TOPSIS model in effectively ranking alternatives, depending on their closeness to the optimal solution. The relative closeness (RC) values assigned to each class provide a

doi:10.6342/NTU202503692

robust framework for prioritizing potential RWH sites and contribute to spatially informed decision making supported by quantitative multi-criteria evaluation.

5.3.2 Application of the TOPSIS Method for Mapping RWH Suitability

The resulting dataset, comprising 68,454 alternatives with their corresponding Relative Closeness (RC) values, was exported as a CSV file and integrated with a spatial sampling grid (1000 m × 1000 m) within a GIS environment to associate each RC value with its geographic location. To facilitate the spatial visualization of RWH suitability, the joined dataset was rasterized as a 30-meter resolution. As illustrated in Figure 28: (a) Potential mapping for RWH sites, (b) Area of different classes and (c) percentage distribution of area through TOPSIS (a), the final output map classified RC values into five suitability categories, enabling a spatially explicit interpretation of optimal locations for RWH site selection based on the TOPSIS evaluation.

Figure *28* (b) shows the total land area covered by each suitability class. The unsuitable category accounted for the largest portion of the study area, covering approximately 17852.02 km², and represented locations that were least favorable for effective RWH implementation. This is followed by the low suitability (24434.64 km²) and suitable (11121.13 km²) classes, which denote areas of moderate feasibility. The highly suitable and most suitable categories occupy smaller areas of the region, covering 8135.12 km² and 5973.63 km², respectively. This descending trend from less to more suitable classifications underscore the selective spatial distribution of the optimal sites for RWH site selection.

doi:10.6342/NTU202503692

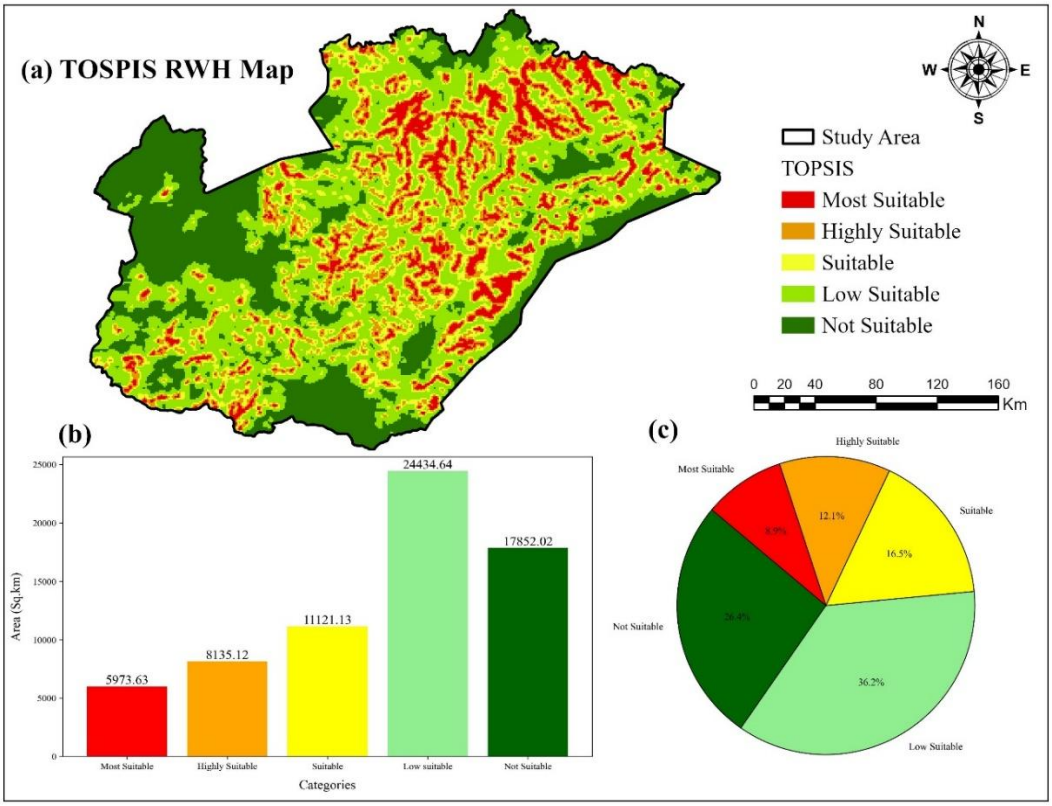

Figure 28: (a) Potential mapping for RWH sites, (b) Area of different classes and (c) percentage distribution of area through TOPSIS

As shown in Figure *28* (c), the relative proportion of each suitability class is calculated as a percentage of the entire area. The unsuitable category accounted for 26.40% of the total area, followed by low suitability (36.2%), suitable (16.50%), Highly Suitable (12.1%), and Most Suitable (8.9%). These proportions reaffirm the predominance of less favorable zones within the region and emphasize the limited spatial extent of highly suitable areas for the selection of potential RWH locations. Furthermore, these visualizations substantiate the spatial interpretation presented in the TOPSIS-based suitability map by quantifying the distribution of the suitability classes. The findings confirm the TOPSIS model's ability to effectively differentiate between regions, with varying potential for RWH. Although the suitability map generated by the TOPSIS method does not exactly mirror the spatial distribution created by the Fuzzy-AHP model,

doi:10.6342/NTU202503692

it demonstrates a significant level of agreement in identifying the most advantageous areas. Importantly, regions labeled as Most Suitable, Highly Suitable, and Suitable in the TOPSIS results tend to coincide with the equivalent zones on the Fuzzy-AHP map. To further evaluate and measure the extent of concordance between these two approaches, subsequent sections offer a comparative analysis of their results.

5.4 Comparative Analysis of Fuzzy-AHP and TOPSIS Outputs

5.4.1 Change Detection

Figure 29 presents a comparative spatial analysis of site suitability classification outputs derived from the Fuzzy-AHP and TOPSIS models along with the resulting change detection raster. Both maps employ a consistent five-class system ranging from unsuitable to the most suitable. This raster was generated using the Categorical Difference method with the changed pixel-only filter, focusing exclusively on areas of disagreement. A comprehensive visual representation of the change detection workflow is provided in Appendix, Figure A1.

The change detection map was color-coded to indicate the direction of transitions between suitability classes, as defined in the accompanying legend. Green represents areas where both models agree (No Change), while various shades of red and other colors depict transitions between classes (e.g., suitable to unsuitable, highly suitable to most suitable). These transitions visually demonstrate how classification differences are distributed, and how intense they are throughout the study area.

doi:10.6342/NTU202503692

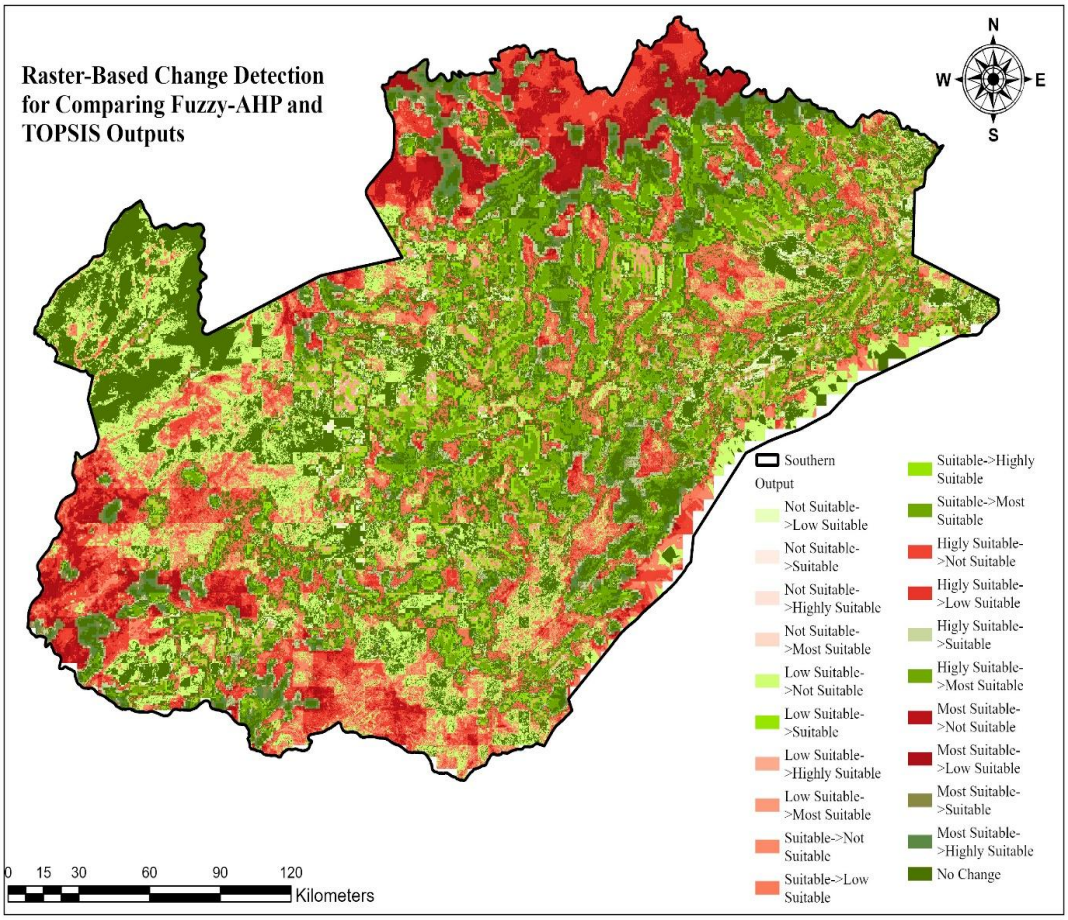

Figure 29: Change Detection Map Comparing Suitability Classifications from Fuzzy-AHP and TOPSIS

To enhance the understanding of the model agreement, Table *20* presents the evolution from the Fuzzy-AHP results (input raster) to TOPSIS results (comparison raster). Approximately 63% of the study area exhibited spatial agreement between the two models, either through precise alignment or minor shifts between adjacent suitability categories. As shown in Table 20, these minor changes include transitions from unsuitable to low suitable (1.6%), low suitability to not suitable (12.72%), Suitable to Highly Suitable (4.53%), and Highly Suitable to Suitable (3.93%). Given the conceptual closeness of neighboring categories, these transitions are regarded as spatially consistent. Furthermore, 29.14% of the area experienced no change, with both models categorizing

doi:10.6342/NTU202503692

it into the same suitability class, further emphasizing the level of concordance between the Fuzzy-AHP and TOPSIS results.

Table 20: Spatial Agreement Analysis of Suitability Scores

Class From (Fuzzy-AHP)	Class To (TOPSIS)	Transition	Count Pixels	Area (sq.km)	Per-Area %
Not Suitable	Low Suitable	Not Suitable ->Low Suitable	1178086	1067.41	1.6
Low Suitable	Not Suitable	Low Suitable ->Not Suitable	9387842	8505.88	12.72
Suitable	Highly Suitable	Suitable->Highly Suitable	3345320	3031.04	4.53
Suitable	Most Suitable	Suitable->Most Suitable	2145460	1943.90	2.91
Highly Suitable	Suitable	Highly Suitable ->Suitable	2901419	2628.84	3.93
Highly Suitable	Most Suitable	Highly Suitable ->Most Suitable	3337862	3024.28	4.52
Most Suitable	Suitable	Most Suitable ->Suitable	1352891	1225.79	1.83
Most Suitable	Highly Suitable	Most Suitable ->Highly Suitable	1340797	1214.83	1.82
Same	Same	No Change	21502755	19482.63	29.14
				Percent-Area	**63%**

In contrast, 37% of the area exhibited notable classification differences between Fuzzy AHP and TOPSIS, as indicated in Table 21. These differences involved reclassification across non-adjacent categories, highlighting a more pronounced methodological divergence. Significant instances include transitions from suitable to unsuitable (7.49%), highly suitable to unsuitable (5.5%), and most suitable to unsuitable (2.72%). These inconsistencies might significantly influence the prioritization of RWH sites, potentially leading to inefficient resource allocation and difficulties during execution. The spatial distribution of these differences was prominently visible in the red-dominated areas of the change detection map.

doi:10.6342/NTU202503692

Table 21: Spatial Discrepancies in Suitability Classifications

Class From (Fuzzy-AHP)	Class To (TOPSIS)	Class name	Count Pixels	Area (sq.km)	Per-Area %
Not Suitable	Suitable	Not Suitable->Suitable	305488	276.79	0.41
Not Suitable	Highly Suitable	Not Suitable->Highly Suitable	109528	99.24	0.15
Not Suitable	Most Suitable	Not Suitable->Most Suitable	27210	24.65	0.04
Low Suitable	Suitable	Low Suitable->Suitable	2430305	2201.98	3.29
Low Suitable	Highly Suitable	Low Suitable->Highly Suitable	1327754	1203.02	1.8
Low Suitable	Most Suitable	Low Suitable->Most Suitable	498471	451.64	0.68
Suitable	Not Suitable	Suitable->Not Suitable	5524456	5005.45	7.49
Suitable	Low Suitable	Suitable->Low Suitable	5630136	5101.20	7.63
Highly Suitable	Not Suitable	Highly Suitable->Not Suitable	4059163	3677.82	5.5
Highly Suitable	Low Suitable	Highly Suitable->Low Suitable	3344570	3030.36	4.53
Most Suitable	Not Suitable	Most Suitable->Not Suitable	2003300	1815.10	2.72
Most Suitable	Low Suitable	Most Suitable->Low Suitable	2028077	1837.54	2.75
				Percent-Area	**37 %**

The change detection analysis highlighted both the similarities and differences between the Fuzzy-AHP and TOPSIS models, indicating the need for a more thorough evaluation to accurately assess their spatial consistency. Although the models generally concur in identifying the most and least suitable areas for rainwater harvesting, they show significant discrepancies in categorizing zones that are marginally or moderately suitable. These variations underscore the importance of systematic comparative evaluations, such

doi:10.6342/NTU202503692

as confusion matrices and correlation analyses, to assess the consistency of the classification results. Considering that methodological differences can greatly influence site prioritization, especially in critical applications, such as selecting sites for harvesting, a confusion matrix analysis was subsequently utilized to assess the binary classification agreement between the models in Section 5.4.2.

5.4.2 Confusion Matrix Analysis

To assess the spatial agreement between the outputs of the Fuzzy-AHP and TOPSIS models, confusion matrix analysis was performed. Figure 1 demonstrates the use of a confusion matrix to assess the overall precision and reliability of the two models in identifying potential RWH sites. In this evaluation, the Fuzzy-AHP binary raster acted as the reference layer, whereas the TOPSIS binary raster was used as the input, and pixels were categorized into two groups: unsuitable (0) and suitable (1) as illustrated figure. The evaluation process involved three steps: (1) creating random points for accuracy assessment, (2) revising the classifications according to the reference raster, and (3) utilizing the confusion matrix tool to measure the agreement between the two models as illustrated in Figure 30. The resulting matrix provides a summary of the classification performance and the degree of alignment between the methods.

doi:10.6342/NTU202503692

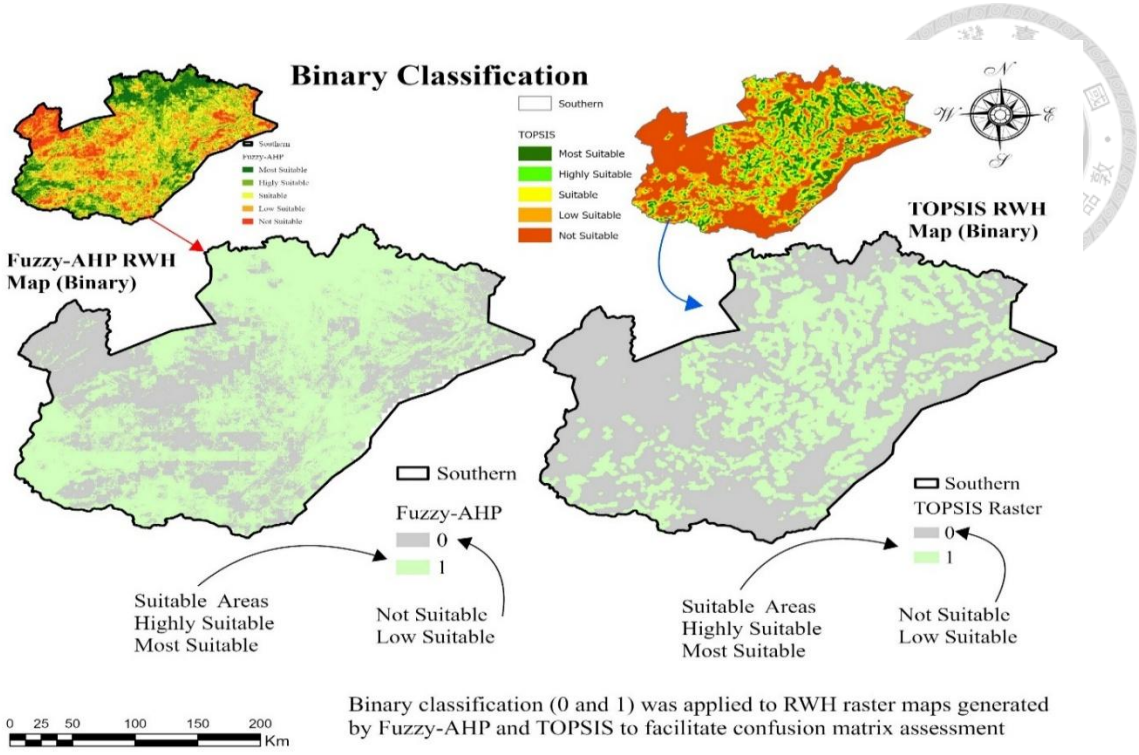

Figure 30: Binary classification of TOPSIS and Fuzzy-AHP suitability maps

As observed in Figure 31, the overall classification accuracy was determined to be 67%, indicating that approximately two-thirds of the pixels were consistently classified using both approaches. The user accuracy for suitable areas was relatively high at 80%, indicating a strong consensus in identifying favorable zones for RWH implementation. Conversely, the user accuracy for unsuitable areas was significantly lower at 53%, suggesting that TOPSIS tends to assign higher suitability to areas deemed unsuitable by Fuzzy-AHP. Additionally, the producer's accuracy for unsuitable areas was 72%, showing that most areas identified as unsuitable in the Fuzzy-AHP model were similarly classified by TOPSIS. However, the producer's accuracy for suitable areas decreased to 63%, indicating moderate consistency in this category.

doi:10.6342/NTU202503692

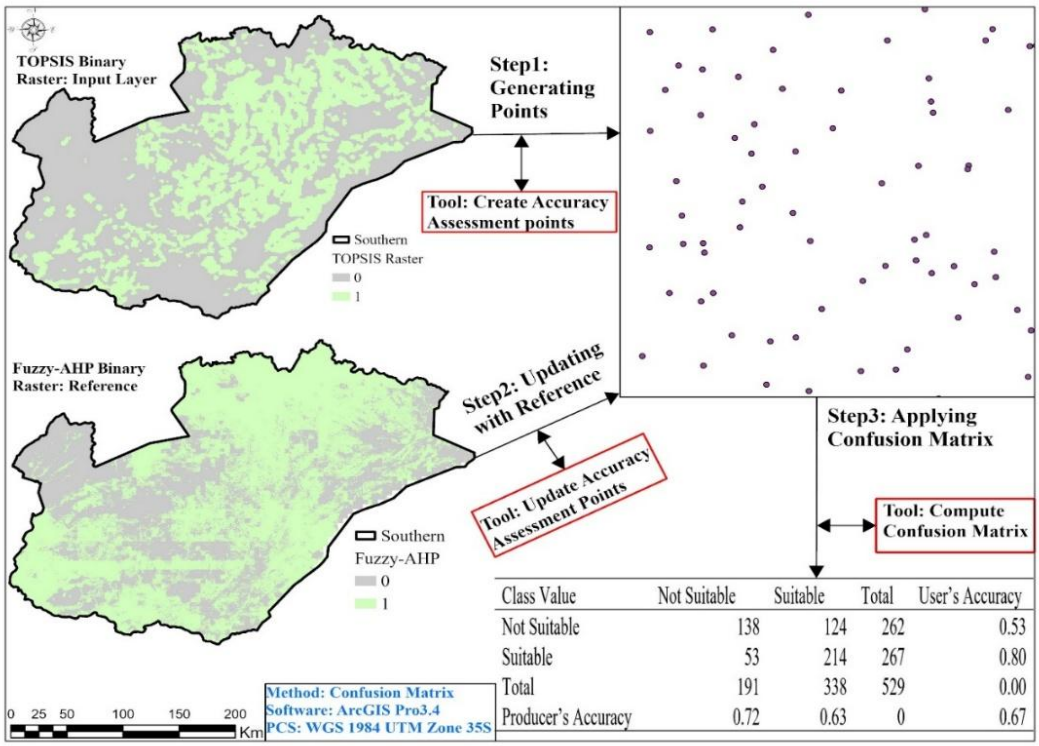

Class Value	Not Suitable	Suitable	Total	User's Accuracy
Not Suitable	138	124	262	0.53
Suitable	53	214	267	0.80
Total	191	338	529	0.00
Producer's Accuracy	0.72	0.63	0	0.67

Figure 31: Accuracy results of confusion matrix

The variations in classification outcomes between the Fuzzy-AHP and TOPSIS models highlight their methodological differences, particularly in how they interpret regions of marginal or transitional suitability. In some cases, TOPSIS rated the locations as more suitable, whereas Fuzzy-AHP deemed them unsuitable. Despite these discrepancies, confusion matrix analysis indicated a moderate level of spatial agreement, suggesting a basic alignment between the two models. However, the binary nature of the confusion matrix does not fully reflect the variability of the continuous suitability scores produced by each method. To overcome this limitation and evaluate the capability of the consistent association between the model outputs, Spearman's rho was used on the pixel-based suitability scores extracted from both raster maps, as explained in the following section.

doi:10.6342/NTU202503692

5.4.3 Correlation Analysis

To evaluate the results of the TOPSIS and Fuzzy-AHP models, an association analysis was conducted to supplement the insights from the change raster analysis and confusion matrix. Both approaches involved categorizing the raster maps into five levels of suitability and using binary classification for confusion matrix analysis. To determine a suitable sample size for data extraction, Cochran's formula was utilized, taking into account the overall accuracy derived from the confusion matrix. This calculation indicates that a minimum sample size of 340 points is necessary. To ensure comprehensive spatial representation throughout the study area, 500 random sampling points were generated for each raster map using fuzzy AHP and TOPSIS.

Table 22: Descriptive Statistics for ANOVA

	Fuzzy-AHP data		TOPSIS data	
Sample size	$\overline{X}$	S^2	$\overline{X}$	S^2
(n=500)	0.5083	0.0164	0.390	0.0562
(n=500)	0.507	0.0168	0.391	0.0551
(n=500)	0.5083	0.0157	0.392	0.0545
	P-Value	**0.9832**	P-Value	**0.9964**

To improve the reliability of the comparison, the sampling process was repeated three times for each map, with 500 points being randomly selected in each iteration. The values obtained were then subjected to statistical analysis using one-way ANOVA (single-factor analysis). As shown in Table 22, the findings reveal that the three samples taken from each model output do not show significant differences, confirming that they come from the same population and that random sampling was consistent. For the correlation analysis explained in the subsequent sections, the initial data of the extracted sample points were utilized for both the Fuzzy-AHP and TOPSIS raster layers.

doi:10.6342/NTU202503692

5.4.3.1 Descriptive Statistical Analysis and Normality Testing

Table 23 provides an overview of the descriptive statistics of the suitability scores derived from the fuzzy analytical hierarchy process (AHP) and TOPSIS methods. The results obtained using Fuzzy-AHP indicate a distribution that is nearly symmetrical, as the mean (0.508) is very close to the median (0.504), with a low skewness of 0.178 and a slightly negative kurtosis of −0.271, suggesting a distribution that is flatter than a normal curve. Conversely, the TOPSIS scores revealed a lower central tendency, with a mean of 0.390 and median of 0.302, and showed greater variability, as evidenced by a higher standard deviation of 0.237. This distribution is more right-skewed, with a skewness of 0.899, and has a more pronounced negative kurtosis of −0.437, indicating a flatter and more asymmetrical shape. The distributional properties justify the use of non-parametric statistical techniques such as Spearman's rho to compare the results of the two models.

Table 23: Descriptive Statistics

Fuzzy_AHP		TOPSIS	
Sample mean	0.508	Mean	0.390
Standard Deviation	0.128	Median	0.302
Sample median	0.504	Standard Deviation	0.237
Skewness	0.178	Kurtosis	-0.437
Kurtosis	-0.271	Skewness	0.899
Maximum	0.844	Minimum	0.111
Minimum	0.206	Maximum	0.993
No. of Observations	500	No. of Observations	500

The normality of suitability scores derived from the Fuzzy-AHP and TOPSIS models was evaluated using the Anderson–Darling (AD) test, as shown in Figure 32 and Figure 33. For the Fuzzy-AHP data, the AD test statistics were 0.45773, which was below the critical value of 0.781, indicating statistical acceptance at a significance threshold of 5%. As a result, there was not enough evidence to dismiss the null hypothesis of normality. This conclusion is further corroborated by the histogram, which exhibits a symmetric

doi:10.6342/NTU202503692

shape, and the Q–Q plot, in which the observed values align closely with the theoretical quantiles for both, suggesting that the Fuzzy-AHP scores approximate a normal distribution.

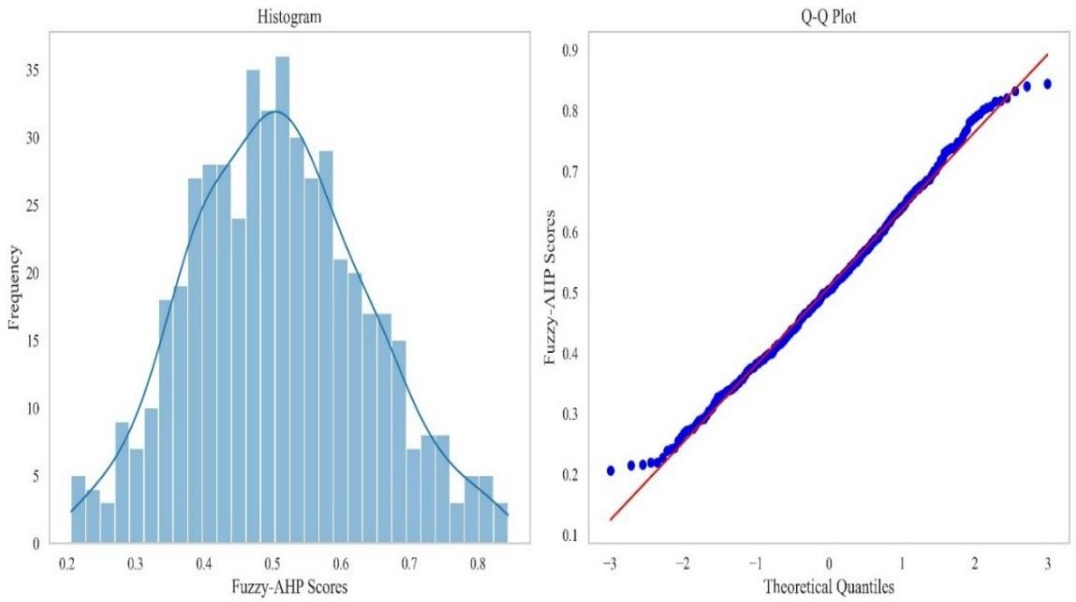

Figure 32: normality testing for data extracted from Fuzzy-AHP map

On the other hand, TOPSIS scores demonstrated a clear departure from normality. The AD test yielded a statistic of 24.149, which greatly exceeded the critical value, leading to the null hypothesis being rejected. The associated histogram highlights a significant right-skewed distribution, whereas the Q–Q plot shows a notable divergence from the diagonal reference line. Owing to the non-normal distribution of the TOPSIS scores, utilizing Spearman's rho coefficient is more suitable for comparing the outcomes of the two models.

doi:10.6342/NTU202503692

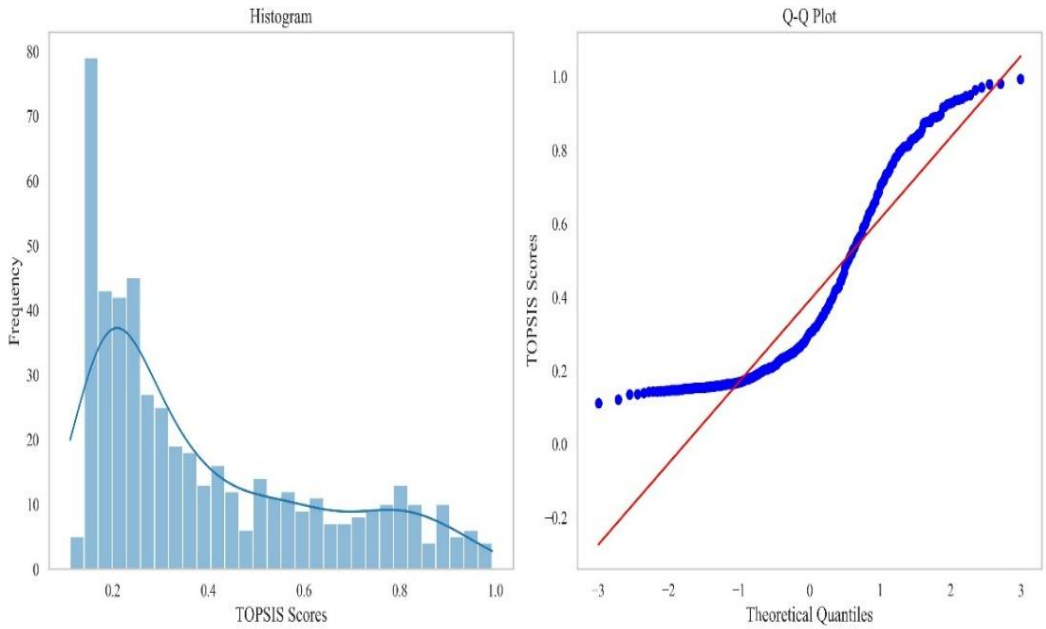

Figure 33: Normality test for data extracted from TOPSIS map

5.4.3.2 Spearman's Correlation Analysis

Table 24 presents a summary of the output analysis, showing that the Spearman's coefficient (ρ) between the Fuzzy-AHP and TOPSIS suitability scores is 0.46, derived from a dataset of 500 observations. This coefficient reflects a moderate positive correlation, indicating that areas deemed highly suitable by one method are likely to be ranked similarly by the other. Although the correlation is not particularly strong, the findings suggest a fair level of agreement between the two methods in prioritizing potential sites for harvesting rainwater (RWH).

Table 24: Spearman's rho coefficient

Parameters	Value	Interpretation
Spearman's ρ	0.46	Moderate positive correlation
t-statistics (H_o=0)	11.52	p < 0.001 (reject H_o)
Degrees of Freedom (DF)	498	—

doi:10.6342/NTU202503692

The rankings produced by Fuzzy-AHP and TOPSIS show a statistically significant correlation ($p < 0.001$), providing strong evidence to reject the null hypothesis that there is no relationship between these two methods. The observed correlation is statistically significant and unlikely to have arisen from random variation, thereby reinforcing the credibility of the comparative analysis. Specifically, the integration of change detection using the Compute Change Raster tool, confusion matrix evaluation, and Spearman's rank correlation enabled a comprehensive assessment of spatial agreement and model consistency.

The change detection revealed notable transitions in suitability classifications, with a spatial agreement of 63% between the Fuzzy-AHP and TOPSIS models. The confusion matrix further quantified classification accuracy, yielding an overall agreement rate of 67%, which indicates a moderate level of consistency between the predicted suitability outputs. Additionally, the Spearman's rho coefficient of 0.46 demonstrated a moderate positive monotonic relationship between the suitability rankings generated by the two models. Collectively, these findings indicate that, despite methodological differences, both models exhibit converging spatial patterns in identifying appropriate RWH sites. This complementarity underscores their potential as integrated tools within spatial decision-support frameworks, offering a more robust and reliable foundation for sustainable water resource planning.

doi:10.6342/NTU202503692

Chapter 6: Conclusions and Recommendations

6.1 Conclusion

In Zambia's Southern Province, where climate variability exacerbates water insecurity, identifying optimal rainwater harvesting (RWH) sites is critical for sustainable water resource management. This study focused on developing a climate-responsive, geospatial decision-making framework to pinpoint the best sites for RWH. This was achieved by combining GIS with MCDA. The study employed twelve carefully selected criteria encompassing physical, environmental, and socioeconomic factors. The inclusion of the SPI notably improved the model's capacity to identify areas vulnerable to drought, thereby enhancing the spatial accuracy of site selection. Utilizing the Fuzzy-AHP, the study found rainfall, curve number, and slope to be the most significant determinants of RWH suitability, maintaining consistent influence across varying levels of uncertainty.

The findings present important implications for climate-resilient water resource planning and management. Suitability assessments using both Fuzzy-AHP and TOPSIS indicate that approximately 62% and 37.5 %, respectively, of the study area exhibits moderate to high potential for placing RWH structures. The regions identified as Most Suitable and Highly Suitable were mainly situated in the northern and southeastern areas of the province, where advantageous environmental and socioeconomic factors align. While minor discrepancies were observed in marginal suitability classes, the spatial concordance between the two models was substantial, with a 63% overlap, 67% classification accuracy, and a Spearman's rank correlation coefficient of 0.46, demonstrating methodological reliability and consistency. These outcomes affirm the robustness and complementary nature of the applied approaches and underscore the framework's value in guiding spatially informed decision-making.

doi:10.6342/NTU202503692

This research primarily benefits government, water resource investors and planners, NGOs, and local communities involved in climate adaptation and sustainable rural development. The framework provides spatially detailed insights into the suitability of RWH, facilitating data-driven decisions and aiding in the strategic distribution of resources for water infrastructure. The integration of climatic indicators alongside conventional criteria enhances the framework's adaptability to changing environmental conditions, ensuring its continued relevance in regions affected by climate stress.

This research lays strong groundwork for future studies focused on improving the model's accuracy and relevance. Potential extensions include the incorporation of advanced hydrological modeling, expanding socioeconomic factors and cost-benefit analyses to improve operational functionality across different geographic and administrative scales. Applying this framework in other semi-arid or arid environments could generate comparative insights and facilitate the development of scalable, transferable strategies for sustainable water resource management. Ultimately, this research contributes not only to academic scholarship but also to practical, actionable solutions for enhancing water security in vulnerable, climate-sensitive regions.

6.2 Recommendations

This research offers several key suggestions to improve the planning and implementation of RWH projects in areas with limited water resources, focusing particularly on Zambia's Southern Province. Priority should be given to developing RWH infrastructure in areas classified as very high and highly suitable, which collectively comprise around 62% of the area of interest. These high-potential locations are predominantly within the districts of Choma, Kalomo, Pemba, Monze, Mazabuka, and Livingstone, where conditions are optimal for the successful deployment of RWH

doi:10.6342/NTU202503692

interventions. Although these areas should be the primary focus, moderately suitable regions also warrant consideration, particularly where local needs or constraints justify their inclusion. To ensure efficient allocation of resources, investments should be strategically directed toward the most favorable sites to enhance the overall impact and sustainability of RWH initiatives.

Second, the inclusion of SPI within the site selection framework proved valuable for identifying drought-prone areas, highlighting the importance of incorporating dynamic climatic indicators into spatial planning processes. It is recommended that national and regional agencies integrate the SPI or similar indices to enhance climate resilience and improve the anticipation of rainfall variability. Third, the combined application of Fuzzy-AHP and TOPSIS, validated through a spatial agreement rate of 63% and a computed Spearman coefficient of 0.46, illustrated the advantages of employing multiple MCDA methods. This integrated approach improves analytical robustness and provides decision makers with greater confidence in prioritizing suitable RWH sites. To enable the broader adoption of this GIS–MCDA framework in other regions, targeted investments in high-resolution spatial data, remote sensing tools, and capacity building in GIS and MCDA methodologies are essential.

Fourth, the design of rainwater harvesting (RWH) systems should be meticulously aligned with key biophysical parameters such as rainfall distribution, curve number, and slope to ensure hydrological feasibility. Particular attention should be given to areas where discrepancies between the two models are most pronounced, as these zones require targeted field validation and iterative refinement to improve site-specific accuracy and adaptability. Moreover, RWH should be advanced not merely as a localized water management solution, but as an integral component of broader national strategies for climate adaptation and disaster risk reduction. Realizing this vision necessitates the

doi:10.6342/NTU202503692

establishment of supportive policy frameworks and sustained engagement of local communities throughout the planning, implementation, and maintenance stages. Collectively, these strategies can foster the sustainable management of water resources and bolster climate resilience in SAR areas that are at risk.

doi:10.6342/NTU202503692

Reference

Adham, A., Riksen, M., Ouessar, M., & Ritsema, C. J. (2016). A methodology to assess and evaluate rainwater harvesting techniques in (semi-) arid regions. *Water (Switzerland)*, *8*(5), 1–23. https://doi.org/10.3390/w8050198

Ahana, B. S., Posite, V. R., Maouly, D. K., Abdelbaki, C., Kantoush, S. A., Nguyen, B. Q., & Kumar, N. (2024). Changing Rainfall Patterns in the Northeastern South Kivu Region, Democratic Republic of the Congo: A Detailed Analysis Using CHIRPS Rainfall Data (1981–2023). *Earth Systems and Environment*, 1733–1750. https://doi.org/10.1007/s41748-024-00510-0

Ahmad, B. A., Salar, S. G., & Shareef, A. J. (2024). An integrated new approach for optimizing rainwater harvesting system with dams site selection in the Dewana Watershed, Kurdistan Region, Iraq. *Heliyon*, *10*(6), e27273. https://doi.org/10.1016/j.heliyon.2024.e27273

Ahmad, R., Gabriel, H. F., Alam, F., Zarin, R., Raziq, A., Nouman, M., Young, H. W. V., & Liou, Y. A. (2024). Remote sensing and GIS based multi-criteria analysis approach with application of AHP and FAHP for structures suitability of rainwater harvesting structures in Lai Nullah, Rawalpindi, Pakistan. *Urban Climate*, *53*(January), 101817. https://doi.org/10.1016/j.uclim.2024.101817

Ahmed, S., Jesson, M., & Sharifi, S. (2023). Selection Frameworks for Potential Rainwater Harvesting Sites in Arid and Semi-Arid Regions: A Systematic Literature Review. *Water (Switzerland)*, *15*(15). https://doi.org/10.3390/w15152782

Al-Adamat, R. (2008). GIS as a decision support system for siting water harvesting ponds in the basalt aquifer/NE Jordan. *Journal of Environmental Assessment Policy and Management*, *10*(2), 189–206. https://doi.org/10.1142/S1464333208003020

Al-adamat, R., Alayyash, S., Al-amoush, H., Al-meshan, O., & Rawajfih, Z. (2012). *The Combination of Indigenous Knowledge and Geo-Informatics for Water Harvesting Siting in the Jordanian Badia*. *2012*(August 2012), 366–376.

Al-Adamat, R., Diabat, A., & Shatnawi, G. (2010). Combining GIS with multicriteria decision making for siting water harvesting ponds in Northern Jordan. *Journal of Arid Environments*, *74*(11), 1471–1477. https://doi.org/10.1016/j.jaridenv.2010.07.001

Al-Hasani, B., Abdellatif, M., Carnacina, I., Harris, C., Al-Quraishi, A., Maaroof, B. F., & Zubaidi, S. L. (2023). Integrated geospatial approach for adaptive rainwater harvesting site selection under the impact of climate change. *Stochastic Environmental Research and Risk Assessment*, *38*(3), 1009–1033. https://doi.org/10.1007/s00477-023-02611-0

Alfonsov, V. A., McKenna, C. E., Bayandina, E. V., Kashemirov, B. A., Yarmieva, L. N., Punegova, L. N., & Kataeva, O. N. (2008). Stereoselective synthesis of enantiopure cyclic α-aminophosphonic acids: Direct observation of inversion at phosphorus in phosphonate ester silyldealkylation by bromotrimethylsilane. In *Heteroatom Chemistry* (Vol. 19, Issue 6). https://doi.org/10.1002/hc.20480

doi:10.6342/NTU202503692

Ali, K., & Al-Hameed, A. (2022). Spearman's correlation coefficient in statistical analysis. *Int. J. Nonlinear Anal. Appl*, *13*(October 2021), 2008–6822. http://dx.doi.org/10.22075/ijnaa.2022.6079

Ammar, A., Riksen, M., Ouessar, M., & Ritsema, C. (2016). Identification of suitable sites for rainwater harvesting structures in arid and semi-arid regions: A review. *International Soil and Water Conservation Research*, *4*(2), 108–120. https://doi.org/10.1016/j.iswcr.2016.03.001

Baalousha, H. M., Younes, A., Yassin, M. A., & Fahs, M. (2023). Comparison of the Fuzzy Analytic Hierarchy Process (F-AHP) and Fuzzy Logic for Flood Exposure Risk Assessment in Arid Regions. *Hydrology*, *10*(7). https://doi.org/10.3390/hydrology10070136

Banko, G. (1998). A review of assessing the accuracy of and of methods including remote sensing data in forest inventory. *Internation Institute for Applied Systems Analysis, Interim Report IT-98-081*, *November*, Laxenburg,_ Austria.

Behzadian, M., Khanmohammadi Otaghsara, S., Yazdani, M., & Ignatius, J. (2012). A state-of the-art survey of TOPSIS applications. *Expert Systems with Applications*, *39*(17), 13051–13069. https://doi.org/10.1016/j.eswa.2012.05.056

Broek, Thea Van Den, and R. H. (2022). An Integrated Approach to Climate Security and Peacebuilding in Somalia. *International Affairs*, *98*(5), 1475–1493.

Buraihi, F. H., & Shariff, A. R. M. (2015). Selection of rainwater harvesting sites by using remote sensing and GIS techniques: A case study of Kirkuk, Iraq. *Jurnal Teknologi*, *76*(15), 75–81. https://doi.org/10.11113/jt.v76.5955

Chang, D. Y. (1996). Applications of the extent analysis method on fuzzy AHP. *European Journal of Operational Research*, *95*(3), 649–655. https://doi.org/10.1016/0377-2217(95)00300-2

Chisanga, C. B., Nkonde, E., Mubanga, K. H., Phiri, D., Chemura, A., & Kipkulei, H. K. (2025). SPI-based drought characteristics using CHIRPS over Zambia: 1981–2024. *All Earth*, *37*(1), 1–19. https://doi.org/10.1080/27669645.2025.2472574

Chisanga, C. B., Nkonde, E., Phiri, E., Mubanga, K. H., & Lwando, C. (2023). Trend analysis of rainfall from 1981-2022 over Zambia. *Heliyon*, *9*(11). https://doi.org/10.1016/j.heliyon.2023.e22345

Chubaka, C. E., Whiley, H., Edwards, J. W., & Ross, K. E. (2018). A review of roof harvested rainwater in Australia. *Journal of Environmental and Public Health*, *2018*. https://doi.org/10.1155/2018/6471324

Coskun, M., & Musaoglu, N. (2004). Investigation of Rainfall- Runoff Modelling of the Van Lake Catchment By Using Remote Sensing and Gis Integration Abstract : F = (P − I) − Q Q =. *Civil Engineering*, *June*, 2–5.

Cruz, J. (2013). *Water Harvesting Proposals*.

de Winnaar, G., Jewitt, G. P. W., & Horan, M. (2007). A GIS-based approach for identifying potential runoff harvesting sites in the Thukela River basin, South Africa. *Physics and Chemistry of the Earth*, *32*(15–18), 1058–1067. https://doi.org/10.1016/j.pce.2007.07.009

doi:10.6342/NTU202503692

Ekmekcioğlu, Ö., Koc, K., & Özger, M. (2021). District based flood risk assessment in Istanbul using fuzzy analytical hierarchy process. *Stochastic Environmental Research and Risk Assessment*, *35*(3), 617–637. https://doi.org/10.1007/s00477-020-01924-8

Elewa, H. H., Qaddah, A. a, El-feel, A. a, Brows, J., St, T., Nozha, E., Gedida, E., & Alf-maskan, P. O. B. (2012). Determining Potential Sites for Runoff Water Harvesting using Remote Sensing and Geographic Information Systems-Based Modeling in Sinai Department of Water Resources , National Authority for Remote Sensing and Space Sciences (NARSS), Environmental GIS L. *American Journal of Environmental Sciences*, *8*(1), 42–55.

Faisal, R. M., & Abdaki, M. (2021). Multi-Criteria Analysis For Selecting Suitable Sites Of Water Harvesting In Northern Al Tharthar Watershed. *Journal of Sustainability Science and Management*, *16*(7), 218–236. https://doi.org/10.46754/jssm.2021.10.017

Falkenmark, M., & Rockström, J. (2004). Balancing water for humans and nature: The new approach in ecohydrology. *Balancing Water for Humans and Nature: The New Approach in Ecohydrology*, 1–247. https://doi.org/10.4324/9781849770521

FAO. (2015). *HLPE Report on Water for food security and nutrition High Level Panel of Experts on Food Security and Nutrition Extract from the Report Water for food security and nutrition*. *6*, 1–14. http://www.fao.org/fileadmin/user_upload/hlpe/hlpe_documents/HLPE_S_and_R/HLPE_2015_Water_for_Food_Security_and_Nutrition_Summary-and-Recommendations.pdf

Foody, G. M. (2001). Land Cover Classification Accuracy Assessment. *Springer Geography*, *80*, 105–118. https://doi.org/10.1007/978-981-16-5149-6_6

Forzieri, G., Gardenti, M., Caparrini, F., & Castelli, F. (2008). A methodology for the pre-selection of suitable sites for surface and underground small dams in arid areas: A case study in the region of Kidal, Mali. *Physics and Chemistry of the Earth*, *33*(1–2), 74–85. https://doi.org/10.1016/j.pce.2007.04.014

Ghosh, S., Kour, S., Taron, A., Kaywala, K., & Rajakaruna, P. (2024a). Assessing El Niño-induced drought in Zambia and its effects using earth observation data. *Natural Hazards*, *121*(4), 4505–4530. https://doi.org/10.1007/s11069-024-06976-5

Ghosh, S., Kour, S., Taron, A., Kaywala, K., & Rajakaruna, P. (2024b). Assessing El Niño-induced drought in Zambia and its effects using earth observation data. *Natural Hazards*, *0123456789*. https://doi.org/10.1007/s11069-024-06976-5

Gupta, K. K., Deelstra, J., & Sharma, K. D. (1997). Estimation of water harvesting potential for a semiarid area using GIS and remote sensing. *IAHS-AISH Publication*, *242*(January 1997), 53–62.

Handia, L., Tembo, J. M., & Mwiindwa, C. (2003). Potential of rainwater harvesting in urban Zambia. *Physics and Chemistry of the Earth*, *28*(20–27), 893–896. https://doi.org/10.1016/j.pce.2003.08.016

Hwang, C.-L., & Yoon, K. (1981). *Methods for Multiple Attribute Decision Making*. 58–191. https://doi.org/10.1007/978-3-642-48318-9_3

doi:10.6342/NTU202503692

Iradukunda, P., Mwanaumo, E. M., & Kabika, J. (2023). Hydroclimatic trend analysis and projection in Africa tropical urban regions: Cases of Lusaka, Zambia and Kigali, Rwanda. *Urban Climate*, *52*(January), 101680. https://doi.org/10.1016/j.uclim.2023.101680

Ishizaka, A., & Labib, A. (2011). Review of the main developments in the analytic hierarchy process. *Expert Systems with Applications*, *38*(11), 14336–14345. https://doi.org/10.1016/j.eswa.2011.04.143

Jaafar, H. H., Ahmad, F. A., & El Beyrouthy, N. (2019). GCN250, new global gridded curve numbers for hydrologic modeling and design. *Scientific Data*, *6*(1), 1–9. https://doi.org/10.1038/s41597-019-0155-x

Joanes, D. N., & Gill, C. A. (1998). Comparing measures of sample skewness and kurtosis. *Journal of the Royal Statistical Society Series D: The Statistician*, *47*(1), 183–189. https://doi.org/10.1111/1467-9884.00122

Kafi, K. M., Shafri, H. Z. M., & Shariff, A. B. M. (2014). An analysis of LULC change detection using remotely sensed data; A Case study of Bauchi City. *IOP Conference Series: Earth and Environmental Science*, *20*(1). https://doi.org/10.1088/1755-1315/20/1/012056

Kahinda, J. M., Lillie, E. S. B., Taigbenu, A. E., Taute, M., & Boroto, R. J. (2008). Developing suitability maps for rainwater harvesting in South Africa. *Physics and Chemistry of the Earth*, *33*(8–13), 788–799. https://doi.org/10.1016/j.pce.2008.06.047

Kaluba, P., Verbist, K. M. J., Cornelis, W. M., & Van Ranst, E. (2017). Spatial mapping of drought in Zambia using regional frequency analysis. *Hydrological Sciences Journal*, *62*(11), 1825–1839. https://doi.org/10.1080/02626667.2017.1343475

Karakuş, C. B., & Yıldız, S. (2022). Gis-multi criteria decision analysis-based land suitability assessment for dam site selection. *International Journal of Environmental Science and Technology*, *19*(12), 12561–12580. https://doi.org/10.1007/s13762-022-04323-4

Khan, Z., Alim, M. A., Rahman, M. M., & Rahman, A. (2021). A continental scale evaluation of rainwater harvesting in Australia. *Resources, Conservation and Recycling*, *167*(December 2020), 105378. https://doi.org/10.1016/j.resconrec.2020.105378

Koudahe, K., Kayode, A. J., Samson, A. O., Adebola, A. A., & Djaman, K. (2017). Trend Analysis in Standardized Precipitation Index and Standardized Anomaly Index in the Context of Climate Change in Southern Togo. *Atmospheric and Climate Sciences*, *07*(04), 401–423. https://doi.org/10.4236/acs.2017.74030

Libanda, B., Zheng, M., & Ngonga, C. (2019). Spatial and temporal patterns of drought in Zambia. *Journal of Arid Land*, *11*(2), 180–191. https://doi.org/10.1007/s40333-019-0053-2

Mahendra, H. N., Pushpalatha, V., Mallikarjunaswamy, S., Rama Subramoniam, S., Sunil Rao, A., & Sharmila, N. (2024). LULC change detection analysis of Chamarajanagar district, Karnataka state, India using CNN-based deep learning method. *Advances in Space Research*, *74*(12), 6384–6408.

doi:10.6342/NTU202503692

https://doi.org/10.1016/j.asr.2024.07.066

Mahmoud, S. H., Adamowski, J., Alazba, A. A., & El-Gindy, A. M. (2016). Rainwater harvesting for the management of agricultural droughts in arid and semi-arid regions. *Paddy and Water Environment*, *14*(1), 231–246. https://doi.org/10.1007/s10333-015-0493-z

Mahmoud, S. H., & Alazba, A. A. (2015). The potential of in situ rainwater harvesting in arid regions: developing a methodology to identify suitable areas using GIS-based decision support system. *Arabian Journal of Geosciences*, *8*(7), 5167–5179. https://doi.org/10.1007/s12517-014-1535-3

Maina, C. W., & Raude, J. M. (2016). Assessing land suitability for rainwater harvesting using geospatial techniques: A case study of njoro catchment, Kenya. *Applied and Environmental Soil Science*, *2016*. https://doi.org/10.1155/2016/4676435

Mati, B. M., Malesu, M., Oduor, A., & ICRAF. (2005). *Promoting rainwater harvesting eastern and southern Africa, The RELMA experience, ICRAF working paper*. 36.

Matomela, N., Li, T., & Ikhumhen, H. O. (2020). Siting of Rainwater Harvesting Potential Sites in Arid or Semi-arid Watersheds Using GIS-based Techniques. *Environmental Processes*, *7*(2), 631–652. https://doi.org/10.1007/s40710-020-00434-7

McKee, Thomas B., N. J. D., & Kleist, J. (1993). Preoperative serum value of sialyl Lewis X predicts pathological nodal extension and survival in patients with surgically treated small cell lung cancer. *Journal of Surgical Oncology*, *105*(8), 818–824. https://doi.org/10.1002/jso.23002

Meghanadh, D., Bharti, K., Maurya, V. K., & Dwivedi, R. (2022). Identification of Potential Sites for Harvesting Rainwater Using Geospatial Techniques. *International Geoscience and Remote Sensing Symposium (IGARSS)*, *2022-July*(November), 6364–6367. https://doi.org/10.1109/IGARSS46834.2022.9884550

Mosase, E., Kayombo, B., Tsheko, R., & Tapela, M. (2017). Assessment of the Suitability of Rain Water Harvesting Areas Using Multi-Criteria Analysis and Fuzzy Logic. *Advances in Research*, *10*(4), 1–22. https://doi.org/10.9734/air/2017/33983

Mouhoumed, R. M., Ekmekcioğlu, Ö., Başakın, E. E., & Özger, M. (2023). Integrated Fuzzy AHP-TOPSIS Model for Assessing Managed Aquifer Recharge Potential in a Hot Dry Region: A Case Study of Djibouti at a Country Scale. *Water (Switzerland)*, *15*(14). https://doi.org/10.3390/w15142534

Mouhoumed, R. M., Ekmekcioğlu, Ö., & Özger, M. (2024a). A holistic multi-tiered decision framework for evaluating rainwater harvesting potential in arid regions: A case study of the southeastern basin of Djibouti. *Groundwater for Sustainable Development*, *25*(January). https://doi.org/10.1016/j.gsd.2024.101090

Mouhoumed, R. M., Ekmekcioğlu, Ö., & Özger, M. (2024b). A holistic multi-tiered decision framework for evaluating rainwater harvesting potential in arid regions: A case study of the southeastern basin of Djibouti. *Groundwater for Sustainable*

doi:10.6342/NTU202503692

Development, *25*(September 2023). https://doi.org/10.1016/j.gsd.2024.101090

Moumane, A., Enajar, A. A., Ghazali, F. E. El, Khouz, A., Karmaoui, A., Al Karkouri, J., & Batchi, M. (2024). GIS, remote sensing, and analytical hierarchy process (AHP) approach for rainwater harvesting site selection in arid regions: Feija Plain case study, Zagora (Morocco). *Applied Geomatics*, 861–880. https://doi.org/10.1007/s12518-024-00585-4

Murray, R. S., John, J. S., & R. Alu, S. (2009). *Schaum's Probability and Statistics*.

Musonda, B., Jing, Y., Iyakaremye, V., & Ojara, M. (2020). Analysis of long-term variations of drought characteristics using standardized precipitation index over Zambia. *Atmosphere*, *11*(12), 1–20. https://doi.org/10.3390/atmos11121268

Mwelwa, D., Mwaanga, P., Nguvulu, A., & Tena, T. M. (2024). Heliyon Assessment of catchment water resources allocation under climate change in Luwombwa sub-catchment , Zambia. *Heliyon*, *10*(21), e39962. https://doi.org/10.1016/j.heliyon.2024.e39962

Nam, W. H., Choi, J. Y., & Hong, E. M. (2015). Irrigation vulnerability assessment on agricultural water supply risk for adaptive management of climate change in South Korea. *Agricultural Water Management*, *152*, 173–187. https://doi.org/10.1016/j.agwat.2015.01.012

Ngoma, H., Lupiya, P., Kabisa, M., & Hartley, F. (2021). Correction to: Impacts of climate change on agriculture and household welfare in Zambia: an economy-wide analysis (Climatic Change, (2021), 167, 3-4, (55), 10.1007/s10584-021-03168-z). *Climatic Change*, *169*(3–4), 1–20. https://doi.org/10.1007/s10584-021-03251-5

Odhiambo, K. O., Iro Ong'Or, B. T., & Kanda, E. K. (2021). Optimization of rainwater harvesting system design for smallholder irrigation farmers in Kenya: A review. *Aqua Water Infrastructure, Ecosystems and Society*, *70*(4), 483–492. https://doi.org/10.2166/aqua.2021.087

Olofsson, P., Foody, G. M., Herold, M., Stehman, S. V., Woodcock, C. E., & Wulder, M. A. (2014). Good practices for estimating area and assessing accuracy of land change. *Remote Sensing of Environment*, *148*, 42–57. https://doi.org/10.1016/j.rse.2014.02.015

Padmavathy, A. S., Ganesha Raj, K., Yogarajan, N., Thangavel, P., & Chandrasekhar, M. G. (1993). Checkdam site selection using GIS approach. *Advances in Space Research*, *13*(11), 123–127. https://doi.org/10.1016/0273-1177(93)90213-U

Ramya, S., & Devadas, V. (2019). Integration of GIS, AHP and TOPSIS in evaluating suitable locations for industrial development: A case of Tehri Garhwal district, Uttarakhand, India. *Journal of Cleaner Production*, *238*, 117872. https://doi.org/10.1016/j.jclepro.2019.117872

Rane, N. L., Achari, A., Choudhary, S. P., Mallick, S. K., Pande, C. B., Srivastava, A., & Moharir, K. N. (2023). A decision framework for potential dam site selection using GIS, MIF and TOPSIS in Ulhas river basin, India. *Journal of Cleaner Production*, *423*(April), 138890. https://doi.org/10.1016/j.jclepro.2023.138890

Rockström, J. (2000). Water resources management in smallholder farms in Eastern and Southern Africa: An overview. In *Physics and Chemistry of the Earth, Part B:*

doi:10.6342/NTU202503692

Hydrology, Oceans and Atmosphere (Vol. 25, Issue 3, pp. 275–283). https://doi.org/10.1016/S1464-1909(00)00015-0

Sacolo, S. J., & Mkhandi, S. H. (2021). Assessment of the potential of rainwater harvesting for maize production in the Lubombo plateau. *Physics and Chemistry of the Earth*, *124*(P1), 102935. https://doi.org/10.1016/j.pce.2020.102935

Sayl, K. N., Sulaiman, S. O., Kamel, A. H., & Al Ansari, N. (2022). Towards the Generation of a Spatial Hydrological Soil Group Map Based on the Radial Basis Network Model and Spectral Reflectance Band Recognition. *International Journal of Design and Nature and Ecodynamics*, *17*(5), 761–766. https://doi.org/10.18280/ijdne.170514

Sazakli, E., Alexopoulos, A., & Leotsinidis, M. (2007). Rainwater harvesting, quality assessment and utilization in Kefalonia Island, Greece. *Water Research*, *41*(9), 2039–2047. https://doi.org/10.1016/j.watres.2007.01.037

Sopper, W. E. (1992). Irrigation with Treated Sewage Effluent. In *Soil Science* (Vol. 153, Issue 3). https://doi.org/10.1097/00010694-199203000-00010

Spearman, & Spearman, C. (1904). The Proof and Measurement of Association between Two Things Author (s): C . Spearman Source : The American Journal of Psychology , Vol . 15 , No . 1 (Jan ., 1904), pp . 72-101 Published by : University of Illinois Press Stable URL : http://www.jstor.o. *The American Journal of Psychology*, *15*(1), 72–101.

Stephens, M. A. (1974). EDF statistics for goodness of fit and some comparisons. *Journal of the American Statistical Association*, *69*(347), 730–737. https://doi.org/10.1080/01621459.1974.10480196

Sun, M., Chen, W., Lapen, D. R., Ma, B., Lu, P., & Liu, J. (2023). Effects of ridge-furrow with plastic film mulching combining with various urea types on water productivity and yield of potato in a dryland farming system. *Agricultural Water Management*, *283*, 108318. https://doi.org/10.1016/j.agwat.2023.108318

Tahraoui, A., & Kheddam, R. (2024). LULC Change Detection Using Combined Machine and Deep Learning Classifiers. *7th IEEE International Conference on Advanced Technologies, Signal and Image Processing, ATSIP 2024*, *1*, 403–408. https://doi.org/10.1109/ATSIP62566.2024.10638952

Tavakoli, M., Motlagh, Z. K., Dąbrowska, D., Youssef, Y. M., Đurin, B., & Saqr, A. M. (2025). Harnessing AHP and Fuzzy Scenarios for Resilient Flood Management in Arid Environments: Challenges and Pathways Toward Sustainability. *Water (Switzerland)*, *17*(9). https://doi.org/10.3390/w17091276

Teuling, A. J., Van Loon, A. F., Seneviratne, S. I., Lehner, I., Aubinet, M., Heinesch, B., Bernhofer, C., Grünwald, T., Prasse, H., & Spank, U. (2013). Evapotranspiration amplifies European summer drought. *Geophysical Research Letters*, *40*(10), 2071–2075. https://doi.org/10.1002/grl.50495

Tiwari, K., Goyal, R., & Sarkar, A. (2018). GIS-based Methodology for Identification of Suitable Locations for Rainwater Harvesting Structures. *Water Resources Management*, *32*(5), 1811–1825. https://doi.org/10.1007/s11269-018-1905-9

Tsubo, M., Walker, S., & Hensley, M. (2005). Quantifying risk for water harvesting

doi:10.6342/NTU202503692

under semi-arid conditions: Part I. Rainfall intensity generation. *Agricultural Water Management*, *76*(2), 77–93. https://doi.org/10.1016/j.agwat.2005.01.008

Ullah, A., Pohl, B., Pergaud, J., Dieppois, B., & Rouault, M. (2022). Intraseasonal descriptors and extremes in South African rainfall. Part I: Summer climatology and statistical characteristics. *International Journal of Climatology*, *42*(9), 4538–4563. https://doi.org/10.1002/joc.7489

Ullah, A., Pohl, B., Pergaud, J., Dieppois, B., & Rouault, M. (2023). Intraseasonal descriptors and extremes in South African rainfall. Part II: Summer teleconnections across multiple timescales. *International Journal of Climatology*, *43*(8), 3799–3827. https://doi.org/10.1002/joc.8059

Usman, M., Liedl, R., Shahid, M. A., & Abbas, A. (2015). Land use/land cover classification and its change detection using multi-temporal MODIS NDVI data. *Journal of Geographical Sciences*, *25*(12), 1479–1506. https://doi.org/10.1007/s11442-015-1247-y

Velmurugan, R., Selvamuthukumar, S., & Manavalan, R. (2011). Multi criteria decision making to select the suitable method for the preparation of nanoparticles using an analytical hierarchy process. *Pharmazie*, *66*(11), 836–842. https://doi.org/10.1691/ph.2011.1034

Vijitha, V., Sayanthan, S., & Mikunthan, T. (2022). A Review on Rainwater Harvesting in Sri Lanka. *Vavuniya Journal of Science*, *1*(1), 31–37. https://doi.org/10.4038/vjs.v1i1.5

Waqed H. Hassan, K. M. Z. K. K. (2025). *GIS-based multi-criteria decision making for identifying rainwater.pdf*.

Water, M. O. F. (2024). *DEVELOPMENT AND SANITATION NATIONAL RAINWATER HARVESTING STRATEGY AND IMPLEMENTATION PLAN*. *September*.

Weerasinghe, H., Schneider, U. a., & Löw, a. (2011). Water harvest- and storage-location assessment model using GIS and remote sensing. *Hydrology and Earth System Sciences Discussions*, *8*(2), 3353–3381. https://doi.org/10.5194/hessd-8-3353-2011

WMO. (2012). Standardized Precipitation Index User Guide. *Journal of Applied Bacteriology*, *63*(3), 197–200.

Wu, R. S., Molina, G. L. L., & Hussain, F. (2018). Optimal Sites Identification for Rainwater Harvesting in Northeastern Guatemala by Analytical Hierarchy Process. *Water Resources Management*, *32*(12), 4139–4153. https://doi.org/10.1007/s11269-018-2050-1

Yadav, B., Patidar, N., Sharma, A., Panigrahi, N., Sharma, R. K., Loganathan, V., Krishan, G., Singh, J., Kumar, S., & Parker, A. (2022). Assessment of traditional rainwater harvesting system in barren lands of a semi-arid region: A case study of Rajasthan (India). *Journal of Hydrology: Regional Studies*, *42*, 101149. https://doi.org/10.1016/j.ejrh.2022.101149

Yannopoulos, S., Giannopoulou, I., & Kaiafa-Saropoulou, M. (2019). Investigation of the current situation and prospects for the development of rainwater harvesting as a

doi:10.6342/NTU202503692

tool to confront water scarcity worldwide. *Water (Switzerland)*, *11*(10), 1–16. https://doi.org/10.3390/w11102168

Yegizaw, E. S., Ejegu, M. A., Tolossa, A. T., Teka, A. H., Andualem, T. G., Tegegne, M. A., Walle, W. M., Shibeshie, S. E., & Dirar, T. M. (2022). Geospatial and AHP Approach Rainwater Harvesting Site Identification in Drought-Prone Areas, South Gonder Zone, Northwest Ethiopia. *Journal of the Indian Society of Remote Sensing*, *50*(7), 1321–1331. https://doi.org/10.1007/s12524-022-01528-5

ZADEH, L. A., & Department. (1965). Fuzzy Sets*. *Procedia Computer Science*, *207*, 4525–4534. https://doi.org/10.1016/j.procs.2022.09.516

Zhou, L. M., Jin, S. L., Liu, C. A., Xiong, Y. C., Si, J. T., Li, X. G., Gan, Y. T., & Li, F. M. (2012). Ridge-furrow and plastic-mulching tillage enhances maize-soil interactions: Opportunities and challenges in a semiarid agroecosystem. *Field Crops Research*, *126*, 181–188. https://doi.org/10.1016/j.fcr.2011.10.010

Ziadat, F. M., Mazahreh, S. S., & Oweis, T. Y. (2006). *A GIS-based Approach for Assessing Water Harvesting Suitability in a Badia Benchmark Watershed in Jordan*. *2006*(Isco), 1–4.

doi:10.6342/NTU202503692

Appendix A

Figure 34 illustrates the methodology used to compute the change raster between Fuzzy-AHP and TOPSIS suitability classification results. The procedure entails categorizing similar classes for both raster maps from each method and utilizing the Compute Change Raster tool in ArcGIS Pro with the categorical difference method. The output highlights spatial reclassifications and areas of agreement or disagreement between the two models.

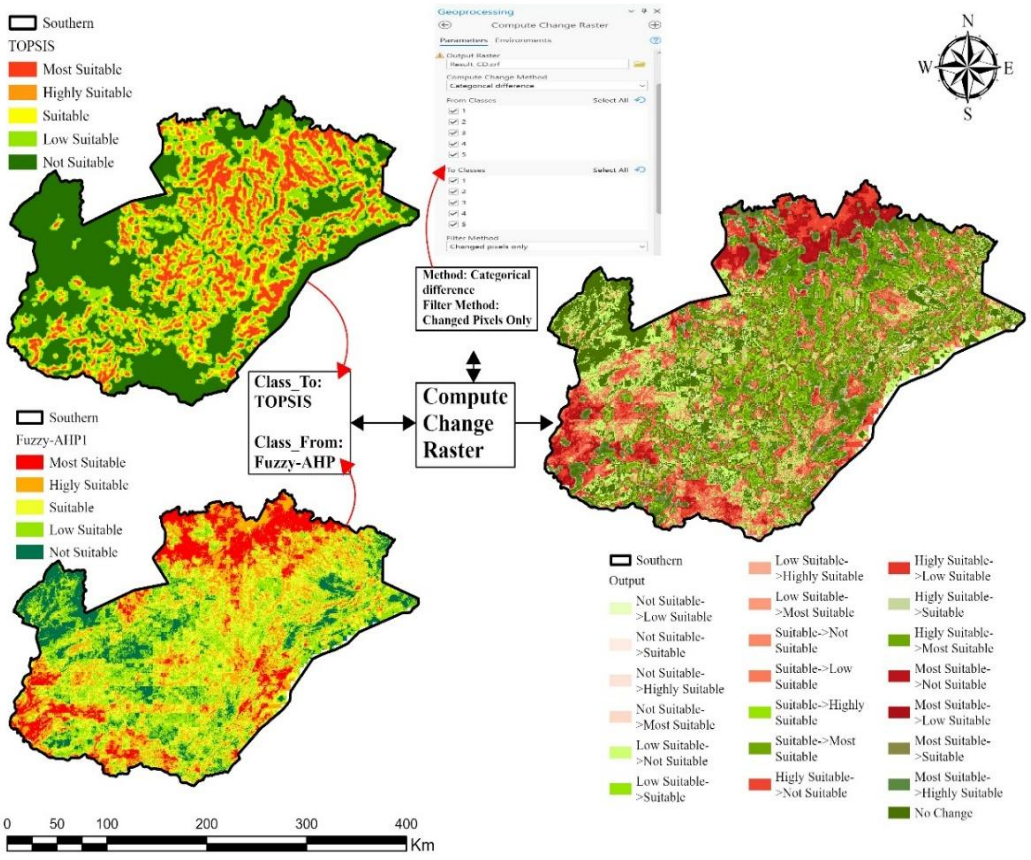

Figure 34:Workflow for Raster-Based Change Detection Between Fuzzy-AHP and TOPSIS Outputs

doi:10.6342/NTU202503692